INSTITUTO SUPERIOR TÉCNICO

ASSOCIATION EURATOM/IST

ASSOCIATED LABORATORY WITH FCT

Centro de Fusão Nuclear
Centro de Física dos Plasmas

2005 Annual Report

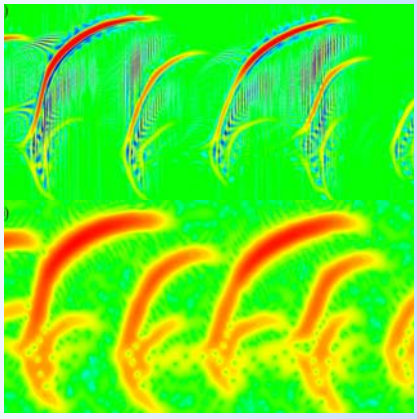

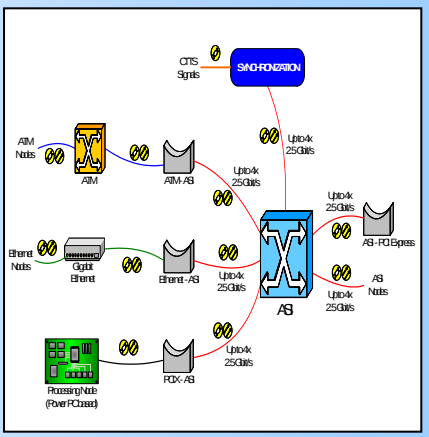

1. INTRODUCTION

1.1. FOREWORD

This document presents the main activities carried out in 2005 in the frame of the Contract of Association (CoA) signed in 1990 by the European Atomic Energy Community (EURATOM) and "Instituto Superior Técnico" (IST), hereinafter referred to as Association EURATOM/IST, and of the Contract of Associated Laboratory on Plasma Physics and Engineering signed in 2001 by "Fundação para a Ciência e a Tecnologia" (FCT) and IST, hereinafter referred to as Associated Laboratory (AL). The CoA activities are described in chapters 2 to 12, while the AL activities are presented in chapters 2 to 9, 12 and 13 to 18. Chapter 19 contains the list of publications, laboratorial prototypes, prizes and awards.

The activities described in this document were mainly performed by "Centro de Fusão Nuclear" (CFN) and "Centro de Física de Plasmas" (CFP), two Research Units of IST (Figure 1.1). The other collaborating Institutions are presented in Figure 1.1 and Table 1.1.

1.2. ASSOCIATION EURATOM/IST

The Contract of Association EURATOM/IST frames the Portuguese participation in the EURATOM Specific Research and Training Programme in the Field of Nuclear Fusion Energy, hereinafter referred as Community Fusion Programme. This Programme has as its long-term objective the development of a prototype commercial fusion power plant. It is presently implemented through several Agreements, in particular: (i) Contracts of Association signed between EURATOM and Institutions of the Member States of the European Union and Switzerland (Associates); (ii) the European Fusion Development Agreement (EFDA); and (iii) the Mobility Agreement, both signed by EURATOM and its Associates.

The work programme of the Association EURATOM/IST includes activities carried out in Portugal (mainly related with the tokamak ISTTOK) and abroad related with the operation and scientific exploitation of large and medium-sized tokamaks and stellarator (JET, (Figure 1.2) ASDEX-Upgrade, TCV, and TJ-II) as well as with the design of the next generation fusion devices (ITER (Figure 1.3) and W7-X).

1.3. MAIN PROJECTS IN 2005

The Association EURATOM/IST had in 2005 the following main Projects:

- Tokamak ISTTOK;
- Participation in the collective use of the JET facilities by the EFDA Associates;
- Participation in the ASDEX-UPGRADE Programme;
- Participation in the TCV Programme;

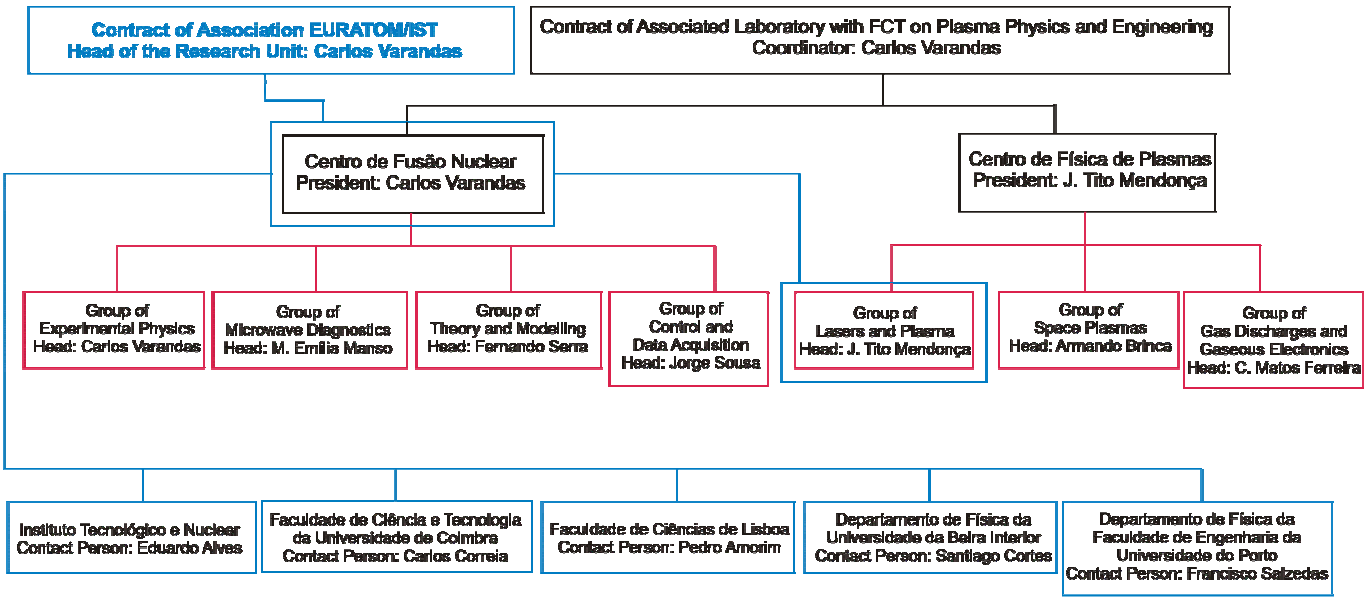

Figure 1.1 – Organization of the Associated Laboratory and Association EURATOM/IST

Project	Responsible Person(s)	Collaborating Institutions	
		Portuguese	Other
Tokamak ISTTOK	Carlos Varandas	CFN[1] UBI[2] CEI[3], CFA[4]	CIEMAT[5], IPP-Kharkov[6], UI[7], IFUR[8], IFUSP[9]
Participation in the collective use of the JET Facilities by the EFDA Associates	Fernando Serra	CFN, CEI, UBI	EFDA[10] CSU[11] Culham UKAEA[12]
Participation in the ASDEX Upgrade programme	Maria Emília Manso Fernando Serra	CFN	IPP-Garching[13]
Participation in the ITER Project	Carlos Varandas Maria Emília Manso	CFN	EFDA CSU Garching
Participation in the TJ-II programme	Carlos Varandas Maria Emília Manso	CFN, CEI	CIEMAT
Participation in the TCV programme	Carlos Varandas	CFN	CRPP[14]
Other studies on theory and modelling	Fernando Serra J. Pedro Bizarro	CFN	IFP[15], PT[16], DFRC[17]
Other activities on control and data acquisition	Carlos Varandas	CFN, CEI	IFUSP
Keep-in-touch activities on inertial fusion energy	J.T. Mendonça	CFP[18]	
Participation in the Fusion Technology Programme	E. Alves	ITN[19]	

Table 1.1 – Responsible person(s) and collaborating Institutions in the 2005 projects of the Association EURATOM/IST

- Participation in the ITER Project;
- Other activities on theory and modelling;
- Participation in the TJ-II Programme;
- Other activities on control, data acquisition and signal processing;
- Keep-in-touch activities on inertial fusion energy;
- Participation in the Fusion Technology Programme;
- Other fusion-related activities.

Table 1.1 presents information about the responsible person(s) and the Institutions involved in each project.

[1] CFN means "Centro de Fusão Nuclear"
[2] UBI means "Universidade da Beira Interior"
[3] CEI means "Centro de Electrónica e Instrumentação da Faculdade de Ciências e Tecnologia da Universidade de Coimbra"
[4] CFA means "Centro de Física Atómica da Universidade de Lisboa"
[5] CIEMAT means "Centro de Investigaciones Energeticas Medioambientales y Tecnologicas"
[6] IPP- Kharkov means "Institute of Plasma Physics of the National Science Center" "Kharkov Institute of Physics & Technology".
[7] UI means "University of Innsbruck".
[8] IFUR means "Institute of Physics of the University of Riga"
[9] IFUSP means "Instituto de Física da Universidade de São Paulo"
[10] EFDA means "European Fusion Development Agreement"
[11] CSU means "Close Support Unit"
[12] UKAEA means "United Kingdon Atomic Energy Authority"
[13] IPP-Garching means "Max-Planck-Institut für PlasmaPhysik"
[14] CRPP means "entre de Recherches en Physique des Plasmas de École Polytechnique Fédérale de Lausanne"
[15] IFP means "Istituto di Física del Plasma"
[16] PT means "Politécnico di Turino"
[17] DFRC means "Department de Recherches sur la Fusion Controlée".
[18] CFP means "Centro de Física dos Plasmas"
[19] ITN means "Instituto Tecnológico e Nuclear"

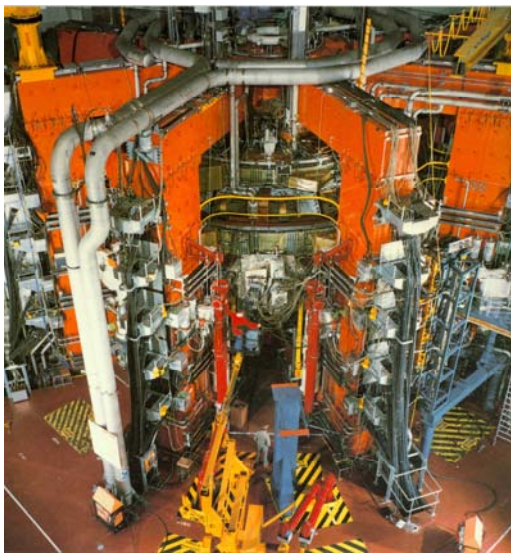

Figure 1.2 – Tokamak JET

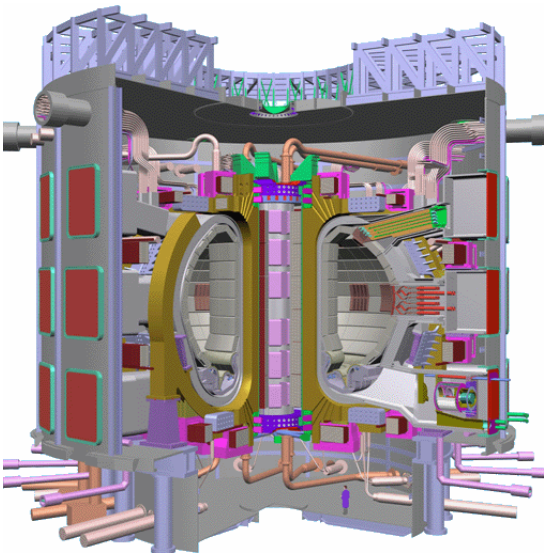

Figure 1.3 – Tokamak ITER

1.4. ASSOCIATED LABORATORY

The Associated Laboratory on Plasma Physics and Engineering has two thematic areas:

- Controlled Nuclear Fusion;
- Technologies of Plasmas and High-Power Lasers

where the following main Projects were carried out in 2005:

- Tokamak ISTTOK;
- Participation in the collective use of the JET facilities by the EFDA Associates;
- Participation in the ASDEX-UPGRADE Programme;
- Participation in the ITER Project;
- Participation in the TJ-II Programme;
- Participation in the TCV Programme;
- Other activities on theory and modelling;
- Other activities on control, data acquisition and signal processing;
- Keep-in-touch activities on inertial fusion energy;
- Other fusion-related activities;
- Theory and simulations on high energy density science and astrophysical and space plasma physics;
- Experimental physics and technological developments on ultra intense lasers, radiation sources, plasma based accelerators and biomedical optics (Figure 1.4);

Figure 1.4 - Detail of the compressor stage at the Laboratory for Intense Lasers.

- Space plasma physics;
- Environmental engineering plasma laboratory;
- Modelling of plasma reactors (Figure 1.5);
- Non-equilibrium kinetics and simulation of discharges, afterglow plasmas and high-speed planetary entries.

Figure 1.5 - Plasma torch, developed at the University of Cordoba (Spain), and modeled at CFP.

2. TOKAMAK ISTTOK

C.A.F. Varandas (Head), H. Fernandes and C. Silva (Deputy Heads), A. Soares, A. Vannucci, B.B. Carvalho, D. Valcárcel, I. Carvalho, I. Nedzelskij, M.P. Alonso, P. Carvalho, R. Coelho, H. Figueiredo, J. Figueiredo, J. Fortunato, R. Gomes, A. Neto, T. Pereira, V. Plyusnin, Y. Tashchev

2.1. INTRODUCTION

ISTTOK is a small-size (R=46 cm, a=8.5 cm), large aspect-ratio, low magnetic field (0.46 T) limiter tokamak with an iron core transformer (flux swing of 0.22 Vs), equipped with a distributed VME control and data acquisition system. Its low temperature (150 eV), low density ($8x10^{18}$ m^{-3}) plasmas are diagnosed by electric and magnetic probes, a microwave interferometer, a heavy ion beam diagnostic and spectroscopic diagnostics.

The main objectives of this project are: (i) development of new diagnostic and control and data acquisition systems; (ii) testing of new operation scenarios (liquid metal limiter and alternating plasma current); (iii) study of the influence of external applied signals on the plasma confinement and stability; and (iv) education and training on tokamak physics and engineering.

This project included in 2005 work in the following main research areas:

- Testing of the liquid metal limiter concept;
- Optimization of the ISTTOK operation;
- Diagnostics;
- Control and data acquisition;
- Plasma physics studies.

2.2. TESTING OF THE LIQUID METAL LIMITER CONCEPT[1]

IST/CFN has proceeded with the testing of the liquid metal limiter concept.

The *liquid metal loop experimental facility* has been successful filled with oxide-free Gallium. The overall setup has been tested showing satisfactory operation of the device.

The *jet stability and reproducibility* has been studied for the 2.30 mm diameter nozzle, which is planned to be used in the tokamak, since it produces a close to 13 cm continuous jet length. The time evolution for a 6 s main valve opening is shown in Figure 2.1. Gallium jet flow velocities and jet Break-Up Length parameter (BUL) have been measured for 1.45, 1.80, 2.09, 2.30 and 2.40 mm nozzle diameters. The results are presented in Figures 2.2 and 2.3.

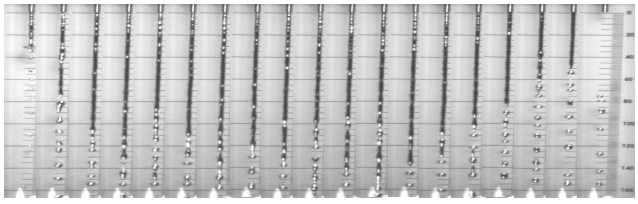

Figure 2.1 - The gallium jet time evolution for a 6 s valve opening using a 2.30 mm nozzle. Each frame was obtained using a 700 μs exposition.

The *influence of a pulsed magnetic field* (0.25 T, 60 ms) *on the jet characteristics* has been analysed for both spatially uniform line distribution and with a high gradient perturbation. Transients in the magnetic field were found not to perturb significantly the jet behaviour;

Finally, careful studies have been carried out on the observed *scattering of Gallium droplets* from the lower collector to the main chamber. A damping device has already been tested. Although it has shown a clear reduction on the number of large size (~ 0.5 to 0.2 mm) droplets, until now, it has been unsuccessful to fully eliminate the appearance of small (~10 to 200 μm size) ones. A more technically advanced damping device is under development in order to achieve a full elimination of the droplets that could reach the tokamak vessel.

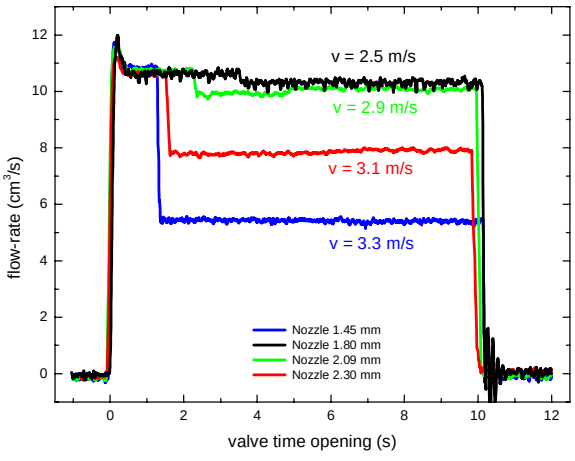

Figure 2.2 - Flow rate and flow velocity for several nozzle sizes.

[1] Work carried out in collaboration with the Association EURATOM/University of Latvia. Contact Person: O. Lielausis

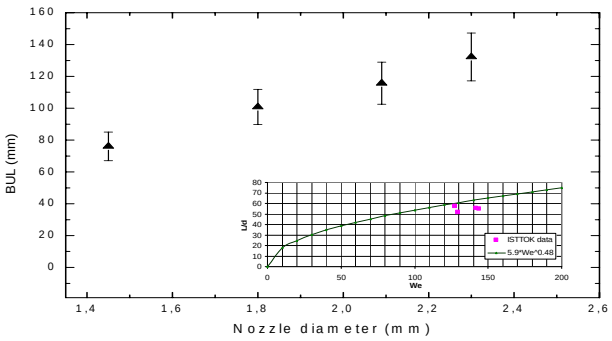

Figure 2.3 - Break-up length (L) for several nozzle sizes and as a function of Weber number.

2.3 OPTIMIZATION OF THE ISTTOK OPERATION

Aiming at optimizing the ISTTOK operation, the *gas injection system* has been upgrade by using a fast valve to allow a better control of the plasma density. The *RF generator* used for the discharge pre-ionization has been replaced by a *biased tungsten filament***.** The *new set of external coils* has been simultaneously used as the transformer primary and as a partial vertical field generator. This approach allows a smaller current on the vertical field quadrupole, with a much higher response time for feedback proposes.

2.4. DIAGNOSTICS

2.4.1. Main activities

This research line included activities on spectroscopy for the analysis of Gallium impurities[2], X-ray tomography, retarding field energy analyzer and emissive probes.

The *spectroscopy diagnostic*, designed to measure neutral Ga density on ISTTOK, has been improved by introducing a multi-channel (x8) fiber in order to acquire Ga spatial density profiles at the plasma edge. The required software has been modified and the diagnostic tested using tokamak cleaning discharges as a plasma source.

A *commercial, low cost, CCD video camera* has been tested. The test proved that these types of cameras are not adequate to be used as detectors in a soft X-ray tomography diagnostic due to the high noise level and the slow acquisition rate. A new diagnostic based on three linear 10-pixel detectors to perform real-time tomography from three different views has been designed.

The design, installation and testing of a *retarding field energy analyzer* for the measurement of the edge ion temperature has been performed.

An improved version of the *multi-pin array of emissive probes* has been installed on ISTTOK (Figure 2.4), which allows the simultaneous measurement of the density, poloidal and radial electric field, and their fluctuations in a spatial scale smaller than the turbulence correlation length.

2.4.2. Retarding Field Energy Analyzer

The retarding field energy analyzer (Figure 2.5) is rather compact (D14×L23 mm^2) and consits of an input 0.6 mm stainless steel pinhole (S), three Ni grids (G1, G2, G3) and a Cu collector plate (C) separated by MICA insulators. The grid stack is assembled in a boron nitride cup with a 14 mm of external diameter and with 2 mm diameter opening on the pinhole side.

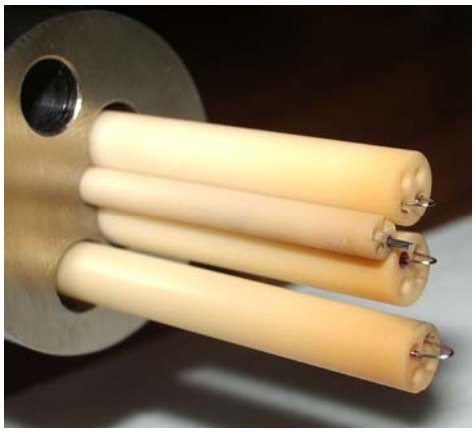

Figure 2.4 - The ISTTOK probe system, consisting of three emissive probes and one cold probe.

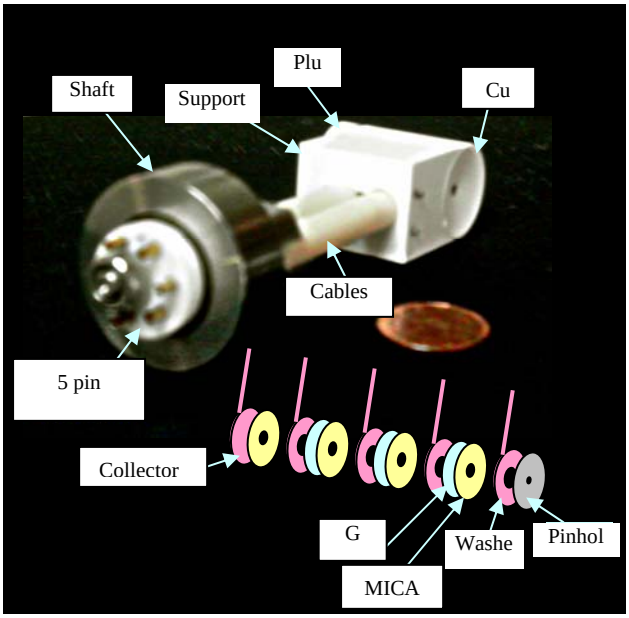

Figure 2.5 - Photograph and schematically illustration of the retarding field energy analyser

[2] Work carried out in collaboration with the Association EURATOM/University of Látvia. Contact Person: Ivars Tale.

A +100 V sawtooth voltage is applied to the second grid G_2 to obtain the ions characteristic, while grids G_1 and G_3 are kept at –50 V to suppress the respective electron flux from plasma and secondary electrons from collector. Figure 2.6 shows a typical characteristic obtained in the ISTTOK scrape-off layer (1.3 cm outside the limiter) as well as an exponential fit to the experimental data. The derived ion temperature (T_i = 14 eV) is typically a factor of two larger than that of the electrons at the same location, which is in agreement with the results of the scrape-off layer models.

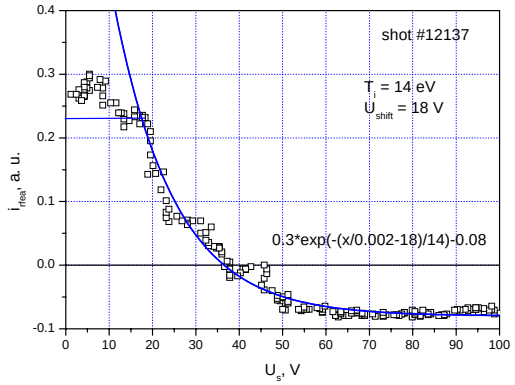

Figure 2.6 - Typical characteristic obtained in the ISTTOK scrape-off layer

2.5. CONTROL AND DATA ACQUISITION

2.5.1. Main activities

In 2005, a *real-time controller* for the horizontal plasma position, a *PCI timing board*, a new version of *software for shared remote data consulting and analysis* and *remote data analysis tools* have been developed. New *power supplies* have been designed and commissioned with optically isolated communication circuits and with local processing capabilities for self-implementation of control algorithms.

2.5.2. Real-time controller for the horizontal plasma position

The real-time controller for the horizontal plasma position allows controlling the vertical magnetic equilibrium field using a novel power supply. This controller is based on an existing PCI module (PCI-TR-256), developed at CFN.

The main technical characteristics of this module are:

- 8 galvanic isolated channels, with 14-bit ADC @ 2 MHz;
- a Texas Instruments Fixed-Point DSP @ 500 MHz (TMS320C6415);
- a Xillinx FPGA (Spartan-IIE XC2S400E);
- 512 MB SDRAM memory module;

The module software acquires data from 8 poloidal magnetic probes, removes the offset present in the signals, numerically integrates them, calculates the plasma position using the current filaments method and generates a power supply control signal with a PI controller. Off-line tests show that this system is capable of performing the plasma position calculation in 74 µs and that its time evolution is similar to the plasma position calculated offline with floating-point numerical codes running in MatLab.

2.5.3. Timing board

A new PCI-EPN board is intended to improve the trigger and the synchronism between the various ISTTOK diagnostics and allowing the migration of the ISTTOK CODAS to an event based system. The boards are on prototype stage and are planned to be operational earlier 2006.

2.5.4 New power supplies

A new concept of switched power supplies (57 kHz) were designed and completed with an embedded microcontroller, for the necessary current drive of the vertical and horizontal magnetic fields. This option allows a direct implementation of PID algorithms with a faster response time. Each power supply will allow a maximum current of 100A, with a very compact design and bipolar capabilities.

2.5.5. Cooperative software for shared tokamak operation

A new version of a multi-user platform, based on standards like CORBA, XML and JAVA, has been developed for remote control and data acquisition experiments. The main objective of this tool is to detach the machine operation from a single computer, allowing hardware configuration, experiment follow and data share by all the connected users. Among the main features it has a built-in chat, profile saving and sharing and remote calculation invocation. Since it was developed in JAVA and deployed with JAVA Web-Start technology, it can run in all the most common operating systems and computer platforms like PCs, Solaris and Mac in a very intuitive way. The software is plugin based, providing an easy way of adding new hardware, data viewers and data calculation algorithms. Since every hardware is described in a XML file, the program automatically creates configurators to the hardware. Every time a configuration is changed, the information is sent to hardware controller so that in the next discharge the hardware is programmed accordingly.

2.5.6. Remote data analysis tools

Based on the Extensible Markup Language (XML) and the Remote Method Invocation (RMI) standards, a client/server remote data analysis application has been developed for intensive data processing. This GRID oriented philosophy presents a powerful tool to maintain centralized computational resources (Figure 2.7). Another major feature is the ability to share proprietary algorithms in remote computers without the need of local code and

libraries installation and maintenance. The 16 CPU Orionte cluster in operation at CFN is currently used to provide remote data analysis. The codes running in languages such as Octave, C, Fortran or IDL are called through a script remote invocation and data is released to the client as soon as available. The remote calculations parameters are described in a XML file containing the configuration for the server runtime environment. Since the execution is made by calling a script any program can be launched to perform the analysis. Some properties of the ISTTOK plasma that require heavy computational resources are already obtained using this approach, allowing ready intershot analysis and parameterization decisions.

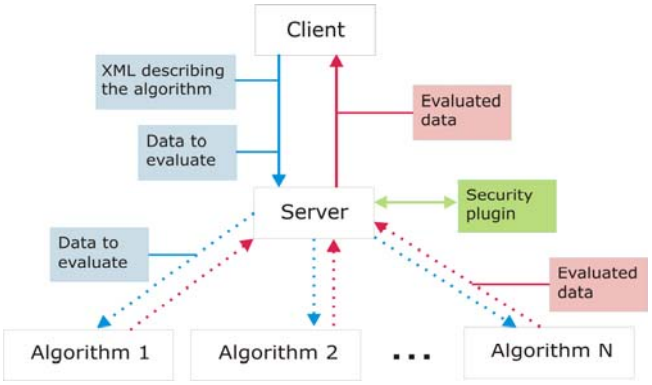

Figure 2.7 - The remote data analysis protocol scheme

2.6. PLASMA PHYSICS STUDIES

2.6.1. Introduction

The ISTTOK plasma physics studies were related in 2005 with:

- Control of edge transport by emissive electrode biasing;
- Plasma SOL flow measurements;
- Emissive probe measurements.

2.6.2. Control of edge turbulent transport by emissive electrode biasing

Emissive electrode biasing experiments have been previously investigated on ISTTOK. Experiments revealed that although a large radial electric field is induced by emissive electrode bias for both polarities (up to ±15 kV/m), a significant improvement in particle confinement is only observed for negative bias. The main motivation for this work is therefore to contribute to the better understanding of the distinct plasma behaviour with positive and negative bias. The boundary plasma was further characterized with focus on the relation between ExB sheared flows and particle transport. The use of emissive electrodes allowed, for the first time, the extension of this investigation to negative bias.

The ExB flow shear has been independently estimated from a radial array of Langmuir probes and a Gundestrup probe, which measures the parallel and perpendicular plasma flows. A good agreement has been found both in the profile and the absolute magnitude. We have observed that the magnitude of the ExB flow shear, in the region just inside the limiter position, is larger for negative bias. The ExB sheared flows induced by negative bias exceeds significantly the turbulence de-correlation time across most of the boundary plasma, while for positive bias this is only valid near the LCFS (r-a>-4 mm). The importance of the ExB flow shear on the global particle confinement has been demonstrated by the good correlation observed between these two quantities for both polarities in a wide range of bias conditions (Figure 2.8). We have found that above a certain threshold value of the ExB shearing rate (~$1x10^6$ kV/m^2) an improvement in particle confinement is observed for both polarities, being that value a factor of three larger than the turbulence de-correlation time. Results support therefore that the distinct particle confinement behaviour observed for positive and negative bias is related with the different ExB flow profile induced by edge biasing.

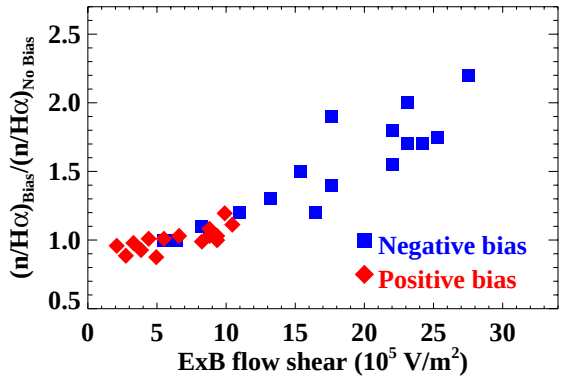

Figure 2.8 - Dependence of the modification in particle confinement induced by electrode biasing ($[n/H_\alpha]_{Bias}/[n/H_\alpha]_{No\ Bias}$) with the ExB shearing rate in the region just inside the LCFS.

The effect of electrode bias on the edge turbulent transport has also been investigated identifying the changes induced on the fluctuations frequency spectrum and probability distribution function, PDF. We have observed that negative electrode bias reduces the large amplitude, low frequency events, resulting in low amplitude fluctuations with a near Gaussian distribution across most of the scanned region. For positive bias, a substantial reduction of the fluctuations is also observed in the SOL. However, large amplitude, broad spectrum fluctuations appear in the core periphery, which increase the cross-field transport and contribute to the observed asymmetry in particle confinement with the bias polarity.

2.6.3. Plasma SOL flow measurements

Plasma SOL flow measurements were made using a Gundestrup Probe. A 1D fluid probe model was used to

deduce the parallel and perpendicular components of the unperturbed flow, taking into account the roundness of the collectors. The radial profile of the Mach numbers is shown in Figure 2.9. We note that the positive bias is not able to drive large sheared flows, which for both type of bias are larger around the limiter radius. The perpendicular Mach number behaves in opposite ways inside the LCFS and in the SOL region when bias is applied. We further note that the unbiased plasma exhibits a toroidal flow of about 0.2 throughout the measured region, being the direction the same as that of the toroidal field and plasma current. Furthermore, we note that the modification induced by biasing in the flows is maximum for negative bias and occurs in the region just inside the limiter for both parallel and perpendicular flows.

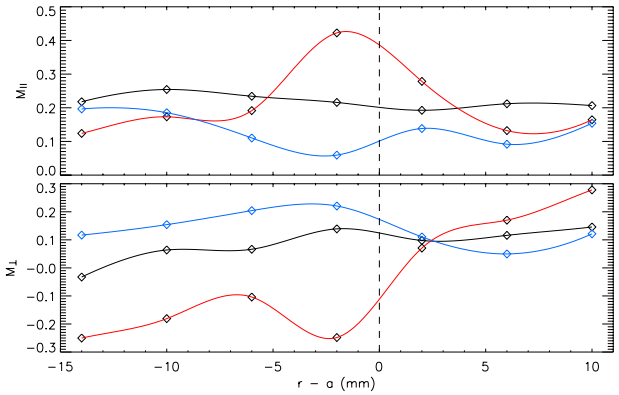

Figure 2.9 - Radial traces of parallel and perpendicular Mach numbers.

2.6.4. Emissive probe measurements[3]

Detailed measurements of the edge quantities with high temporal and radial resolutions have been performed with a multi-pin array of emissive probes. The main aim of this work was to investigate the importance of temperature fluctuations in the turbulent transport estimation. Both the root mean square of the poloidal electric field and the fluctuation-induced particle flux were found to be significantly larger when measured with the emissive probes, indicating that temperature fluctuations are important for the particle flux determination. The flux distribution was also found to be more peaked and asymmetric when measured with the emissive probes (Figure 2.10). A clear reduction of the turbulent particle flux and an improvement of the plasma confinement are observed during the negative emissive electrode biasing.

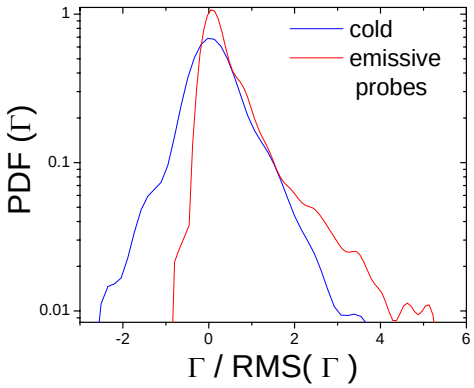

Figure 2.10 - Probability distribution functions for the normalized turbulent particle flux at r = -8 mm inside LCFS.

[3] Work carried out in collaboration with the Association EURATOM/OAW (University of Innsbruck). Contact Person: Roman Schrittwieser.

3. PARTICIPATION IN THE USE OF THE JET FACILITIES BY THE EFDA ASSOCIATES

F. Serra (Head), A. Figueiredo, A. Vannucci, B. Gonçalves[1], C. Silva, C. Varandas, D. Alves, D. Borba[2], F. Nabais, F. Salzedas, I. Nedzelski, I. Nunes, J. Sousa, L. Cupido, L. Fattorini, L. Meneses, N. Cruz, M.E. Manso, M.F. Nave, P. Belo, P. Varela, R. Coelho, S. Cortes, S. Hacquin[3], T. Ribeiro, V. Plyusnin.

3.1. INTRODUCTION

The Association EURATOM/IST has proceeded with its participation in the collective use of the JET facilities, in the frame of the "European Fusion Development Agreement" (EFDA) through the "JET Operation Contract" and the "JET Implementing Agreement".

The main activities carried out during this year were related with:

- Operation;
- Scientific exploitation;
- Performance enhancements;
- Management.

3.2. OPERATION

Two members of the IST/CFN staff have been working in the JET Operation Team:

- One physicist belonged to the *"Electron Kinetics Group"*, being responsible by maintenance and data validation of the X-mode correlation reflectometer (KG8b) and the O-mode fluctuation reflectometer (KG3), as well as completing some shifts as "Diagnostic co-ordinator" (DCO) during the restart campaign;
- The other physicist belonged to the *"Operation Group"*, being involved namely in the development of new plasma scenarios and configurations, in particular for the new divertor, and in the conceptual design of the tiles for all the main JET limiters and antenna (ICRH and LHCD) protections, and acting as first Session Leader in the restart of JET (during September/December 2005).

3.3. SCIENTIFIC EXPLOITATION[4]

3.3.1. Introduction

The participation in the JET 2005 Work Programme had contributions from fifteen physicists who performed post-analysis of data from the experimental campaigns C13 - C14, and who were also involved in the preparation of the Campaigns C15-C17. The work was focused on *code developments and physics studies related mainly with Task Forces M (with contributions to S1,S2, and T) , D and E.*

3.3.2. Integration of transport and MHD codes

(i) Implementation of sawtooth models into the transport code JETTO

The so-called sawtooth crash is thought to start with the onset of the m/n=1/1 internal kink mode. During this crash a reconnection process results in the drop of the central temperature. The corresponding outward transport of energy defines an inversion radius that separates the central region, where energy is lost, from an outer region, where energy is deposited.

Until recently the sawtooth physics available in the transport code JETTO was limited to a simple phenomenological model. At a user specified sawtooth crash time, the bulk plasma profiles of density and pressure were flattened within a user specified radius. No redistribution of the magnetic flux was included. In addition, the code could not be used for predictive sawtooth studies since no sawtooth trigger model was available. Following an assessment of available numerical modules, it has been proposed implementing into JETTO: (i) the NTCC Module KDSAW used in TRANSP; and (ii) the Porcelli's sawtooth trigger model available in the BALDUR code. The first part of this work, the implementation of KDSAW into JETTO, has been carried out and completed (Figure 3.1). KDSAW is now fully integrated and tested. A new interface for JAMS has been written. WEB documentation has been prepared. The second part of the work, i.e. the work on the implementation of the Porcelli model was initiated. A test version of JETTO including the Porcelli model is now available.

(ii) Testing JAMS interface for the equilibrium code HELENA and for the MHD code MISHKA[5]

The MHD codes MISHKA and HELENA have recently been integrated into JAMS. However, in order to simplify the JAMS input panels only a limited number of parameters were offered to the user, for the study of edge stability. Test runs of MISHKA and HELENA were

[1] Member of the Close Support Unit.
[2] Head of Office for the EFDA Associate Leader for JET
[3] Secondee with JOC.
[4] Work carried out in collaboration with the JET EFDA Contributers
[5] Work performed in collaboration with the Association EURATOM/UKAEA, Code Management Group. Contact Person: V. Parail

made to assess the input required in the JAMS interface for the study of core MHD modes. This will be useful for the study of core MHD stability in Optimised shear as well as in ELMy H-mode plasmas. In addition the HELENA and MISHKA codes were tested for the edge MHD analysis of ELM-free discharges with large edge bootstrap currents. Areas for improvement in the input panels, output files and JAMS interface have been identified.

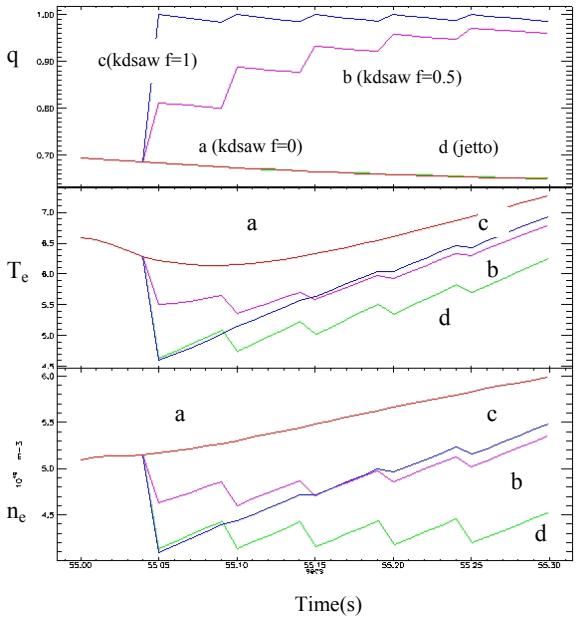

Figure 3.1 – Time traces of central q, T_e and n_e comparing the treatment of sawtooth crashes with KDSAW (curves a (no reconnection), b (partial reconnection) and c (full reconnection)) and the old JETTO (curve d).

3.3.3. JET sawtooth studies

Auxiliary heating be that either from ICRF or NBI has come to be associated with sawtooth stabilization leading to long sawtooth periods. Recent JET experiments challenged our sawtooth knowledge, as observations showed that both types of heating can produce short sawtooth periods, in the range of τ_{ST}=20-100 ms, that are shorter than observed in Ohmic heated plasmas. Experimental results from small sawtooth regimes have continued to be analysed, in particular on sawtooth observations in the reversed B_T campaign. Observations with counter-NBI indicated the important role of rotation on sawtooth stability (Figure 3.2). Two conclusions were made: (i) q-profile modifications from NIB driven current have been excluded as a possible explanation for the different sawtooth observation in co- and counter-NBI; and (ii) qualitatively, the sawtooth period observations may be explained by shear rotation effects on the internal kink stability.

3.3.4 Modelling edge stability of JET quiescent H-mode plasmas

The edge stability of JET QH-mode discharge #59611 has been studied using different versions of the transport code JETTO coupled to an ELM cycle model. Attempts on JET to access the Quiescent H-Mode (QMM) regime with counter-NBI heating, produced plasmas with extended ELM-free phases up to 1.5 s duration. These were characterised by continuous edge n=1 MHD modes similar to the DIII-D "edge harmonic oscillation". The possibility that the edge n=1 mode observed in the QH-mode plasmas may be an external kink mode (similar to the JET Outer Mode observed in Hot-ion H-mode plasmas) is being considered. Different models for the calculation of the Bootstrap Current and Neo-Classical transport were tried (Figure 3.3). A systematic variation of input parameters while searching for continuous ELMs has been made first with the JETTO Default version, then with a JETTO version that is coupled to a Theory Motivated Ballooning/Peeling ELM model. Continuous peeling modes have been obtained with the latter. Sensitivity studies of ELM stability to different edge parameters and to assumptions in the model is in progress. In addition, the edge stability of the n=1 mode is being studied with the codes HELENA and MISHKA.

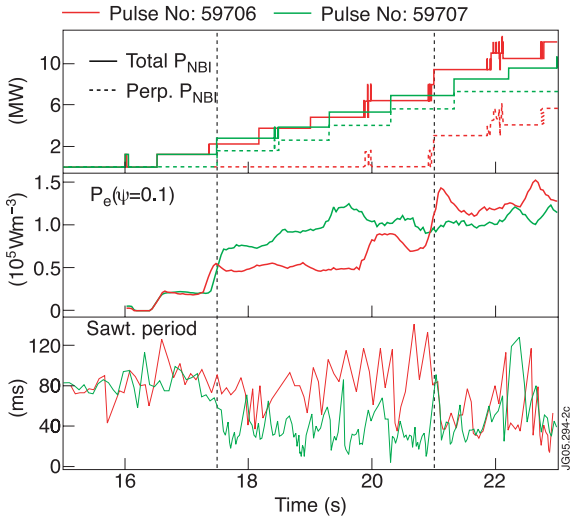

Figure 3.2 – Pair of JET discharges with counter-NBI showing sawtooth periods similar or smaller than observed with Ohmic heating. (a) Total and perpendicular NBI power; (b) Volume averaged power transferred to the electrons, at the flux surface ψ=0.1 (calculated with the PENCIL code); and (c) observed sawtooth period. Vertical lines indicate the times when perpendicular NBI was added: t=17.5 for pulse n. 59707 and t=21 s for pulse n. 59706.

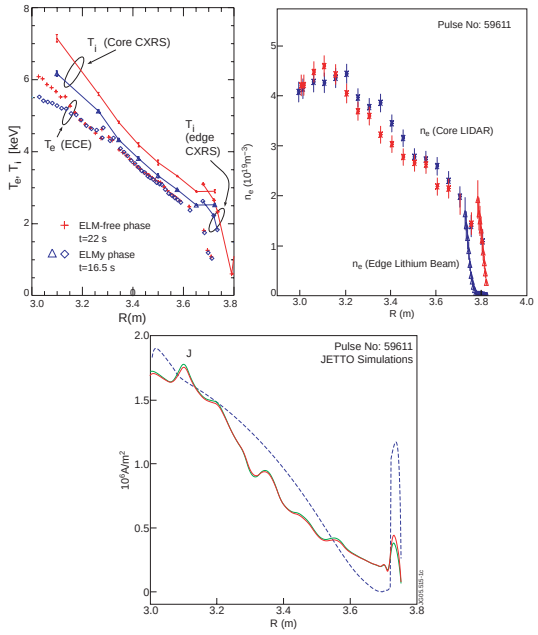

Figure 3.3 - (a) and (b) – Temperature and density profiles measured in a JET Quiescent H-Mode experiment.(c)– Current Density profile modelled with JETTO: (A) Interpretation runs using measured T and n during quiescent phase, for different models for Bootstrap current (Red: NCLASS model, green: JETTO model). (B) Predictive run without ELMs or any other MHD modes (dotted line).

3.3.5. Contribution to DIII-D experiments in the quiescent H-mode (QHM) regime[6]

Current ramps were used to study the stability of edge MHD modes as a function of the plasma current, in quiescent H-mode plasmas. The idea for these experiments originated from a proposal from IST to identify the nature of the Edge Harmonic Oscillator (EHO) and to determine if there were similarities with the MHD observations in JET ELM-free plasmas. It had been proposed that the EHO was likely to be an external kink as the JET Outer Mode and therefore its stability should be sensitive to the edge plasma current. As predicted, the experimental results have shown that the EHO is stabilised by ramping down the plasma current, leading to MHD free periods. In contrast, ramping up the plasma current triggered ELMs. Qualitatively the experiment suggested that the edge of the QHM plasma is marginally stable to external kinks. Both EHO and ELMs behave as external kinks (also known as peeling modes). The EHO observations are consistent with a non-linearly saturated external kink, while the ELMs appear to be linearly unstable external kinks.

3.3.6. Data analysis of n=0 chirping modes observed in JET ion cyclotron heated plasmas.

Persistent rapid up and down frequency chirping modes with a toroidal mode number of zero (n=0) have been observed in the JET tokamak (Figure 3.4). They arise only when energetic ions with a mean energy ~500 keV are created by high field side ion cyclotron resonance frequency heating. A study of fluctuation data from magnetic and reflectometry diagnostics has been performed.

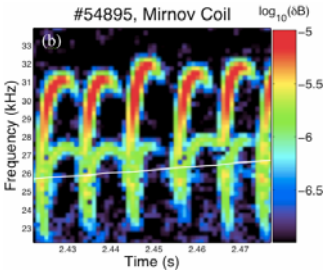

Figure 3.4 – Spectrogram of the signal of a Mirnov coil on JET showing the chirping n=0 mode.

3.3.7. Forecast of tokamak plasma instabilities using artificial neural networks

A research program was initiated to investigate the possibility of using artificial neural networks to forecast the occurrence of major disruptions and ELM instabilities in JET plasmas. The feed-forward neural networks used were chosen to have two hidden layers and were trained using the well known back-propagation algorithm.

Using soft X-ray signals, the major disruptions in some class of plasma discharges could be forecasted up to 2.0 ms in advance, as shown (Figure 3.5). The red and the black curves correspond to the neural network output and to the experimental data, respectively.

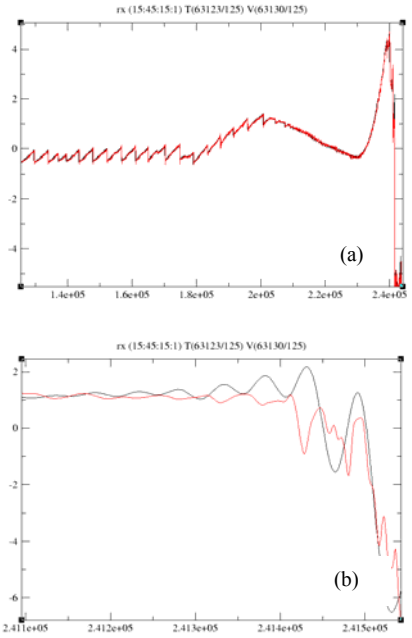

Figure 3.5 – Validation result using JET soft X-ray signal. The red curves represent the output signals from the neural network, forecasted 2.0 ms in advance. In (b) it is shown in detail the last instants of time before the plasma disruption.

[6] Work included in the JET collaboration with DIII-D. Contact person: P. West, who led the experiments

Using magnetic signals, both the disruption event and the ELM occurrences could be forecasted up to 1.2 ms in advance. Figure 3.6 presents the comparison the result of the training process (curve in red) to the experimental data (in black). Figure 3.7 shows in detail, an ELM spike and also the plasma disruption event.

After the neural network has been properly trained it was then put to forecast the ELM occurrences and the plasma disruption events using five other different JET plasma pulses. The results obtained can be considered very good, as illustrated in Figures 8 and 9.

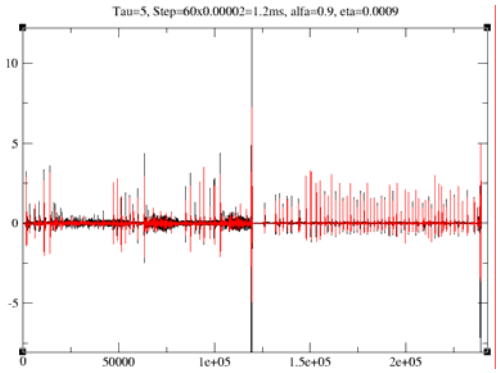

Figure 3.6 – Result of the training process using two JET magnetic signals. The red curve represents the output signals from the neural network, with forecasting time 1.2 ms in advance, and the black curve represent the experimental data.

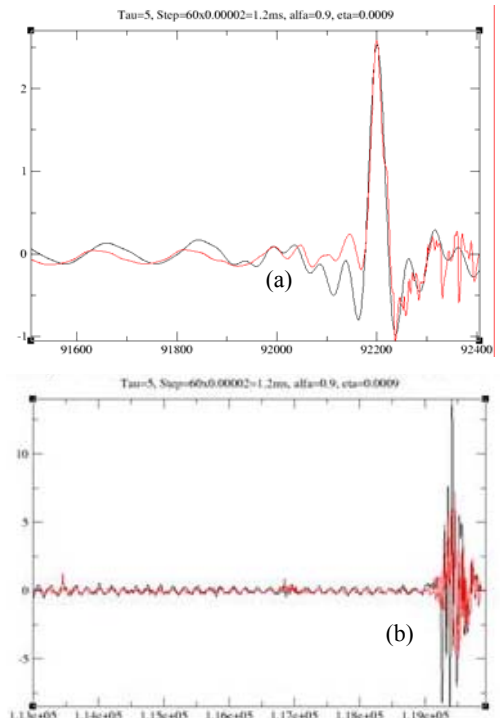

Figure 3.7 – Time expanded signals of figure 6 showing in detail that the neural network closely matches (a) the ELM spike and (b) the plasma disruption event.

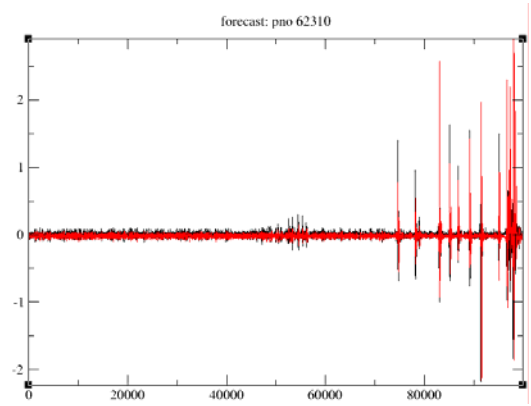

Figure 3.8 – Forecast result (in red) of the JET pulse 62052, using the neural network trained previously. The forecasting time interval is 1.2 ms.

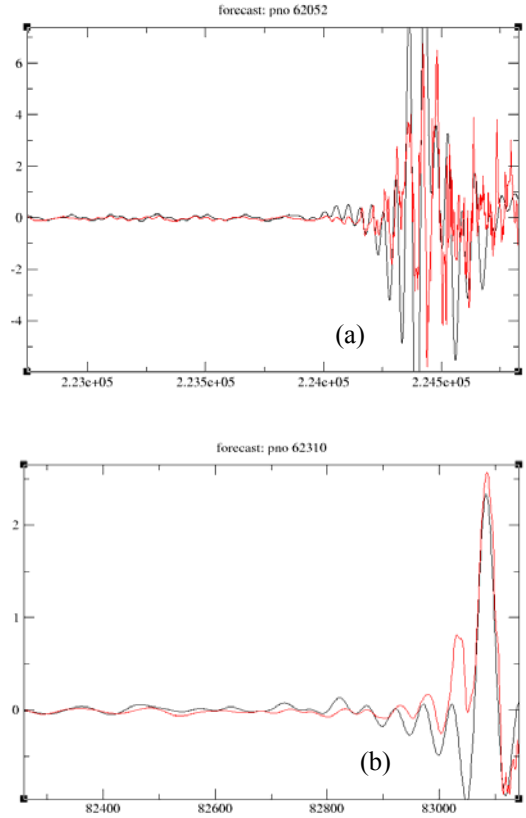

Figure 3.9 – In (a) the disruption event of the JET pulse 62052 (Figure 3.4) is shown in detail. In (b) the time expanded signal of the JET pulse 62310 is presented, showing in detail an ELM spike.

3.3.8. Numerical calculations of the precessional fishbones resonance

A surprising feature of the precessional drift fishbones recently observed in JET low density experiments was its unusually high frequency (around 60 to 90 kHz). To try and explain this, numerical simulations were carried out with the CASTOR-K code. This code allows to calculate the resonant exchange of energy between a mode with an

internal kink structure and populations of ICRH driven fast ions as were used in the experiments. It uses the equilibrium calculated by the HELENA code and the eigenmode calculated by the MISHKA code. Thus, the CASTOR-K code was used to calculate the resonant transference of energy δW_{HOT} between the fast particles population and the mode for different values of T_{HOT}, as function of the mode frequency (Figure 3.10). The modes frequencies that maximize this transference should be around the frequencies observed in the experiments.

Figure 3.10 shows that the best fit between experimental and numerical results is for a fast ions temperature T_{HOT} between 1 MeV and 1.5 MeV, while the value of the fast ions temperature T_{HOT} estimated for these experiments was around 1 MeV. It can also be seen that the mode expected frequency increases rapidly as the fast ions temperature increases. To analyse in more detail what is happening, it is needed an orbits analysis.

Figure 3.11 (upper half) shows the resonant transference of energy between the internal kink mode (f=50 kHz) and three ICRH driven fast ion populations characterized by different temperatures (500, 750 and 1000 keV). The orbits of the particles in stronger resonance with the mode are also represented in Figure 3.11 (lower half). It can be seen that there are two main resonances, one corresponding to particles nearer the magnetic axis centred around 900 keV and the other corresponding to particles farer from the plasma axis centred around 1.8 MeV. This second resonance becomes dominant when the fast ions temperature increases (it is already dominant for T_{HOT}=750 keV). Thus, it can be concluded that there is a change in the type of orbits of the particles that have a stronger interaction with the mode, which cause the mode frequency to increase rapidly with the fast ions temperature and may explain the high frequency of the precessional fishbones observed experimentally.

3.3.9. Improved time–frequency visualization of chirping mode signals in tokamak plasmas using the Choi-Williams distribution

The use of auxiliary heating in tokamak plasmas produces energetic ions that can destabilize a variety of magnetohydrodynamic (MHD) modes. These instabilities may expel energetic ions from the plasma core, reducing the heating efficiency. Often, such MHD instabilities have time-varying frequencies, being referred to as "chirping modes". The best examples are "fishbones", which have decreasing frequency while the mode amplitude increases. Such chirping down has also been observed in JET Alfvén eigenmodes. Upward frequency chirping is less common, although sometimes observed in JET plasmas with ion cyclotron resonant heating (ICRH).

Here, it is shown an unusual class of JET low-frequency chirping modes, with toroidal mode number n = 0, which are rapidly swept upwards and downwards in the 25–40 kHz range. Similar nearly symmetric up and down chirping has recently been observed in toroidal Alfvén eigenmodes in the spherical tokamak MAST with neutral beam heating. The nonstationary character of MHD chirping modes is best seen in a time–frequency image, which can be compared with others from nonlinear theoretical models of kinetic instabilities. These models predict frequency splitting as well as frequency sweeping. The short-time Fourier transform spectrogram has been used to analyze chirping mode signals. Still, images based on the spectrogram are hindered by a trade-off between time and frequency resolution, which is particularly detrimental when nonstationarity is strong. Excellent time–frequency resolution can be achieved with the Wigner distribution, but artifacts may preclude its use for signals with multiple components. The Choi-Williams distribution allows a compromise to be made between good time–frequency resolution and an acceptable level of artifacts.

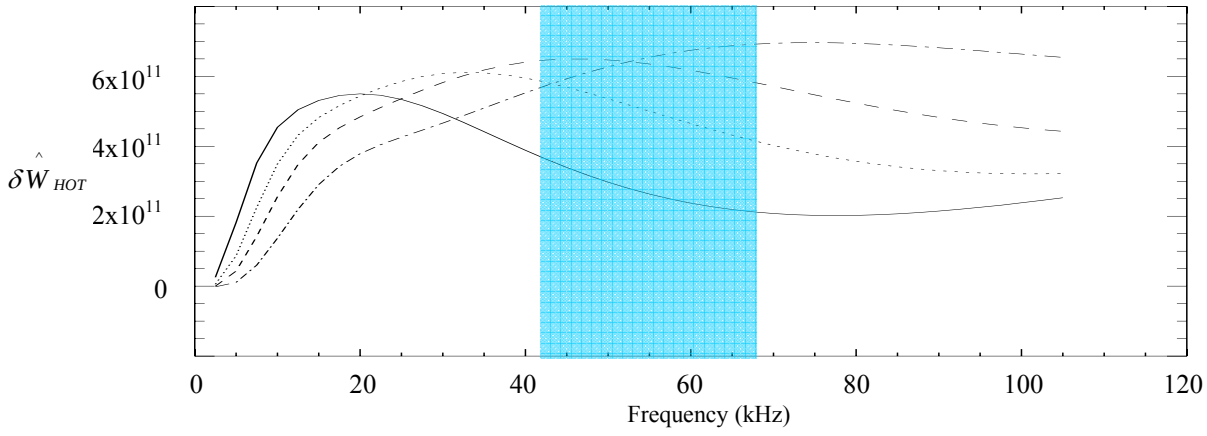

Figure 3.10 - Resonant transference of energy between the internal kink mode and an ICRH driven fast ions population with temperatures of 500 keV (solid line), 750 keV (dotted), 1 MeV (dashed) and 1.5 MeV (dashed/dotted). The observed frequency of precessional fishbones is shadowed.

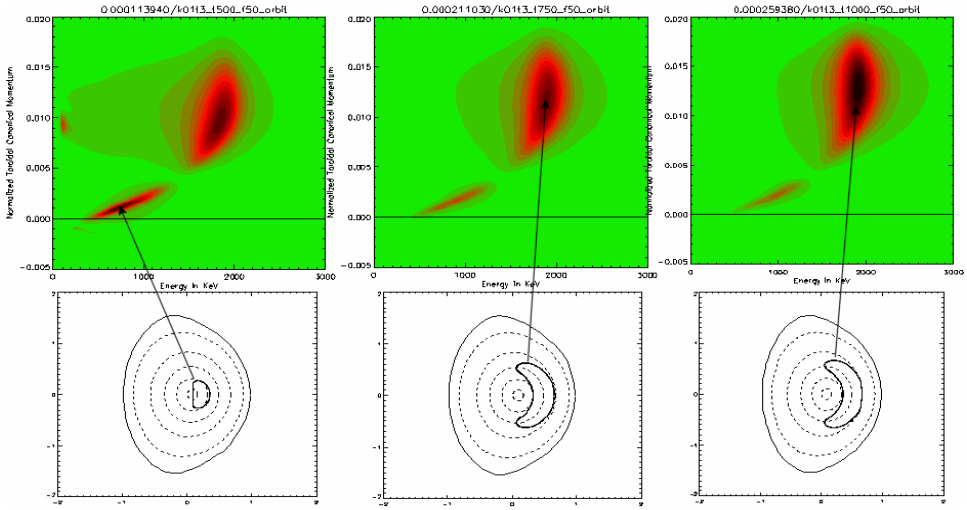

Figure 3.11 - Upper line - Resonant transference of energy between the internal kink mode (f=50 kHz) and an ICRH driven fast ions population as function of the energy and the toroidal canonical moment for three different fast ions temperatures: 500 keV (left), 750 keV (middle) and 1000 keV (right). Lower line: Orbits of the particles with a stronger interaction with the node, for each case.

The images in Figure 3.12 are time–frequency representations of chirping modes in a JET plasma, which are observed during the initial heating phase — when ICRH is applied — of a discharge with a non-monotonic current density profile. Figure 3.12 shows that the Choi-Williams distribution does yield a sharper time–frequency picture than the spectrogram. Artifacts can be recognized in Figure 3. 12(a) by their oscillatory nature, but pose no problems reading the plot since they are separated from the signal components. In Figure 3.12(b), the spectrogram shows each burst of magnetic activity as a pair of modes that start at the same low frequency and then diverge with one mode chirping up and the other chirping down. In Figure 3.12(a) the frequency splitting in two modes is more clearly observed even at the lowest frequency.

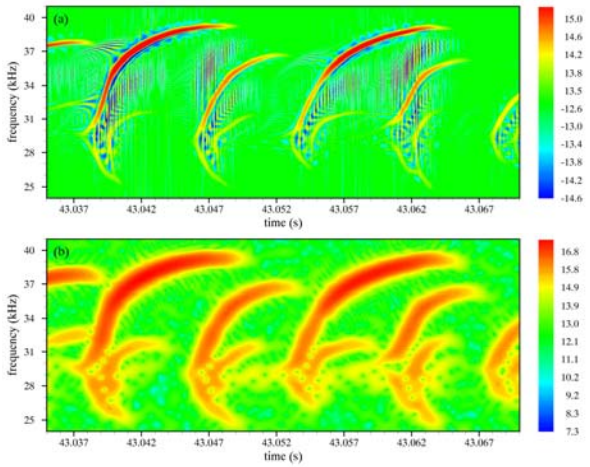

Figure 3.12 - Time–frequency density plots of a chirping mode signal (JET pulse 54893) obtained using (a) the Choi-Williams distribution with $\sigma = 25$ and (b) the spectrogram with a 2 ms window.

3.3.10. Impurity transport studies

The classical friction in the SOL was studied as a mechanism to prevent impurities to reach the plasma core. A 2-D multispecies transport code EDGE2D/NIMBUS was used, for typical MARKIIGB divertor H-mode JET plasmas. To describe H-mode plasma we used a prescribed ad-hoc perpendicular transport coefficients of heat and particle diffusivities, and drifts were not considered. The parallel transport was determined using the 21 moments approximation of the Braginskii equations .

The force balance between the classical parallel friction force and the thermal force are related to Neon content inside the last closed flux surface. The higher is the friction force relatively to the thermal force the lower is the Neon content in the core before the plasma detachment. This study was done for four different main gas inlet positions: top of the vessel, divertor region, inner mid plane and outer mid plane. We found that Neon exhaust is better for the latter case. This conclusion is still valid with the change of impurity boundary conditions although some differences are found: the plasmas detaches at higher densities because the electron temperature at the inner divertor is higher and the Neon enrichment factor is lower because the system allows more impurities inside the last closed flux surface for the steady state boundary condition, $\nabla n_z(\psi_{min}) = 0$, than for the external impurity puff $n_z(\psi_{min}) = 0$ (Figure 3.13).

The Neon core content is lower and the enrichment factor is higher for the simulations with Neon and Carbon than with Neon only but for main ion densities at the plasma detachment. The main influence of Carbon on Neon is the plasma detachment onset happens at lower main ion densities. There is no clear increase of the friction force between Carbon and Neon. The sum of

friction and the thermal forces is lower and closer to zero at onset of plasma detachment making the Neon to be mainly confined in the divertor region in such plasma.

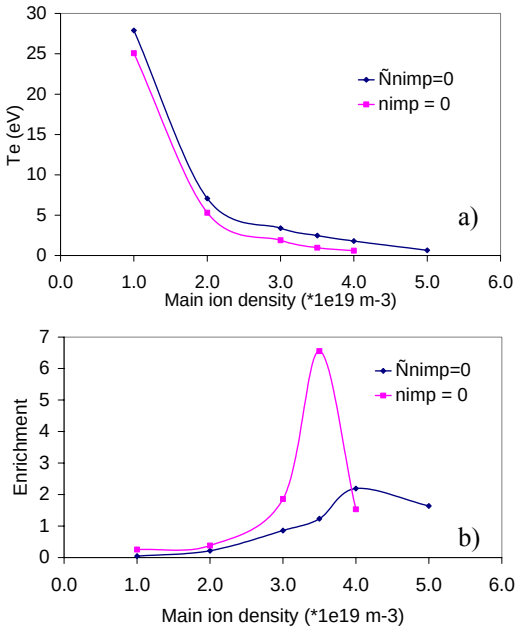

Figure 3.13 - a) Electron temperature at the inner divertor and b) Neon enrichment factor for the two boundary conditions at the last closed flux surface.

A reduction of the core carbon content and a drop of the C^{2+} spectral line intensity in the divertor region were observed in high density seeded impurity JET plasmas after the introduction of the extrinsic impurity . We found the same effects in our simulations with Carbon and with Carbon and Neon of the experiments when we compare the modelling results for the same main ion densities. However these effects are also observed in a pure Carbon simulation but at higher main ion densities, (Figure 3.14). We can conclude that the extrinsic impurity plays an indirect role on the Carbon redistribution and it is the electron temperature in the divertor region that is the main factor. Namely it is the reduction of the electron temperature that leads to and increase in the friction force relatively to the thermal force. As the plasma approaches detachment the electron temperature becomes so low that the efficiency of the carbon chemical sputtering goes down reducing the C^{2+} spectral line intensity in the divertor region (Figure 3.15).

3.3.11. Exploitation of the microwave reflectometry systems[7]

(i) Characterisation of Alfvén Cascades (ACs) in advanced plasma regimes

The excitation and observation of Alfvén Cascades are now used to diagnose advanced plasma scenarios with

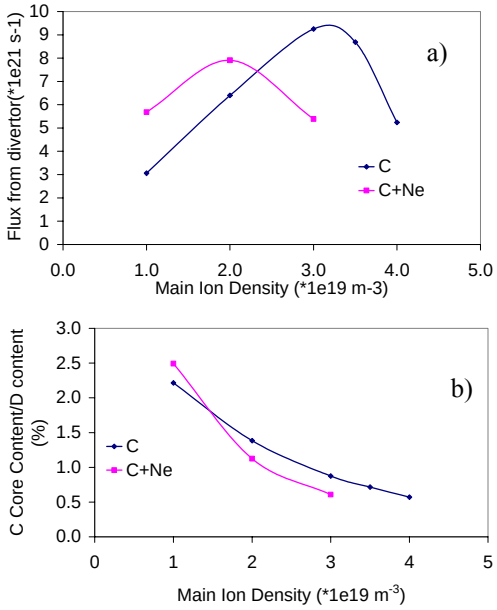

Figure 3.14 - a) Carbon source at the divertor and b) carbon content inside the last closed flux surface / deuterium content, for the simulations with carbon (c) only and with carbon + Neon (c+Ne).

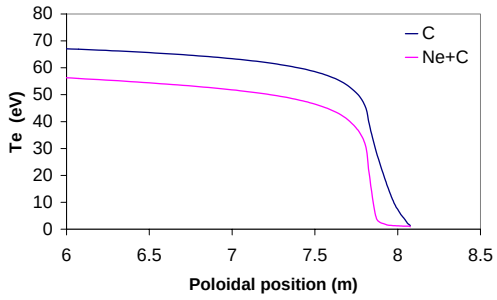

Figure 3.15 – Electron temperature along a poloidal field line 1 cm outside the last closed flux surface, in the SOL of the inner divertor for simulations with C and Ne+C.

Internal Transport Barriers (ITBs). In addition to the determination of the reversed magnetic shear, the time evolution of the safety factor minimum $q_{min}(t)$ can be inferred from the time evolution of the Alfvén Cascade frequency. A good determination of $q_{min}(t)$ is crucial for the development of such scenarios on JET since the ITBs are usually triggered at low order rational magnetic surfaces corresponding to $q_{min}(t)$. The JET O-mode multi-channel reflectometer (KG3 diagnostic) used in the interferometry regime allows routine measurement of Alfvén Cascades with high frequency and time resolution. In addition, the level of density fluctuations induced by an Alfvén Cascade can be inferred from the phase perturbations of the reflectometry signal. This only requires an assumption on the shape of the density fluctuations, which can be obtained from an equilibrium

[7] Work carried out in collaboration with the Association EURATOM/UKAEA. Contact Person: S. Sharapov

reconstruction and MISHKA-H and NOVA-K computations. The level of density fluctuations is then estimated by matching the phase perturbations evaluated experimentally (Figure 3.16) and those computed by WKB simulations.

(ii) Turbulence studies

H-mode access at very low plasma density has been studied on JET, providing valuable information on the physics of the edge transport barrier formation . In particular, a significant reduction of the turbulence level was observed after the L-H transition (Figure 3.17). This is exemplified on the figure below, which displays a clear reduction of the fluctuations of the reflectometer signal reflected in the edge plasma region.

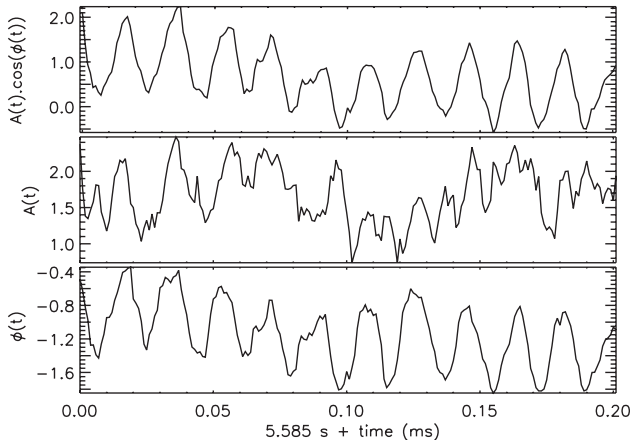

Figure 3.16 - Fluctuations of the reflectometry homodyne signal, of its amplitude and of its phase induced by the presence of an Alfvén cascade

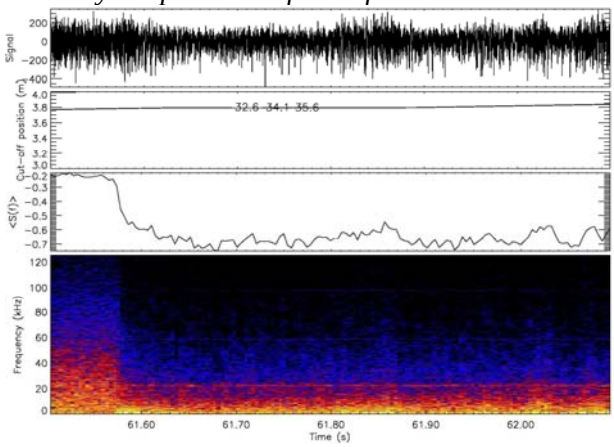

Figure 3.17 - Reduction of plasma turbulence at the L-H transition observed from a O-mode reflectometry signal at fixed frequency 34.1 GHz. From upper to lower parts: Raw reflected signal (b) Radial position of the cut-off layer (c) Averaged level of the reflected signal fluctuations (d) Spectrogram (sliding FFT) of the reflected signal

3.3.12. Turbulence experiments in reversed and standard-B field configurations in the JET tokamak

In 2005 it was performed the analysis of the data collected by the fast reciprocating Langmuir probe system in the plasma boundary region during the campaigns of 2003/2004 with the aim to compare plasma turbulence in normal and reversed field configurations. Basic turbulence properties (e.g. level of fluctuations, ExB turbulent transport) are comparable in normal and reversed field configurations. It was observed that the SOL turbulence is less intermittent in REV-B discharges.

The normalized Probability Distribution Function (PDF) shows that the distributions of fluctuations in the ion saturation current, I_s and the floating potential, V_f are very similar in both magnetic field directions (Figure 3.18). It should also be noted that the PDF's were obtained at different radial positions. Some differences in PDF shape are observed for the measurements from the far SOL (star points).

The normalized PDFs of the turbulent flux are also remarkably similar (Figure 3.19). A reduction of the intermittence is observed in REV-B discharges (closed symbols) being this reduction more pronounced in inward intermittent flux events ($\Gamma_{ExB} < -5 <\Gamma_{ExB}>$, negative tail of the curve). This small difference is not reflected in the turbulent flux profiles because the contribution from intermittent events to the total flux is small.

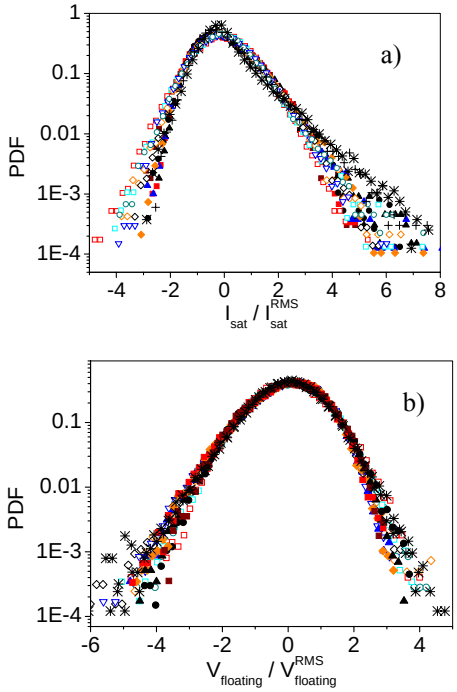

Figure 3.18 - Probability Distribution function of I_s (a)) and V_f (b)) normalized to the level of fluctuations

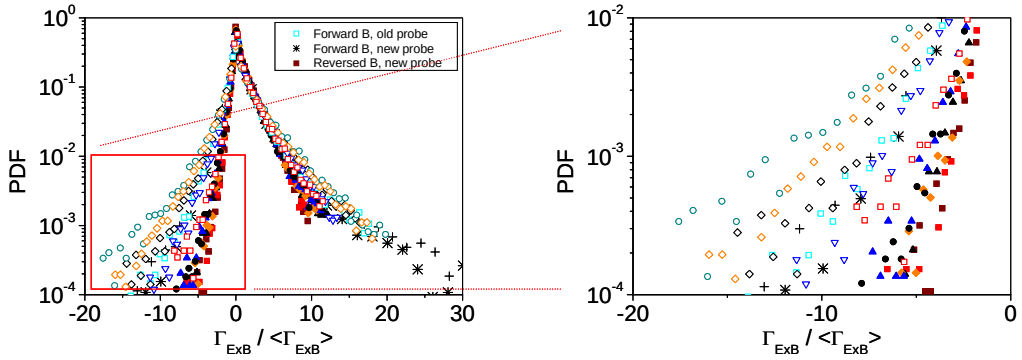

Figure 3.19 - a) PDF of the turbulent ExB flux. b) A detail of the tail of the distribution shows a reduction in the inward intermittent events for the reversed field discharges.

3.3.13. Analysis of generation and loss mechanisms of runaway electrons

A comprehensive understanding of the trends of disruption-generated runaway electrons (REs) is needed to avoid their detrimental consequences on the materials of the plasma facing components (PFC) and vacuum chamber in large tokamaks and ITER. Comparison of experimental results and numerical modeling has allowed further contribution into development of the model for generation of runaway electrons during disruptions. Numerical modelling has been carried out in frame of a test particle model taking into account the evolution of the runaway beam geometry, which has been observed in experiments using soft-X diagnostics. A detailed scan on RE beam size shows that calculated current conversion efficiency can exceed the upper bound of the experimental values if the RE beam will occupy the whole plasma cross-section despite a significant decrease of the RE density (Figure 3.20 (a,b,c)). At some combinations of the disruption parameters the current conversion rate can achieve 100%, which never has been observed in experiments. Similar trends have been also predicted by other studies, where under certain conditions practically all the initial plasma current can be converted into runaways.

Several mechanisms are considered as possible reasons for the observed in experiments a 60% upper bound for the current conversion rate:

(i) REs are sensitive to magnetic fluctuations, which decrease the characteristic life-time of the runaways: $\tau_{RE}=a_{pl}/5.8D_r$, where $D_r \approx \pi q R_0 c(b_r/B_0)^2$ is the coefficient of the radial diffusion caused by the presence of magnetic field perturbations with the magnitude b_r. Very large magnetic perturbations lead to the enhanced losses of fast particles and limit the energy and total amount of REs at the early stage of disruptions. However, with the increase of kinetic energy (W_{kin}) REs become less sensitive to the magnetic turbulence.

(ii) Another loss mechanism can be understood from the analysis of the runaway orbit outward drift as the RE energy increases: $d_r=c/\omega_{ce}\ (q/P_{||})(P_{||}^2+ P_{\perp}^2/2)$. From this expression one can obtain a condition for the energy of runaway electron, at which it will escape outside the confining region created after disruption: $P_{\perp}^2=2(d_r/q^*\omega_{ce}/c^*P_{||}-P_{||}^2)$ (Figure 3.21 (a)). So, that even under conditions of the perfect confinement the runaway electrons can produce intense photo-neutron emission interacting with PFC due to outward shift of the runaway orbit at certain values of the REs energy (Figure 3.21 (b)).

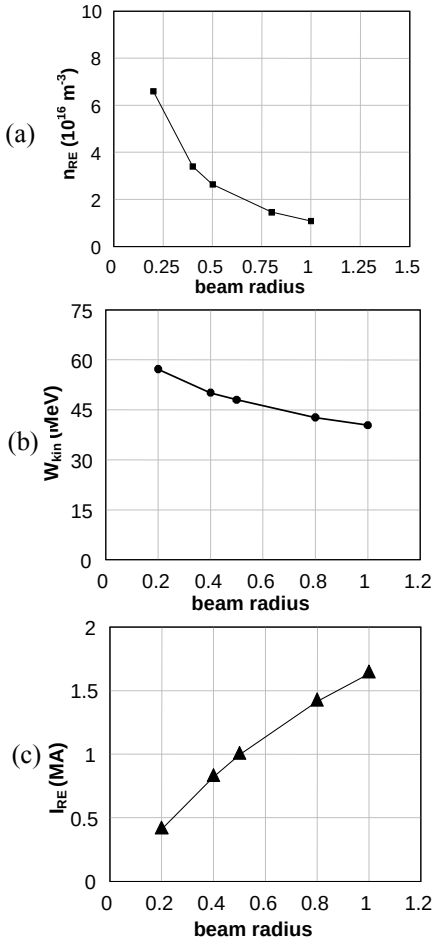

Figure 3.20 - Dependence of the calculated RE density (a), maximal kinetic energy (b), and RE currents vs. dimensionless runaway beam radius.

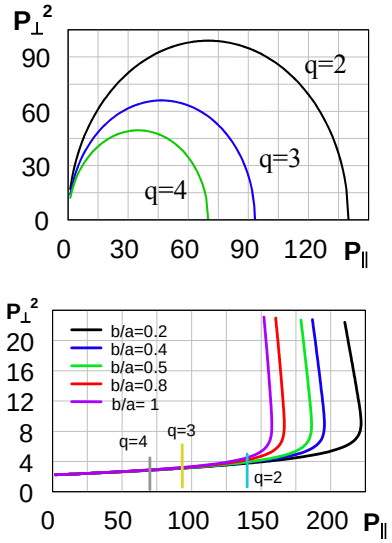

Figure 3.21 - (a) - Trajectories of the test electron in a momentum space at which its orbit outward shift becomes equal to the minor plasma radius (d_r=a, for a=1 m) at different values of safety factor: q=2,q=3 and q=4. (b) - Evolution of the test runaway electron at different values of dimensionless runaway beam radius. Conditions for complete runaway electron diffusion from the confining region are presented by curves calculated at values q=2,3 and 4.

3.4. ENHANCEMENTS

3.4.1. Introduction

The Association EURATOM/IST has been in charge with the following tasks carried out in the frame of the JET Enhanced Performance Project:

- Mw access – Project management and implementation;
- Development of a new fast sweep frequency reflectometer;
- TOFOR – Project design and procurement activities;
- Collaboration in the commissioning of TOFOR and MPRu;
- RTP – Development of a real-time test facility;
- PCU-VS – design of the PCU vertical stabilization;
- DPDT4 – Real-time measurement & control diagnostics & infrastructure project;
- Fast wave reflectometer.

3.4.2. Millimeter wave access (EFDA/01-625)

The installation of both *in-vessel and ex-vessel hardware*, namely antennas and waveguides for both reflectometry and ECE, was completed. A *quasi optical coupling arrangement* to couple five different systems into a waveguide was developed. Calibration of the existing *correlation reflectometrs* to the expected performance within the new waveguides was done.

Tests were performed, first with a mirror in-vessel and later with plasma.

Figure 3.22 shows that significant improvements of the S/N ratio for the KG8b reflectometer signals have been reached. The increase of the raw signal amplitude by a factor of 50 suggests an improvement of at least 17 dB and a clear dynamic can now be observed on the signal spectrum**.**

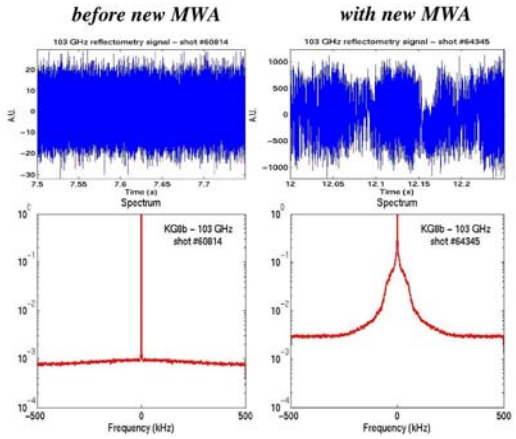

Figure 3.22 - Raw signal and corresponding spectrum from the KG8b 103 GHz channel before (on the left) and after (on the right) the installation of the new MWA

3.4.3. Development of a new fast swept frequency reflectometer (KG8a diagnostic).

A *new fast swept-frequency heterodyne reflectometer* (KG8a diagnostic) dedicated to density profile measurement is being developed and should be operational for the next JET experimental campaigns in 2006. Providing routine measurement of the edge density profile with high spatial (< 1 cm) and temporal (< 30-50 μs) resolution, this diagnostic will be of the greatest importance for the pedestal studies on JET. In addition to the development of the routine for density profile inversion, some theoretical studies were carried out in order to estimate the spatial resolution of these measurements. The influence of the misalignment between the plasma magnetic axis and the probed region was especially assessed. As depicted in the figure below, a spatial resolution better than 1 cm is expected from the KG8a measurements in a large majority of the JET discharges.

3.4.4. TOFOR – Project design and procurement activities[8]

Five *time digitizer boards* (TDB) were assembled and delivered to JET after successfully tested at the Uppsala University. Since the TDB power needs require that no more than three boards coexist in the same computer, the *control software* was modified for three plus two boards in two computers, with an implementation of a TCP

[8] Work carried out in collaboration with the Swedish Euratom Association Contact Person: J. Kelme

based synchronism server and a client. Better synchronization links were tested and found operative for the required length. Integration of the boards in the diagnostics was performed by the VR Association in close collaboration with IST/CFN.

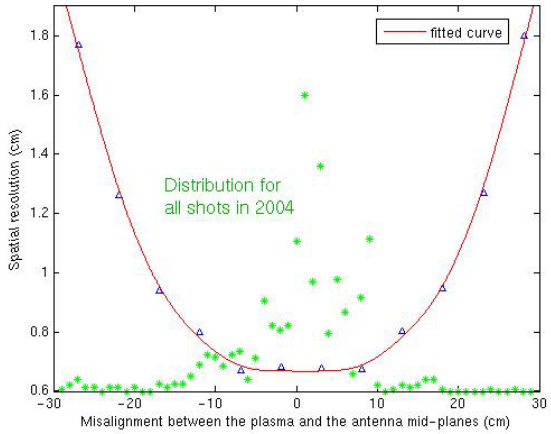

Figure 3.23 - Estimation of the spatial resolution of the KG8a reflectometer diagnostic as a function of the misalignment between the plasma and the reflectometry antenna mid-planes

3.4.5. RTP – Development of a real-time test facility

The *complete unit providing 32 waveform generator (WG) plus 8 transient recorder channels* was assembled. Requirements compliance tests were performed at IST/CFN. Integration to CODAS and functional tests were performed at JET by the IST/CFN staff with success. Minor accuracy corrections on the WG outputs and additional software features allowing local unit control were incorporated. Software and hardware manuals have been finished.

3.4.6. PCU-VS – Design of the PCU vertical stabilization

The implementation of a new vertical stabilization controller will require the increment of the number of input signals to over 50, while maintaining the control loop delay under 50 µs, and aiming to reducing it to fewer than 10 µs. The design of an *ATCA-based hardware platform (Figure 3.24) for the low-latency controller* was proposed aiming at:

- Reducing the delays on the acquisition/generator endpoints and data interconnect links;
- Providing high processing power near the acquisition/generator endpoints and on the system controller;
- Providing the synchronism of all digitizer/generator endpoints;
- Having an architecture designed for maintainability, upgradeability and scalability;
- Targeting the specificities of the VS controller including low cost per channel;
- Decreasing risks during implementation and testing.

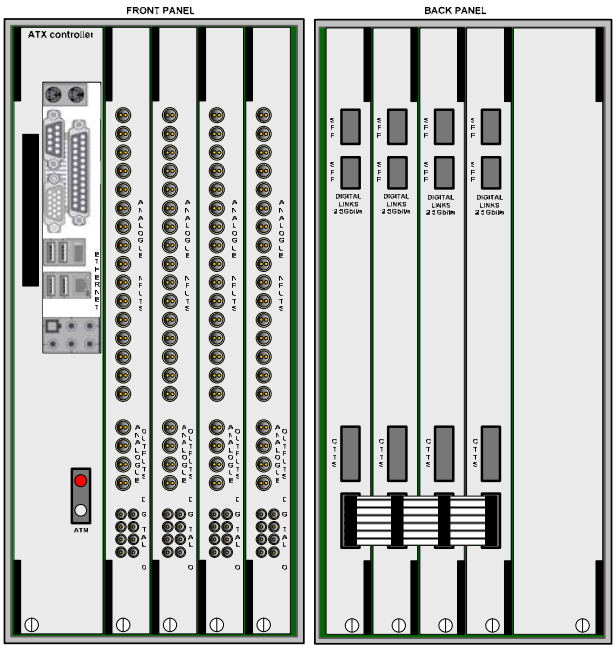

Figure 3.24 - Vertical stabilization controller

3.4.7. DPDT4 – Real-time measurement & control diagnostics & infrastructure project

The essential aim of this project is to expand JET real-time diagnostics and control capabilities required to fulfil the programme objectives of JET in the proposed FP7 phase of operation dedicated to ITER preparation. In particular the objective is to optimize the control of the plasma during operation and to enable control schemes for the main plasma scenarios and in particular profile control. In response to the call for participation in the diagnostic enhancements, Associations IST, CEA and UKAEA declared interest in the project. IST offered to lead the project and proposed the workgroup organization chart of Figure 3.25.

3.5. Management

The Association EURATOM/IST has collaborated on the management of the use of the JET facilities by the EFDA Associates in the following manner:

- Dr. Duarte Borba, as Head of Office for the EFDA Associate Leader for JET,
- Dr. Bruno Gonçalves as a member of the staff of the Close Support Unit to the EFDA Associate Leader for JET;
- Prof. Horácio Fernandes and Dr. Paulo Varela as members of the Remote Participation Users Group.

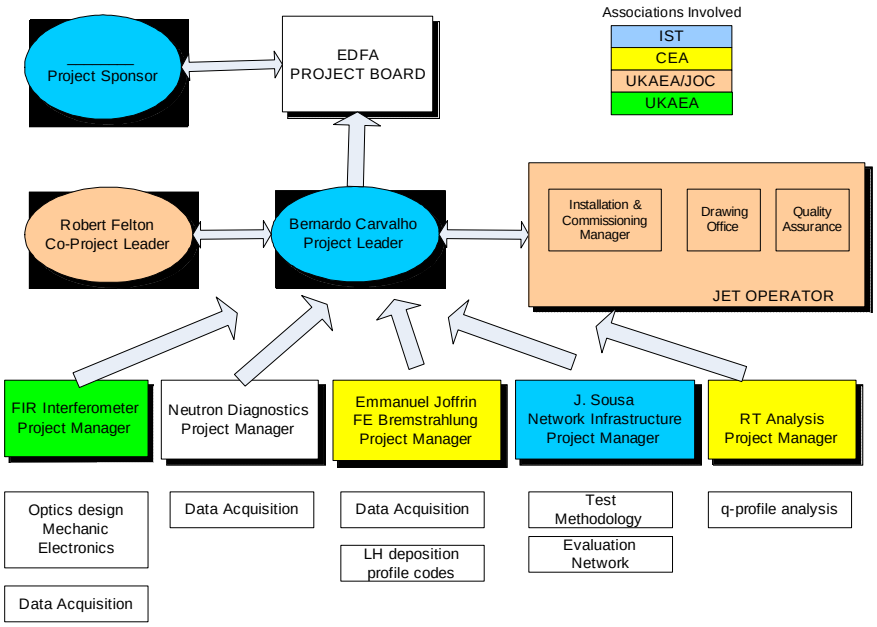

Figure 3.25 – Organization of the DPDT4 project

4. PARTICIPATION IN THE ASDEX UPGRADE PROGRAMME[1]

M.E. Manso (Head), F. Serra (Deputy Head), A. Combo, A. Ferreira, A. Silva, D. Borba, F. Salzedas, F. Silva, I. Nunes, J. Santos, L. Cupido, L. Fattorini, L. Guimarãis, L. Meneses, P. Varela, R. Coelho, S. Hacquin, S. Graça, T. Ribeiro

4.1. INTRODUCTION

The Portuguese participation in the ASDEX Upgrade[2] (AUG) programme has been mainly focused in two research lines:

- Microwave reflectometry;
- MHD, turbulence and transport.

4.2. MICROWAVE REFLECTOMETRY

4.2.1. Introduction

This research line included in 2005 activities on microwave systems and electronics, control and data acquisition, diagnostic developments, data processing, modelling and plasma physics studies.

Concerning *microwave systems and electronics,* the V band LFS channel was tested and electronics had to be modified for homodyne detection due to the degradation of the mixer. After its repair it was changed back again to heterodyne. The main control switch board of the system was calibrated and a faulty optical coupler was replaced. The pig-back of the optical analogue signal transmitters was changed. V band/X-mode channel was tested and changed from heterodyne to homodyne detection. All the diagnostic channels were inspected and tested. Part of the transmission line of the Q/X-mode channel was disassembled, tested and calibrated after high losses that were found to be caused by metal peaces of soldering material inside one of the waveguides. The V/X-mode antenna was modified to correct a construction error. A new transmission line for the HFS channels is being studied in order to protect the diagnostic in AUG forthcoming experiments with increased ECRH power.

Regarding *control and data acquisition,* the firmware of all of the eight control boards was upgraded to use a high level language, like the one used in the fluctuations monitor control system. This makes the communication more robust. Control software for a new "hopping" frequency system has being installed and tested. Also a new system has started to be developed.

Concerning *diagnostic developments,* the new hopping diagnostic was completed and first turbulence results were obtained.

Regarding *data processing*, a new algorithm was developed for the time-frequency analysis of broadband signals which allows the length of the analysis window of the spectrogram to be adapted to automatically to the local time-frequency characteristics of the signals while maintaining a good time-frequency resolution. Several upgrades were also made to the interactive data analysis tools for better efficiency and less computing time.

Concerning *modelling,* dedicated tools were developed to simulate Doppler reflectometry. A code was developed for the analysis of turbulence and transport in the SOL.

The *plasma physics studies:* were focused mainly in pellet experiments as well as MHD, turbulence and transport. The studies could be extended to higher densities with the W band channel in full operation.

4.2.2. Frequency calibration

The frequency calibration system was upgraded with a delay line. The output of the detected signal resulting from interference between the non delayed and the delayed signal as well as the spikes from the frequency markers are shown in Figure 4.1. The interference data was used to obtain a continuous the frequency versus time characteristics of the oscillators in ultrafast swept operation.

The instantaneous phase evolution of the signal shown in Figure 4.1a is obtained with an Hilbert Transform and the resulting frequency step is depicted in Figure 4.1b. The spectrogram of a signal reflected from a metallic mirror obtained with the frequency marker calibration shows significant deviations from a constant value corresponding to the distance between the antenna and the mirror (Figure 4.2a), whereas in the case of the delay line calibration an almost constant time delay is recovered (Figure 4.2b). The novel method greatly improved the accuracy of density profiles.

4.2.3. Control and data acquisition

In order to exploit full diagnostic capabilities of the ASDEX Upgrade tokamak it is mandatory to upgrade the data acquisition and control system. This will cope with faster frequency sweep times and improved time resolution as well as accuracy allowing, for example, plasma position and shape measurements for control purposes, as it is foreseen for ITER. A new PCI-based

[1] Work carried out in collaboration with the ASDEX-Upgrade Team. Contact Person: Dr. G. Conway.

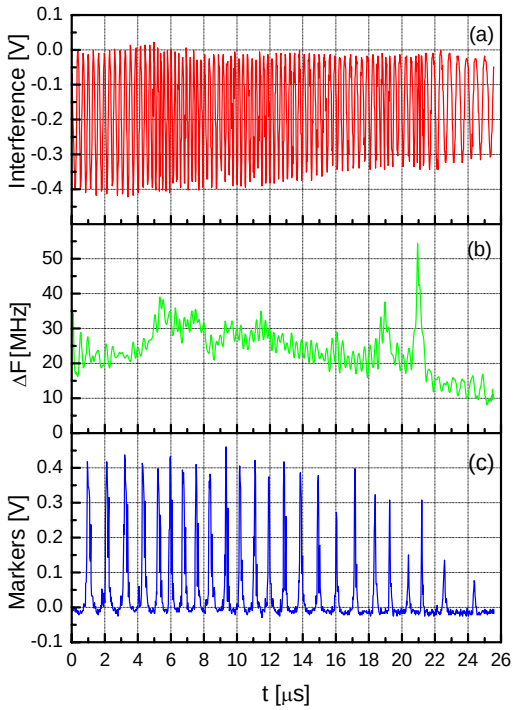

Figure 4.1 - a) Interference signal. b) Frequency step from the interference signal. c) Frequency markers signal.

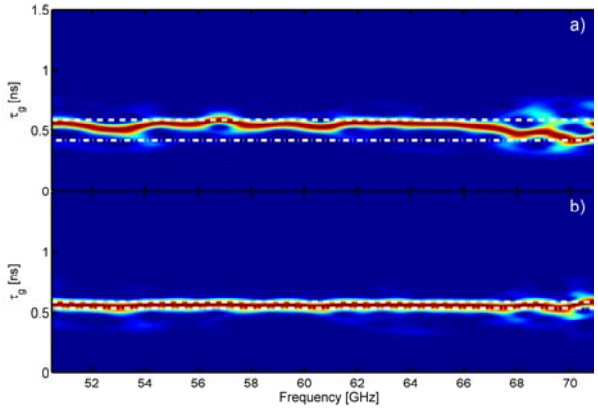

Figure 4.2– Spectrogram of a signal reflected from a metallic mirror: a) frequency marker calibration and b) delay line calibration.

system (Figure 4.3) is being developed based on a digitizer card with 2 channels, 12-bit resolution and a waveform generator with one channel, 14-bit resolution. Both cards will have 512 Mbytes of memory, a Digital Signal Processor (DSP) for advanced processing modes and a Field Programmable Gate Array (FPGA) for real-time algorithms and complex trigger managing modes. The system will be able to support multiple cards (digitisers and signal generators) operating synchronously at a maximum speed of 210 MHz. The development of the fast digitizers and generators was started with the schematic and layout design of the PCI cards.

4.2.4. Numerical studies for plasma position

The sensitivity and robustness of reflectometry to track plasma movements in a steady state ELMy H-mode scenario was studied aiming to fully demonstrate the use of reflectometry for control purposes as foreseen for ITER. Position curves after ELM removal were averaged using a window of 3 measurements or 26 ms, roughly equivalent to averaging three ITER individual measurements (at a 10 ms rate). To compensate the errors in the profile inversion due to the non probed plasma region with O-mode reflectometry, a dynamic initialization procedure was developed.

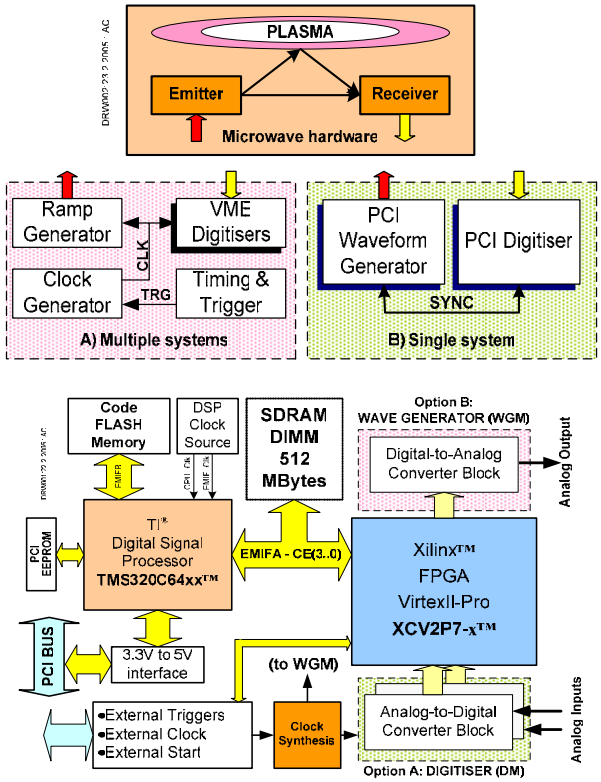

Figure 4.3 - Current (A), new (B) data acquisition system and PCI module diagram.

To track the separatrix position from reflectometry profiles two estimations for the density at the separatrix were used one from diagnostic XPTO and multiplying the average density by a factor α (with $\alpha \in [0.15, 0.65]$). Position results obtained using the dynamic estimation for the ratio between the separatrix density and the average density after removing measurements performed during ELMs, were impressively good (Figure 4.4). In this case, shot #19701, the tracking of the separatrix position using

a fixed scaling of 30% of the average density to estimate the density at the separatrix would result in a match to the magnetic separatrix with a radial error of 2.5 mm and standard deviation of 2.5 mm both at HFS and LFS.

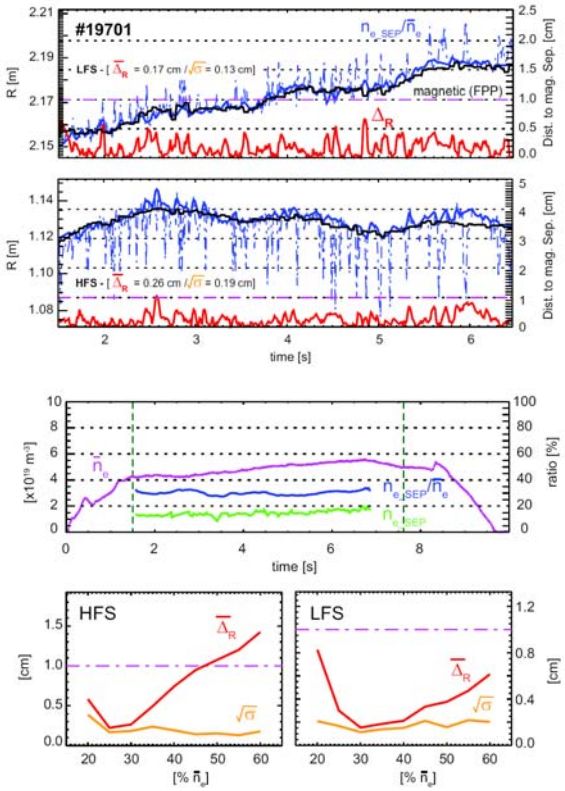

Figure 4.4 - Position of density layers corresponding to $n_{e\_sep}/\overline{n}_e$ after removing during-ELM measurements and averaging during a 26 ms window (thick blue) and the corresponding distance to the magnetic separatrix, $\overline{\Delta}_R$ (red), in discharge #19701; $\overline{n}_e, n_{e\_sep}$ and corresponding ratio curve (top right plots); $\overline{\Delta}_R$ and $\sqrt{\sigma}$ as a function of a static percentage of $\overline{n}_e$ (bottom right plots).

4.2.5. Modelling[2]

The previously developed 2D code is being equipped with the tools to explore the possibilities of extracting information from reflectometry about thin velocity shear layers as those occurring, for example, in internal transport barriers and zonal flows.

The numerical results can be applied to any reflectometry system, namely in ASDEX Upgrade or Tore Supra[3].

[2] Work carried out in collaboration with Dr. Stephan Heuraux (Université Poincaré, Nancy, France.)

[3] Modelling analysis more focused on reflectometry for ITER is presented in section 8.

The plasma is modelled with a generic density profile, across circular or elliptical iso-density lines (slab model corresponds to an infinitely elongated ellipsis). Turbulence is taken into account as a sum of modes with random phase. The density perturbation at each point obeys to,

$$\delta n_{eTRB} = \sum_{i_m}^{i_M} \sum_{j_m}^{j_M} A(i,j) \cos\left[k_x(i)x + k_y(j)y + \varphi(i,j)\right] \quad (1)$$

The choice of the coefficients $A(i,j)$ is in agreement with the Tore Supra experimental data. The columns of the original turbulence matrix on the shear region are shifted poloidally, each column sliding at a speed given by the imposed velocity shear profile. Figure 4.5 shows the columns of the original turbulence matrix $n_e(r,t)$ (top left), as the simulation runs its course, slide with a velocity given by the shear profile. Its effect on the turbulence structure is shown on Figure 4.5 (bottom left). This model for velocity shear implies a modification of the wavenumber spectrum (k-spectrum) on the shear layer (both poloidal and radially). Figure 4.5 shows the original spectrum (top right) and the spectrum at iteration 50×10^3 (bottom left) are shown. They reveal the deformation of the density fluctuation spectrum in the shear zone reflecting the elongation of the turbulent structures along the poloidal direction and the radial squeezing as the matrix columns slide in the shear region.

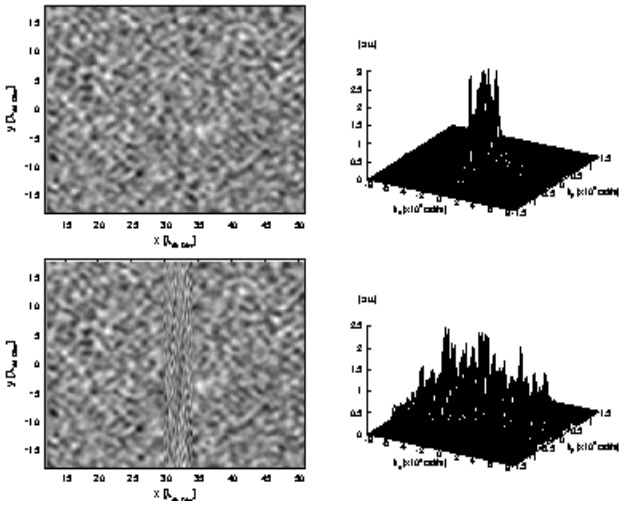

Figure 4.5 - Original turbulence matrix (top left) and the amplitude k-spectrum (top right). Matrix of turbulence at iteration $50 \cdot 10^3$ (bottom left) and the modified spectrum at the poloidal velocity shear region with a radial profile in the x-direction (bottom right).

In classical reflectometry the code is usually run in a monostatic setup (same antenna used for emission and reception) and the signal is excited in the waveguide using a Unidirectional Transparent Source (UTS) allowing

unidirectional injection of a wave. Figure 4.6 (upper plot) presents a monostatic setup for a 2D H-plane horn with a half power beam width of 30° appears on top. The Doppler effects in this configuration appears due to lateral probing of the plasma through the relatively large antenna radiation pattern. The contribution to the frequency spectrum from the direct reflection on the plasma is stronger than the Doppler effects and the Doppler frequency shift arises on a wide frequency range according to the Bragg law at the turning point (oblique cut-off).

The 2D code was adapted to typical Doppler reflectometry using an optical system (Figure 4.6 bottom plot). The use of a lens allows the emission of a quasi non-diverging beam with a planar wave front which will respond to a single wave number according to the injection angle chosen by the prism. The same impulsive response (IR) technique utilized to implement the UTS is used to eliminate the spurious reflection from the lens and prism.

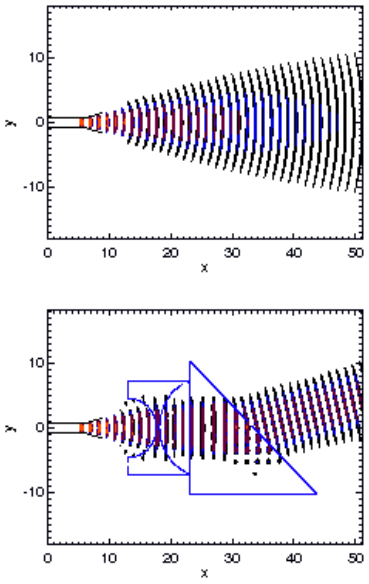

Figure 4.6 Classical reflectometry with a horn (top) and Doppler setup with a converging lens and prism to launch beams with high directivity.

4.2.6. Pedestal evolution in the presence of ELMs

The study of the pedestal evolution in AUG discharge #1991, where four intrinsic type I ELMs and one pellet triggered ELM occurred, is presented in Figure 4.7, along with the time traces of the line average density obtained with the interferometer diagnostic, and the H_α radiation associated with the outward particles flux into the divertor plates.

A further picture of edge profile dynamics under ELMs was obtained from the detailed profile evolution at the LFS (Figure 4.8). At the LFS the density time traces show clearly the two distinct regions separated by ~ 1cm around 2.17 m. This should be the position of the last closed flux surface, separating the pedestal (< 2.17 m) and the scrape of layer (SOL) (> 2.17 m). Transport during the ELM (period of enhanced D_α light emission) increases the SOL density during that period of time.

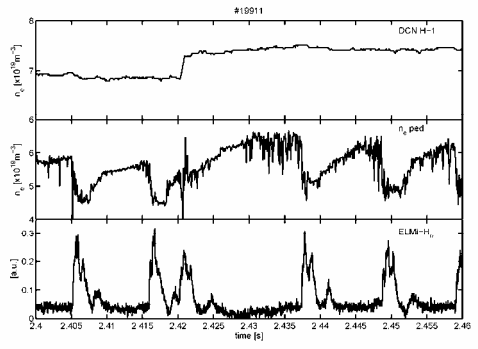

Figure 4.7 – Time traces of: (a) line average density from interferometry (DCN H-1); (b) pedestal heigth from reflectometry (ne-ped); (c) H_α radiation (ELM-H_α).

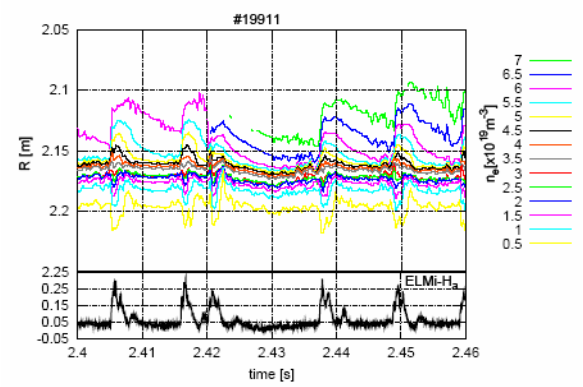

Figure 4.8 – Density contour plots showing the time evolution of the edge density profile at the LFS. The bottom plot depicts the time trace of Hα radiation (ELM-Hα).

The high SOL density is maintained during the ELM, but is back to pre-ELMs values immediately after the end of the period of enhanced D_α light emission. This corresponds to a low confinement expected for the SOL and the higher density can only be maintained by the strong influx of particles to the SOL from the core during the ELM. The density in the pedestal also collapses very quickly, within 100 μs time scale, but recovers more slowly to the pre-ELM values taking ~ 10-20 ms, which is approximately the ELM repetition time. This means that the confinement in the pedestal is good between ELMs, allowing the profiles to recover, but poor during the ELMs. This is consistent with the expected picture of the density evolution in the pedestal and SOL regions during the ELM cycle.

4.2.7. Localization of TAE modes

The new hopping reflectometer has the capability of probing several density cutoff layers (in the Q and V

bands at LFS) during each discharge. The position of density layers is determined using ne profiles from the broadband FM-CW reflectometry system.

First results (Figure 4.9) show that in TAE experiments (AUG shot #20489), with low density ($\bar{n}_e = 3.25 \times 10^{19}\, m^{-3}$), 5 MW of ICRH power and L-mode, the "hopping frequency system" allows the radial localization of modes at the edge as well as TAEs and sawteeth precursor in the core (ρpol = 0.6-0.35) clearly separated from the edge. These results are important to study the radial structure of TAEs modes.

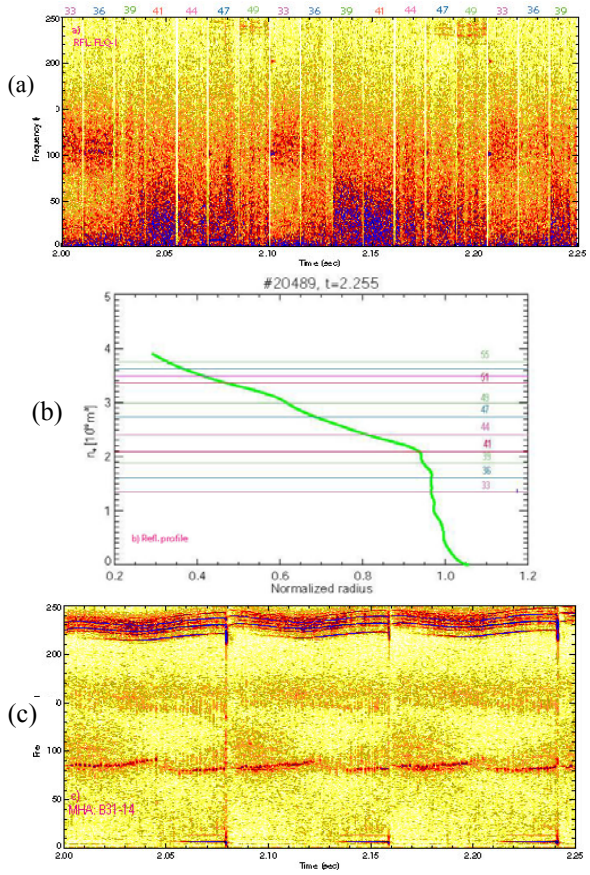

Figure 4.9 - Spectrogram of Q band "hopping frequency millimeter wave reflectometer" for TAE shot #20489 (a), the corresponding density profile from reflectometry for the localization of the density cutoff layers (b) and spectrogram from magnetics (c).

4.3. STUDIES ON MHD, TURBULENCE AND TRANSPORT

4.3.1. Introduction

This research line included in 2005 code development for turbulence and transport analysis in the SOL of ASDEX-Upgrade.

4.3.2. Code development for turbulence and transport analysis in the SOL of ASDEX Upgrade

The boundary of tokamak plasmas is characterised by electromagnetic interactions between wavelike and fluidlike motions on space scales down to the ion gyroradius. The two moment gyrofluid flux tube model GEM3 was used to investigate electromagnetic turbulence and the associated transport phenomena both in the edge and scrape-off layer (SOL) of such region of the plasma.
The comparative study between edge and SOL conditions was concluded . The main results include the observation of the dominance of a convective cell mode ($k_\perp \neq 0$ and $k_\parallel = 0$) whenever the limiter was included, i.e., whenever the SOL boundary conditions were applied, in accordance with the experimental observations for the SOL region. The turbulent transport values were also found to increase in the latter situation, where the large scale interchange dynamics became dominant, due to the absence of the adiabatic response of the electrons in the convective cell mode. Conversely, with closed field lines boundary conditions, the field line connection of tokamak sheared magnetic fields suppresses the convective cell mode, when the flux surfaces are closed, leaving the drift wave character typical of the plasma edge, with the parallel electron dynamics keeping the electrostatic potential coupled to the electron pressure through parallel forces mediated by parallel currents.

The study of the effect of the equilibrium magnetic field geometry of a tokamak (ASDEX Upgrade with diverted geometry) was continued, including the investigation of the issue of the spatial resolution of the simulations. This also included verifications made within the geometry code METRICS to check the consistency of the coordinates transformations made, and also the implementation of a Savitzky-Golay smoothing filter, constituting an improvement of the filtering that is necessary to apply to the curvature operators in the case of grids coming from the CARRE code.

The results for closed flux surfaces regions showed a well spatially resolved system, even at the locations along the field lines where the grid cells are most severely deformed, due to the variations of the perpendicular (contravariant) metric components of the metric (Figure 4.10). When compared to the corresponding results obtained with the simplified geometry model (Figure 4.11), which retained only the poloidal dependence of the curvature operators, they revealed a reduction of the measured E × B turbulent transport, which brought the figures closer to experimentally measured values. This result supports the scenario whereby the local magnetic shear, that affects directly the polarisation dynamics (the main mechanism behind a fluid drift model) and is particularly strong close to the magnetic separatrix (Figure 4.11–left), facilitates the nonlinear decorrelation processes by twisting the turbulent perpendicular vortical structures, which are then torn apart to smaller scales.

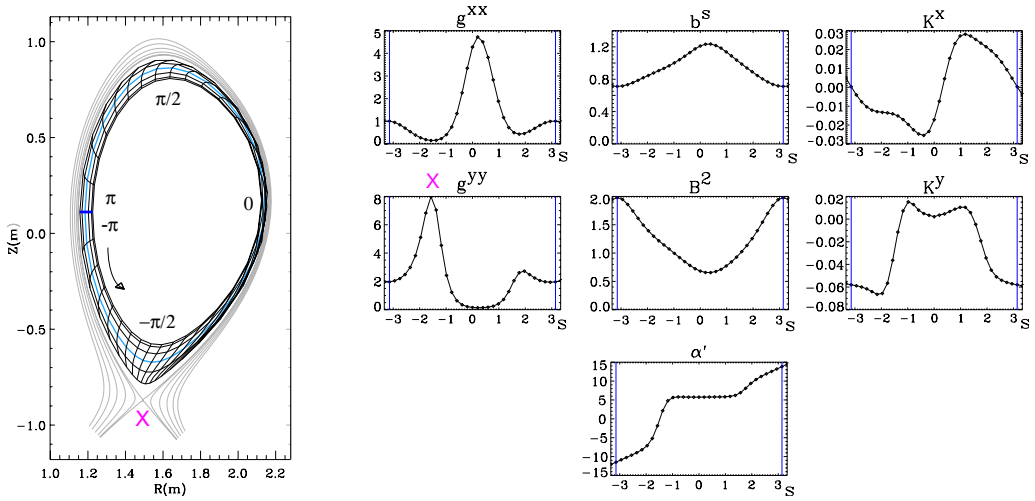

Figure 4.10 - (left) Representation of the ASDEX Upgrade diverted equilibrium magnetic field used herein; (right) 7 geometrical quantities necessary describing the equilibrium on the left side figure, which are needed to be provided to GEM or GEM3 models. The curves were calculated for the flux surface highlighted in blue on the left side figure.

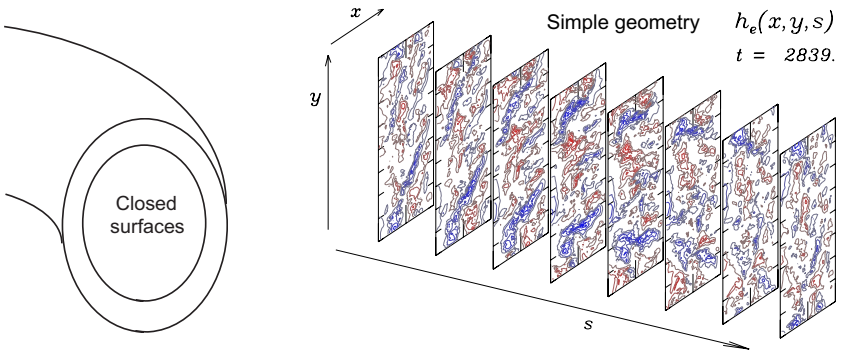

Figure 4.11 - 3D spatial morphology of the nonadiabatic electron density "he=ne-ϕ" (ne is the electron density and ϕ is the electrostatic potential) in the computational domain for closed flux surfaces (edge), using the simplified model for the tokamak geometry. Negative values are represented in blue and positive in red.

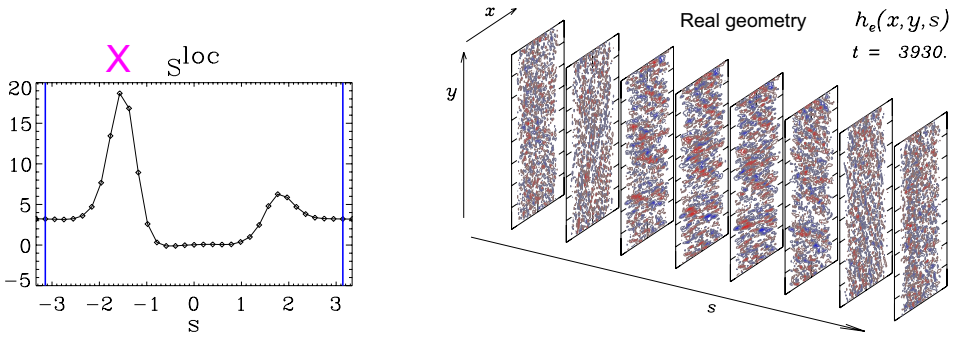

Figure 4.12 - (left) Local shear along a magnetic field line, a quantity which is absent in the simplified geometry model used for figure 2; (right) The same as in figure 2, but using the realistic description of the tokamak (figure 4.10). Note the relation between the maxima of the local shear and the twisting of the vortical structures in the plane perpendicular to the magnetic field. Compare with figure 2, where bigger perpendicular structures are present.

5. PARTICIPATION IN THE ITER PROJECT

C.A.F. Varandas (Head), M.E. Manso (Deputy Head), J.P. Bizarro, J. Belo, L. Cupido, H. Fernandes, A. Ferreira, J. Santos, F. Serra, P. Varela

5.1. INTRODUCTION

This project included in 2005 activities in the following areas:

- Microwave reflectometry;
- Control and data acquisition;
- Non-inductive current drive;
- Information.

5.2. MICROWAVE REFLECTOMETRY

5.2.1. Main activities

The activities on microwave reflectometry have been related with the design analysis of the position reflectometer, development of an advanced FM-CW coherent reflectometer and experimental demonstration studies on ASDEX-Upgrade of plasma position/shape measurements in ITER relevant scenarios.

Concerning the design analysis of *the position reflectometer*, the Association EURATOM/IST has led a Physics Integration Task of the Fusion Technology Programme (TW3-TPDSUP) and is now in charge of a new Task (TW5-TPDS-DIARFA) entitled "Experimental assessment of ITER HFS waveguides".

Regarding the development of a prototype of *a coherent reflectometer*, the frequency synthesizer has been completed.

Concerning *plasma position/shape measurements*, a data base has been built to support a neural network approach towards real time density profile evaluation and first results were obtained.

5.2.2. Coherent reflectometer

The frequency synthesizer, the most complex and extensive part of the coherent reflectometer, was developed during 2005 (Figure 5.1). Both PLL and FPGA frequency control boards were tested and VHDL plus the microcontroller software was developed and fully tested. By the end of 2005 a fully operational hop/fast-hop/sweep synthesizer was fully tested and proven to work within the thigh timing requirements. Only minor software adjustments remain to be done to conclude this block. The remaining part of the coherent reflectometer system will be developed during 2006.

5.2.3 Plasma position reflectometer

5.2.3.1. In-vessel waveguide routing

The design of the in-vessel waveguide routings for gaps 3, 4, 5, and 6 modelled using CATIA was carried out. The routings for gaps 4, 5, and 6 are completed up to the port flange and await definition of the vacuum interface. The corresponding 3D CATIA models were sent to the ITER IT for validation and integration. As an example, the routing for gap 4 is shown in Figure 5.2.

Figure 5.1 – Prototype of the Frequency Synthesizer for Coherent Reflectometers

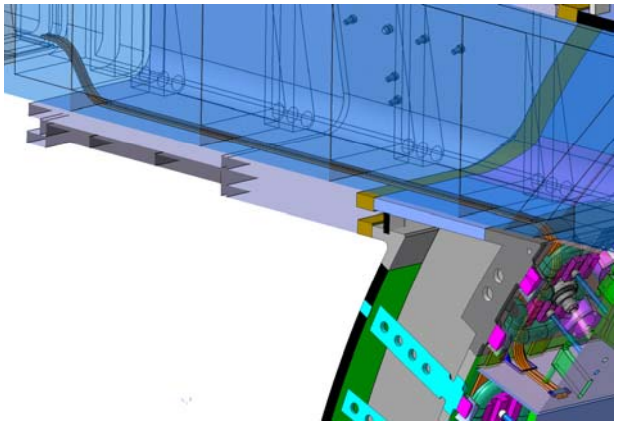

Figure 5.2 – Waveguide routing for gap 4, located between blanket modules 11 and 12. The waveguides are depicted in orange. The antenna and support structure can also be seen.

5.2.3.2. Waveguide electromagnetic performance[1]

In order to evaluate the electromagnetic performance of the waveguides, critical sections of the routing were simulated using the HFSS code. Both a straight section of waveguide and the most demanding bend were simulated. Because such complex waveguide chains will use joints/flanges, simulations contemplate also the assessment of the sensitivity to misalignments.

Numerical results indicate that straight sections of waveguide propagating the TE_{01} mode are essentially loss free except for resistive wall losses.

Figure 5.3 shows that no mode conversions are observed in the frequency range 15 – 60 GHz.

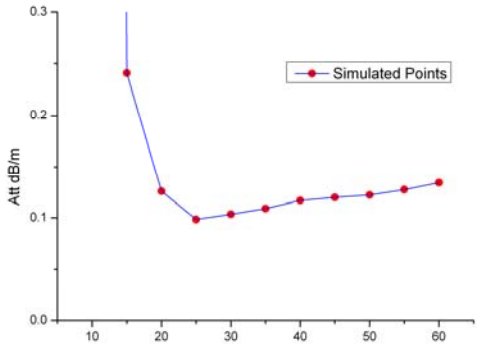

Figure 5.3 – Evolution of the transmission losses of a straight section of waveguide propagating the TE01 mode in the frequency range 15 – 60 GHz.

Curved sections of oversized waveguides may be more problematic as with mode conversion transmission losses increases which in the end may also modify the antenna pattern. Cross polarization can also occur as an effect of mode conversion.

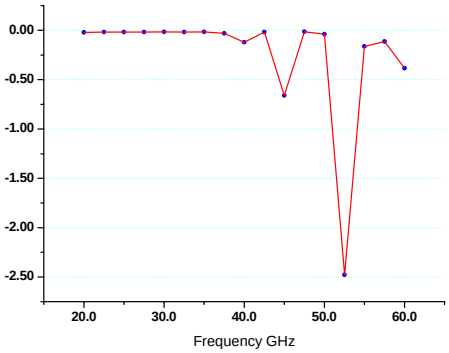

Figure 5.4 – Transmission losses for the most critical bend (gap 6). Simulation uncertainty is below $\pm$ 0.1 dB at 40 GHz and $\pm$ 0.5 dB at 60 GHz.

The above results show that transmission is essentially resonance free up to 40 GHz. Above this frequency the system performance can be reduced or even disable operation.

A straight section of waveguide was also used to investigate the sensitivity to misalignments in both E and H directions. As depicted in Figure 5.5, the waveguides are moderately sensitive to misalignments both in the E and H directions. However, the tolerance/precision requirements are within the maximum misalignment obtained with normal pin-aligned flanges.

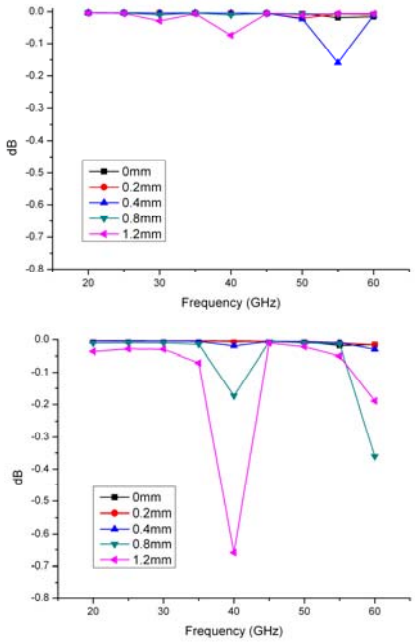

Figure 5.5 – Transmission losses due to misalignments along the E direction (upper) and H direction (lower) in comparison with a reference straight section.

[1] With contributions from Dr. Dietmar Wagner (EURATOM/IPP Association – IPP, Germany) and Dr. Burkhard Plaum (IPF Stuttgart, Germany).

5.2.3.3. Thermal analysis

The antennas of the plasma-position reflectometer for ITER will be located between two blanket modules (for gaps 4, 5, and 6) and directly exposed to the plasma, thus being submitted to both nuclear heating and plasma radiation heating. Two major types of heat loads were considered in the simulations: plasma radiation and nuclear heating.

The results (Figures 5.6 and 5.7) show that the initial reference materials (copper and stainless steel) are not adequate to endure the predicted heat load.

The modified geometry made very clear the importance of adequate dimensioning and positioning of the support plates. With the introduction of another support and by using thicker plates the convergence temperature was strongly reduced, as more heat is conducted to the upper blanket, keeping the front section of the antenna at lower temperatures. Also, positioning the first support closer to the antenna front section (although exposing it to a higher nuclear load), prevents the accumulation of heat. Another important improvement is that the back support remains at a lower temperature. Although this setup allows the use of copper and stainless steel, a combination of a tungsten (or molybdenum) antenna and two thicker support plates, carefully positioned along the antenna body, would be a better solution.

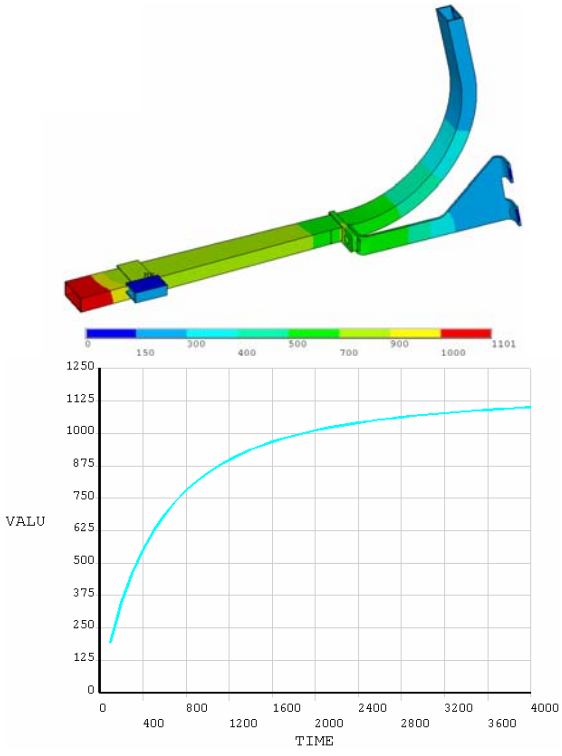

Figure 5.6 - Temperature distribution on the antenna plus waveguide structure after 4000 s.

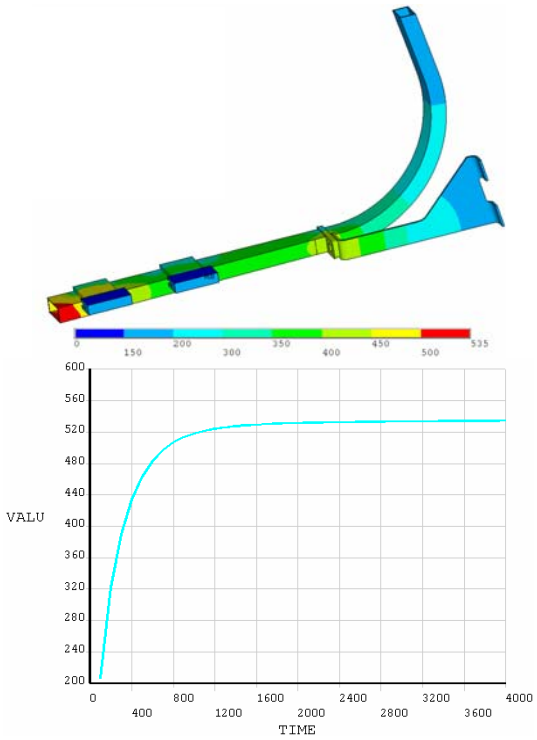

Figure 5.7 - Temperature distribution after 4000 s.

5.2.4. Plasma position/shape measurements in ITER relevant scenarios

To demonstrate real time profile evaluation a neural network based approach is being pursued; preliminary studies using experimental data from ASDEX Upgrade gave promising results[2].

An extensive density profile database for H-mode discharges was built, based on O-mode reflectometry data obtained in ASDEX Upgrade. This data base allows a statistical evaluation of the performance of the real-time profile inversion method. The application of the neural approach applied to those plasma scenarios proved to be quite robust to the effects that may decrease profile accuracy, namely plasma turbulence. It was also found that the method is not very sensitive to the lack of density profile data below $n_e=3.6x10^{18}$ m^{-3}, which cannot be obtained with O-mode probing. This is illustrated in Figure 5.8 where the performance of a trained neural network is compared with the results from the application of the traditional Abel inversion. In the case of the Abel inversion three different methods of initializing the density profile were used: (i) the initial assumed density profile; (ii) a curve obtained with a dynamic procedure and (iii) a linear extrapolation down to zero frequency.

The observed robustness is expected to provide a relief on the requirements and sophistication of the procedures

[2] Details in chapter IV.

for group delay evaluation, allowing the use of more real-time friendly signal processing techniques.

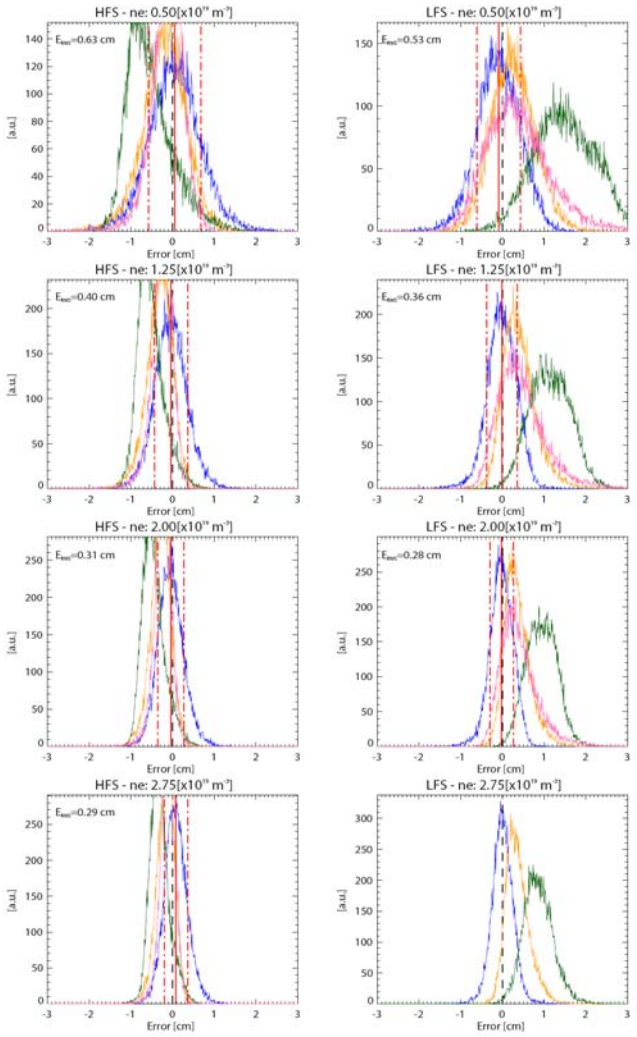

Figure 5.8 – Statistical distributions of position errors at four plasma density layers (ne=0.5, 1.25, 2.0 and 2.75x1019 m-3) corresponding to the inversion of a set of 17952 density profiles (affected by a density fluctuation level of 5% ne_sep). The output of the neural network is represented in blue. Shown also are: (i) the result of applying the standard Abel inversion to the probed group delay initialized with the assumed density profile (in orange); (ii) with a dynamical initialization (in magenta) and with a linear initialization (in green).

5.3. CONTROL AND DATA ACQUISITION

IST has started a formal collaboration with the ITER team on control and data acquisition. A senior researcher participated in Garching in a meeting for the definition of the working programme in this area.

5.4. NON-INDUCTIVE CURRENT DRIVE

5.4.1. Introduction

IST was envolved in 2005 in the design of ITER-like PAM lower hybrid current drive (LHCD) antennas[3]

5.4.2. ITER-like PAM LHCD antennas

5.4.2.1. Collaboration on the design of ITER-like PAM LHCD antennas

In response to a call from the EFDA Associate Leader for JET concerning the upgrade activities of its LHCD system, a project was set-up to design a new launcher based on the PAM (Passive Active Multijunction) principle, with CEA-Cadarache as the Leader Association. The first preliminary studies for this new LH launcher were carried out (in collaboration with CEA-Cadarache) mainly with regard to its coupling and directivity properties as a function of the electron density (above the cut off) — diverse studies being performed by the other intervening Associations — and were focused on the two most basic multi-junction shapes: the tri-junction and the bi-junction, together with the corresponding sets of internal phase shifters. The former was designed to launch a spectrum with the main peak located at $N//_0$=2.027

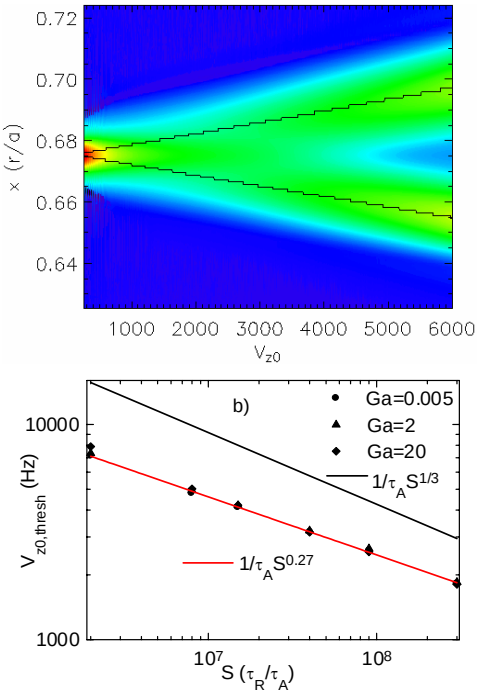

Figure 5.9 – Contour of the toroidal braking force exerted by static m=2,n=1 external magnetic fields on a rigid rotating plasma. Vertical axis indicates the radial direction and the plasma rotation lies on the x-axis (a). Rotation threshold for the transition between both regimes of reconnection (b).

[3] Work carried out in collaboration with the Association Euratom/CEA. Contact Person: Alain Becoulet.

whereas for the latter $N//_0$=1.9 was chosen instead. Passive waveguides with various depths (λ/8, λ/4, 3λ/8 and λ/2), including most of their combinations, were investigated for both designs and for every situation various feeding phases were tested as well. With the adoption of the bi-junction based antenna, an important study was carried out to allow for the largest injected power compatible with other constrains. This led to a launcher design having 20 mm wide active waveguides and with the passive ones reduced to an 8mm width, as the one being proposed for implementation, due to its coupling endowments as well as to the potential to reach an injected power somewhat in excess of 5 MW (at a 25 MW/m^2 power density). These studies were included in the final report of the entire project.

This year saw also the start of a thorough study (also in collaboration with CEA-Cadarache) of the coupling features of Tore Supra's LH antenna known as C3, for which the properties of the full launcher (in what its coupling to the plasma is concerned) will be modelled and the ensuing theoretical results compared to the corresponding experimental measurements. It is the first time that a study of this magnitude, i.e. including the full waveguide array of the entire launcher, is undertaken for the C3 (with its 288 waveguides divided in 16 modules). The ultimate goal, though, is to characterise the behaviour of LH launchers in general when they face the plasma and, in particular, that of the new PAM (Passive Active Multijunction) antenna under construction for Tore Supra, thus creating important tools for the analysis of experiments.

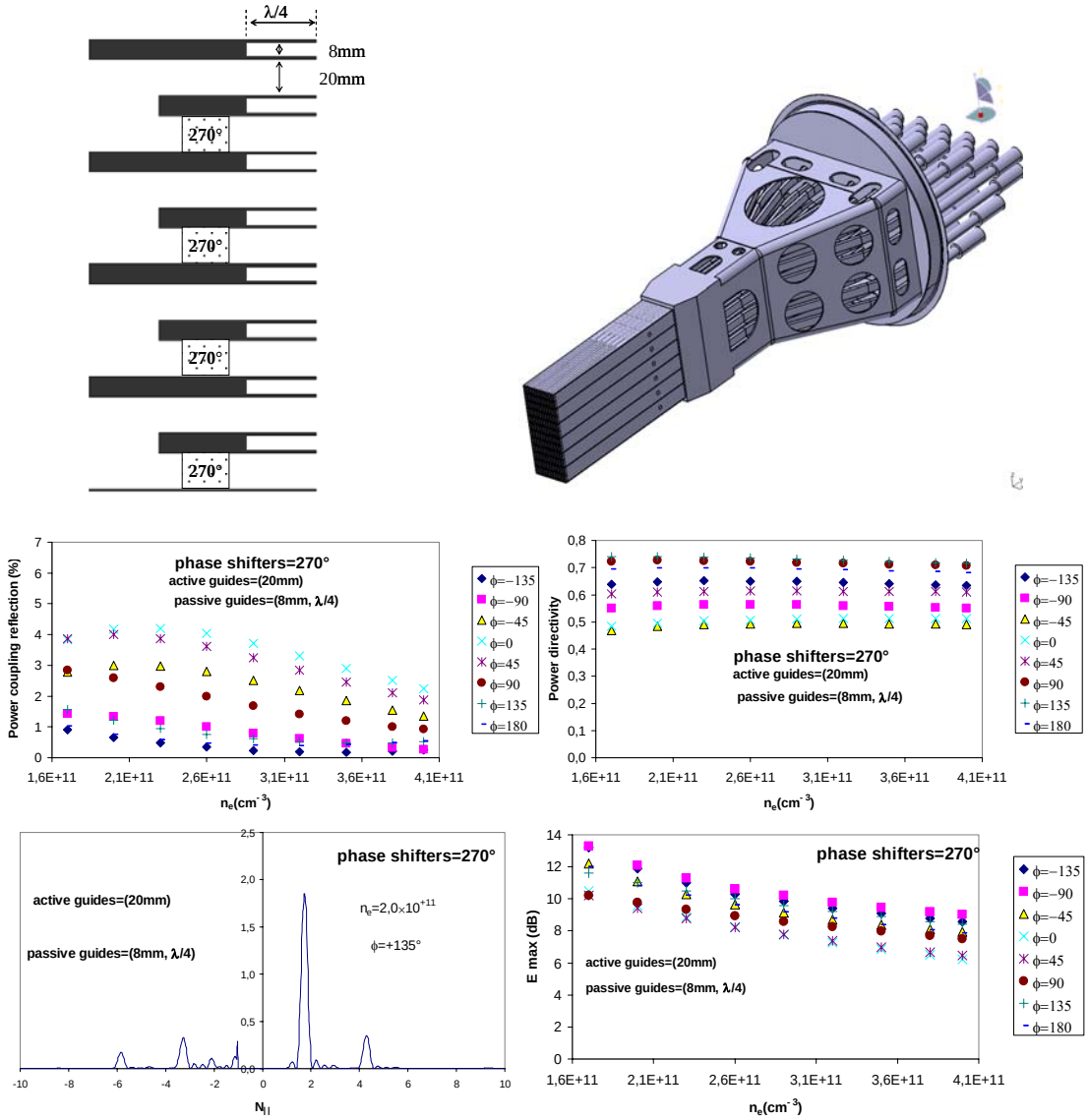

Figure 5.10 – View of the PAM LHCD launcher designed for JET, and analysis of its coupling capabilities.

5.5. INFORMATION

IST has proceeded with the divulgation of the ITER project to the general public, industry and research units. The following actions were performed in 2005:

- Participation in the Fusion-Industry Workshop, held in Madrid, in 1 and 2 June. Prof. Carlos Varandas was the Co-chair of the working group on Industrial Policy Issues;
- Publication of articles in the main Portuguese newspapers and participation in television programmes about ITER;
- Organization of a Workshop in 24 November, at IST, for the divulgation of the ITER project to the Portuguese Industry and Research Units. This Workshop had about 114 participants;
- Participation in the workshop “ITER: Opportunities for European Industry”, held in 13-14 December, in Barcelona, with a stand and 500 participants.

6. PARTICIPATION IN THE TJ-II PROGRAMME[1]

C. Varandas (Head), M. Manso (Deputy Head), A. Silva, C. Silva, I. Nedzelskij, L. Cupido, L. Pereira, Y. Tashchev.

6.1. INTRODUCTION

The Portuguese participation in the TJ-II programme has been mainly focused in three research areas:

- Microwave reflectometry;
- Electrode biasing experiments;
- Heavy ion beam diagnostic.

6.2. MICROWAVE REFLECTOMETRY[2]

CFN has developed in 2004 a *fast frequency hopping reflectometer*, operating in the Q-band (33-50 GHz), with wave propagation in X-mode. It can be tuned to any selected frequency, within a fraction of a ms, enabling to probe several plasma layers within a short time interval. This gives the possibility to study important characteristics of radial distribution of plasma turbulence. First results have been obtained in 2005 showing the formation of a velocity shear layer above a certain critical density and demonstrating the good spatial resolution of the reflectometry measurements. In view of the good results obtained with the diagnostic, a new system is being developed to study correlation properties of plasma turbulence. It uses basically the same design of the previous hopping system. The final design has been assessed and the procurement has been initiated.

6.3. ELECTRODE BIASING EXPERIMENTS[3]

Following earlier investigations on the effect of electrode bias on the TJ-II boundary plasma, a detailed comparison between *positive and negative bias at densities above the threshold value to trigger the spontaneous development of ExB sheared flows* has been performed. We found that at high densities negative voltages are easier to impose when compared with positive ones as the forced plasma rotation is in the same direction of the natural rotation. Figure 5.1 shows the time evolution of the main plasma parameters for discharge with negative bias. As the bias is applied, a strong reduction in the H_α emission is observed associated with an increase in the density up to the ECRH cut-off frequency. A stronger reduction of recycling is observed for negative bias, when compared with that observed for positive bias at similar plasma density, resulting therefore in a larger increase in the ratio $\bar{n}/H_\alpha$ (~70%). These results are in agreement with observation in other devices where improvement in particle confinement is in general observed for both polarities, being larger with negative bias.

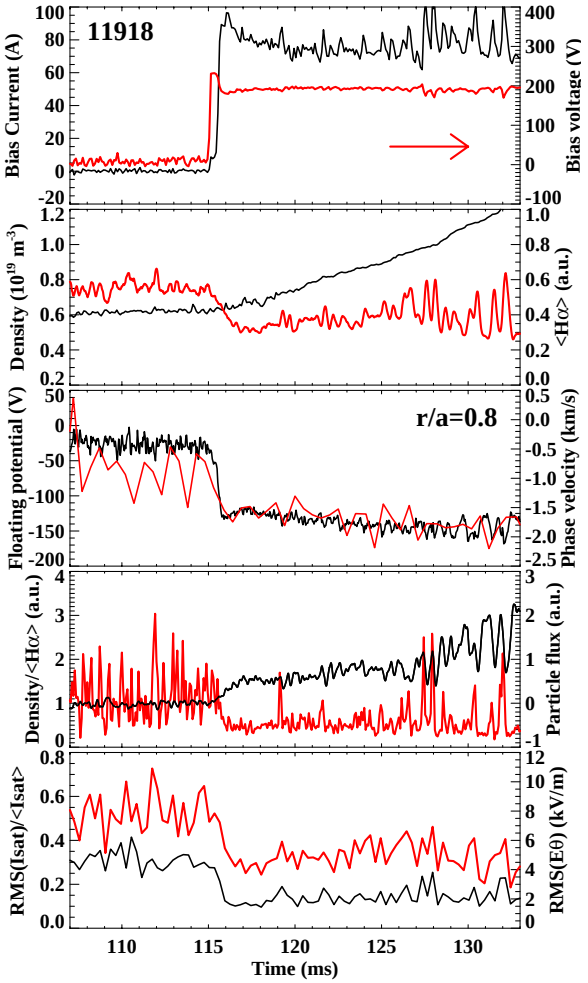

Figure 6.1 – Time evolution of the main plasma parameters for a discharge with negative electrode bias (V_{bias}=200V, $r_{elec}/a \approx 0.9$) at high density.

6.4. HEAVY ION BEAM DIAGNOSTIC[3]

6.4.1. Introduction

This research line included in 2005 the improvement of the multiple cell array detector (MCAD), the revision of the conditioning electronics, the development and testing of a new control and data acquisition system and the beginning of the diagnostic operation.

The revision of the *multiple cell array detector* was finished, including repair of the damaged contacts and cells, duplication of the contacts of the working cells and insulation of the MCAD housing and biasing grids from

[1] Work carried out in collaboration with the Association EURATOM/Ciemat. Contact Person: J. Sanchez
[2] Contact Person: J. Sanchez
[3] Contact Person: C. Hidalgo

the TJ-II vacuum vessel. The cells have been modified and improved by insertion of tantalum "wire-balls" into Faraday cup matrix.

Concerning the *conditioning electronics* eight preamplifiers and amplifiers have been repaired and tested. The preamplifier-connector part has been modified and included in a single box, aiming at decreasing the cable lengths and, therefore, the noise.

A 24-channel *control and data acquisition system* has been developed, tested and pushed into operation.

Regarding the *diagnostic operation*, the fist experimental campaigns have permitted clear observations of the primary ions at energies of 80 keV, 90 keV and 100 keV.

6.4.2. Control and data acquisition system

6.4.2.1. System Overview

The new dedicated control and data acquisition system for the multiple cell array detector of the TJ-II heavy ion beam diagnostic (HIBD) is based on in-house designed VME modules and Linux.

The hardware consists of: (i) a VME host running Linux; (ii) four CFN transient recorder boards; (iii) an analogue output board; and (iv) a commercial 32 bit TTL I/O M-Module mezzanine.

The software for the active control of the primary and secondary beam lines has two major components: (i) a server daemon running on the VME host, receiving operation parameters and waveforms to be programmed and controlling board operation; (ii) client applications with graphical user interfaces running on the control room PC's.

The software for the MCAD acquisition system consists of a daemon controlling acquisition and writing data to the TJ-II database and a graphical application allowing easy configuration of acquisition parameters.

6.4.2.2. Multiple cell array detector

Currently 32 channels are installed, provided by four in-house designed transient recorder modules (VME8i125). Each VME8i125 transient recorder module has 8 channels with 12 bits resolution, 512 kSamples per channel of inboard memory and a sampling rate up to 1.25 MSPS. The end of acquisition signal is defined by a commercial 32 TTL I/O M-Module mezzanine, since the VME8i125 does not provide this information.

The software of the MCAD data acquisition system has two major components (Figure 6.2): a daemon that runs on the VME host and a graphical application that is used to configure all acquisition parameters. The configuration application can be run in any computer (inside or outside the control room). The MCAD daemon: (i) reads the transient recorder module configuration (produced by the MCAD configuration editor application); (ii) programs and arms the transient recorder modules with the configuration provided by the user; and (iii) reads the acquired data from the board memory and writes it (along with configuration parameters) to the TJ-II database.

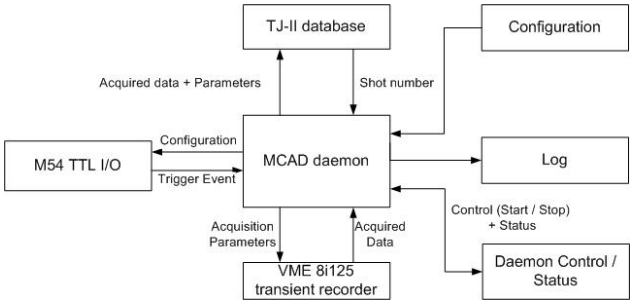

Figure 6.2 - Block diagram of the software of the MCAD data acquisition system

6.4.2.3. Active beam control

The active beam control software has two major components (Figure 6.3): a server daemon that receives the board configuration and waveforms and a pair of clients with graphical user interfaces. Both clients allow the user to configure the trigger type (external or internal), the update rate and the waveform. The main difference between the two clients is the way how the waveform is selected: one client has a set of predefined waveforms (sinus, triangular, sawtooth, and constant) and the other allows the user to interactively design a waveform with the mouse.

The link between the clients and the server is achieved with an Ethernet connection. The communication is done using a custom protocol over TCP/IP. The daemon only accepts connections from specific computers in the control room. Additionally, at a given moment only one client is allowed to be connected to the server. To prevent the possibility of the VME8O board being loaded with garbage (due to waveform data corruption in the network transmission) all the waveform data passes through a software limiter in order to maintain the high voltage power supply within a safe voltage range.

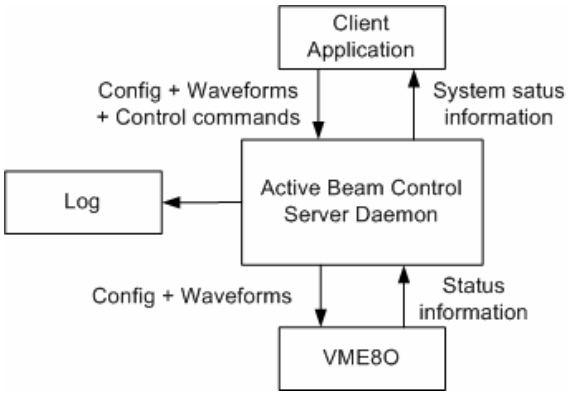

Figure 6.3 - Block diagram of the software for active beam control

7. PARTICIPATION IN THE TCV PROGRAMME

C. Varandas (Head), A.P. Rodrigues P. Amorim, L.A. Pereira, T.I. Madeira

7.1. INTRODUCTION

This project had in 2005 two research lines:

- X-ray diagnostics
- Advanced plasma control system (APCS)

7.2. X-RAY DIAGNOSTICS

7.2.1. Introduction

This research line included in 2005 activities related with:

- The operation and scientific exploitation of the horizontal pulse height analysis (PHA) diagnostic;
- The commissioning, testing and implementation on TCV of the vertical PHA diagnostic;
- The transformation of the vertical PHA diagnostic into a real-time system;
- The commissioning and testing of the rotating crystal spectrometer.

7.2.2. Analysis of the data from the horizontal PHA diagnostic

Since its commissioning, the horizontal PHA diagnostic has provided data which has contributed to many experimental studies particularly in the fields of impurity injection aided particle confinement and plasma heating scenarios: mild (Figure 7.1) to strong (Figure 7.2) deviations of the electron populations from a thermal distribution when additional heating is applied have been observed, and impurities resulting from the erosion of the plasma vessel walls during ECRH have been identified (Figure 7.3). The impurity identification is straightforward as long as the system calibration is known, but to determine the electron temperature, some situations have been treated by employing a single maxwellian fit (Figure 7.4), others are addressed by a bi-maxwellian model (Figure 7.1) in cases of strong non-Maxwellian behavior (Figure 7.2) the approximation of a Maxwellian distribution no longer holds and leads to erroneous results without physical meaning as there is no longer a correspondence between the observed photon energy and the electron energy. A qualitative interpretation of the experimental results is being investigated.

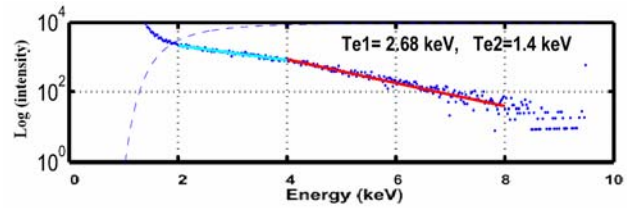

Figure - 7.1 - Example of mild non-maxwellian behavior observed during ECRH

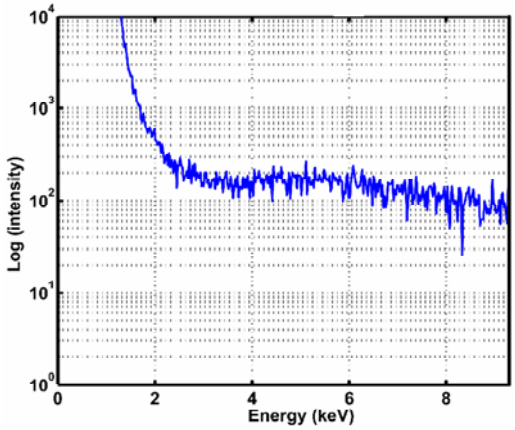

Figure 7.2 - Example of strong non-maxwellian behavior observed during ECRH

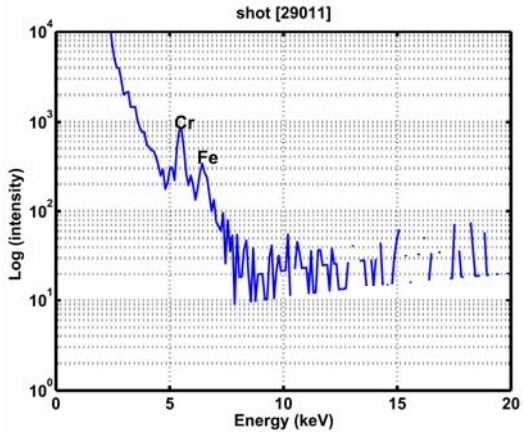

Figure 7.3 - Impurities resulting from erosion of the plasma vessel walls during ECRH.

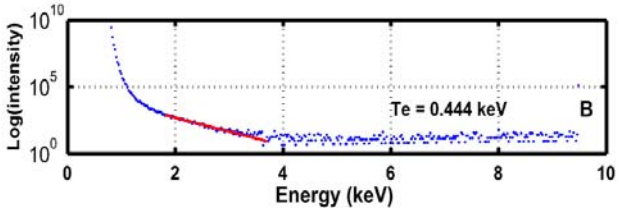

Figure 7.4 - Electron temperature measurement using single Maxwellian fit

7.2.3 Vertical PHA diagnostic

The vertical PHA diagnostic is a modern upgrade of the "classical" horizontal PHA system that has been designed aiming at demonstrating an extremely low *étendue* X-ray

spectral measurement of a hot plasma with a regulated flux permitting real-time measurements of plasma parameters for a wide range of plasma conditions and real-time diagnostic feedback control.

This diagnostic comprises a compact Silicon Drifted Detector (SDD) Peltier cooled diode and two independent systems for signal conditioning and processing: a commercial multiple-frame multichannel analyser (MCA3) with post acquisition analysis and a CFN designed VME hosted DSP card which will provide real-time analysis of the X-ray emission. Both system are designed to remote actuate the stepper motors whilst simultaneously regulating the system *étendue* to maintain an optimal throughput during a single discharge: the analogue system employs an integrator (sensor) together with a comparator that when the throughput limits are surpassed, gives out a signal that actuates the motors and change the position of the aperture. For the DSP system the pre-amplifier pulses are fed into a subsystem with a DAC that supplies the appropriate voltage to actuate the stepper motor. With a regulated input rate, a spectrum, with spectroscopic quality, may be obtained every 100 ms during a 2 s TCV discharge.

Measurements of the central electron temperature have already been obtained with the MCA3 card for some TCV operation regimes (Figures 7.5), with an average throughput of 300 kHz. The DSP algorithms employed to make the histogram and calculate the electron temperature are still being essayed for performance during TCV operation. A set of beryllium filters of 50, 100 and 150 μm are also employed to reduce the dominant lower energy X-ray photon rate and a low power ^{55}Fe source occupies one of the filter holder positions and can be used to diagnose and calibrate the system *in situ*.

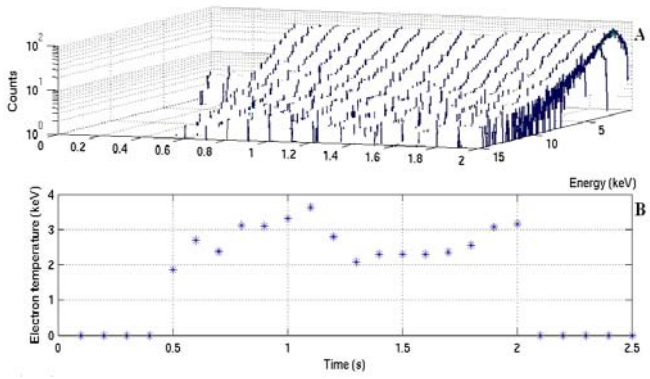

Figure 7.5 - Results obtained with the MCA3. (A) soft x-ray spectrum and (B) Electron temperature, temporal evolution.

7.2.4. Real-time diagnostic

The research and theoretical development of the histograms construction algorithms were carried out. These algorithms, that give real-time results, were implemented using C language and the specific DSP Assembler. The debug and optimization were initially done using a simulation setup with data from the old PHA diagnostic and later with real-time data from the detector system in shot conditions. The synchronization of these algorithms with those that make the data acquisition and the electron temperature calculation has been also tested.

The DSPs system in the TCV control was integrated with the data acquisition system and the detector system was connected with the DSPs module. The TCV trigger and timing system was also connected to the DSP module in order to get external synchronized triggers. These timing signals were programmed in the TCV main database and used to synchronize the real-time electron temperature calculation with the shot of the TCV.

Implementation and test of the VME host CPU software were done. This software configures the DSPs module, gets the histograms and the electron temperature values, calculated during the shot.

The control of the count rate in real-time is absolutely necessary in order to avoid saturation of the acquisition system and to maintain a minimum count rate that gives a minimum statistical error that enables the calculation of the electron temperature of the plasma in real-time. To overcome this need the development and implementation of the diaphragm real-time control algorithm which controls the X-ray count rate were done. The control algorithm must yet be tested in good shot conditions. This task should be concluded during 2006 when the shots of TCV will be stable. Then, the real-time electron temperature calculation can be achieved.

7.2.5. Rotating Crystal Spectrometer

All parts of the diagnostic (the new microchannel plates, new pre-amplifiers and master/slave unit that actuates the stepper motor) have been assembled. The tests to the hardware have been initiated. First essays have shown that the pre-amplifiers were not working properly, their design had to be revised but every new adaptation did not succeed so far. The design of the holding structure at the horizontal port has started but had to be interrupted because the port was attributed to another device. No decisions have been taken so far in what concerns the new localization of the diagnostic.

7.3. ADVANCED PLASMA CONTROL SYSTEM

After some preliminary tests, the main objective of the 2005 activity in this Project was the decrease of the control cycle. Aiming at having a transfer time in the DMBUS less then 10 μs, the control programming logic device (CPLD) that controls the DMBUS was replaced by a faster version. This change has originated the need of the reprogramming of the CPLD with another software tool and a different language.

In parallel, a support library, a set of utilities and test scripts have been developed.

8. OTHER THEORY AND MODELLING STUDIES

F. Serra (Head), J.P. Bizarro (Deputy Head), R.Coelho, J. Ferreira, F. Nave, P. Rodrigues.

8.1. INTRODUCTION

This project included in 2004 three research lines:

- Study of the role of magnetic reconnection processes in the dynamics and confinement of thermonuclear plasmas;
- Modelling of Grad-Shafranov equilibria in tokamak plasmas.

8.2. ROLE OF MAGNETIC RECONNECTION PROCESSES IN THE DYNAMICS AND CONFINEMENT OF THERMONUCLEAR PLASMAS

8.2.1. Introduction

This research line included in 2005 studies on:

- The effect of sheared toroidal rotation on the stability of tearing modes;
- Error field driven reconnection.

8.2.2. Effect of sheared toroidal rotation on the stability of tearing modes

Magnetic reconnection events can degrade plasma confinement and limit fusion plasma performance. The physics of free reconnection, leading to the formation of magnetic island chains localised where the safety factor q(r) is rational, i.e. q=m/n, is a complex problem depending on many plasma figures of merit (collisionality, β_p) and profiles (pressure, current density). For plasmas discharges with significant Neutral Beam Injection (NBI), toroidal rotation could have a strong effect on tearing mode stability. In fact, in a scenario with sheared toroidal plasma rotation, the toroidal component of plasma velocity perturbations (negligible in static plasmas) is no longer expected to be negligible and should be taken into account for inferring mode stability even in a large aspect ratio machine.

Linear numerical MHD simulations in a cylindrical geometry with both perpendicular and parallel (to the equilibrium magnetic field) perturbations allow to conclude that plasma rotation in the equivalent toroidal direction can result both on the increase or decrease of the instability growth rate. A parabolic-like profile is considered for the toroidal rotation, vanishing at the plasma edge. Simulations were performed both for the single helicity model (that considers both parallel and perpendicular perturbations) and the conventional reduced MHD model (neglects parallel components of the perturbed quantities). Anomalous perpendicular plasma viscosity and plasma rotation shear at the modes' rational surface play a key role on assessing the effect of shear flow.

While destabilising for low viscosity plasmas (ratio of the resistive to viscous diffusion time scales $\tau_R/\tau_V<<1$) (Figure 8.1a), for viscous plasmas ($\tau_R/\tau_V>1$) shear flow reduces the growth rate, making possible mode stabilisation above a given rotation frequency (Figure 8.1b). Mode stabilisation is feasible owing to the considerable effect of the parallel component of the plasma velocity perturbations.

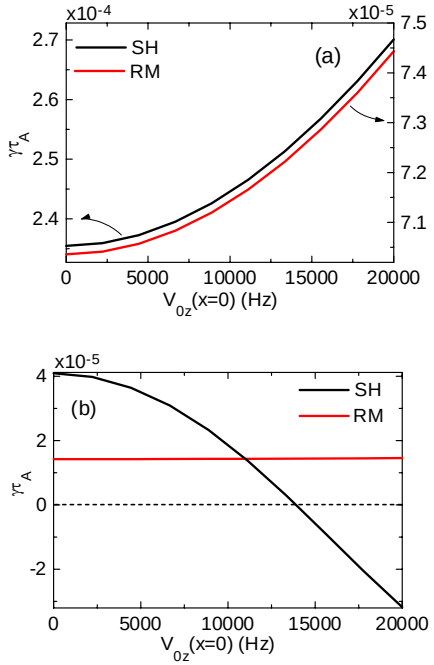

Figure 8.1 – Sheared toroidal plasma rotation is destabilising in low-viscous plasmas for both the single helicity and reduced MHD models (a) and stabilising in viscous plasmas (b).

When extrapolating to more reactor relevant operational conditions (higher Reynolds number $S=\tau_R/\tau_A$), one also notices that above a given threshold in the rotation shear (that decreases with increasing τ_R/τ_V) a tearing mode, unstable in the absence of rotation, can be stabilised (Figure 8.2). In addition, for the same ratio τ_R/τ_V, plasma rotation necessary for mode stabilisation decreases with increasing magnetic Reynolds number.

8.2.3. Error field driven reconnection studies

The penetration and amplification of static external magnetic fields on rotating magnetically confined fusion plasmas imposes serious limitations on the plasma performance, degrading confinement and potentially leading to some disruptions. To gain further insight on the physical mechanisms involved during this penetration, a detailed investigation was carried out. Two distinct

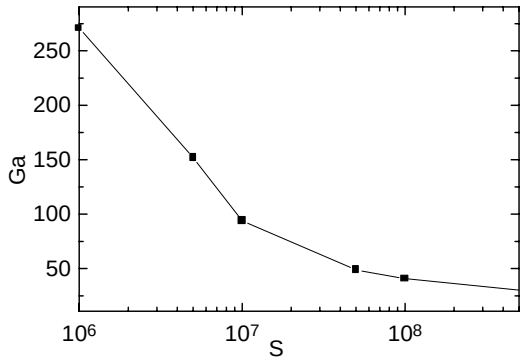

Figure 8.2 – Threshold in Ga ($=\tau_R/\tau_V$) for mode stabilisation as a function of the magnetic Reynolds number S for a rotating plasma with $V_{z0}(x=0)$=20kHz and aspect ratio $A=R_0/a$=3.4.

regimes are found, depending on the plasma rotation frequency with respect to the static external magnetic windings producing the "error-field": a resistive-viscous regime, where plasma inertia plays a minor role in the reconnection; a viscous-ideal regime, where the reconnection layer is greatly affected by ideal MHD effects. The former regime is also known as Alfven Resonance regime (AR) since a resonance pair emerges at both sides of the q=m/n resonant tearing mode rational surface. These two resonances, spreading away from the q=m/n surface (q=2 in the simulations) as plasma rotation increases, play a significant role in the dynamics since they both shield magnetic reconnection at the q=m/n surface and are sinks for the transfer of angular momentum to the plasma. During the transition from a forced reconnection regime to an AR regime, the toroidal induced braking force is found to become an increasing function of plasma rotation frequency as a direct consequence of the emerging contributions at the AR locations, contrasting the decrease in the localised force at the q=2 surface (Figure 8.3). For a magnetic Reynolds number $S=3\times10^8$, transition to the AR regime occurs at ~1.8kHz when the force becomes increasingly localised at the Alfven resonances.

The threshold in plasma rotation for this regimes' transition scales as $\omega_{thr} \propto 1/\tau_A S^{0.27}$ and has a weak dependence on the anomalous plasma viscosity. It is conjectured that the lack of experimental evidence of an AR dominated regime in present tokamaks may be due either to an effective drag on plasma rotation caused by anomalous plasma viscosity or to the plasma collisionality regime (magnetic reconnection in a collisionless regime evolves on much faster time scales, implying a much larger threshold plasma rotation to enter the AR regime).

8.3. MODELLING OF GRAD-SHAFRANOV EQUILIBRIA IN TOKAMAK PLASMAS

The studies on *reversed Grad-Shafranov (GS) equilibria, with negative toroidal current density flowing in the core*

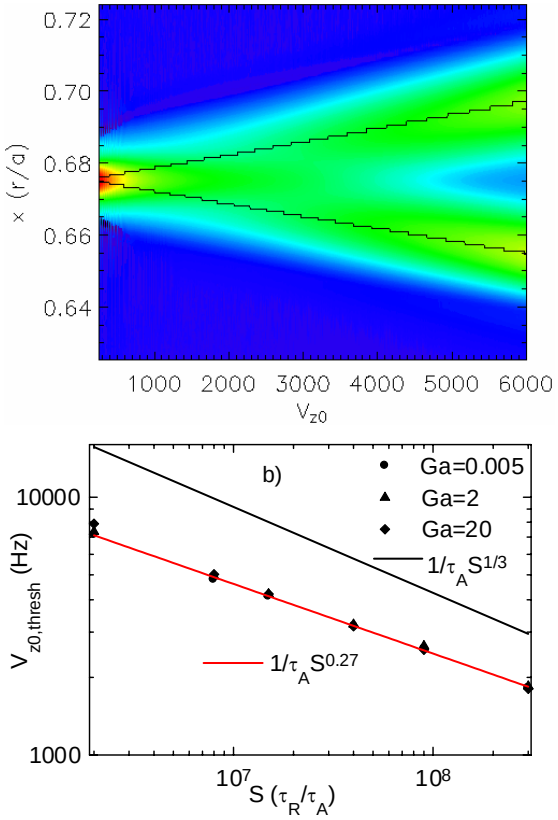

Figure 8.3 – Contour of the toroidal braking force exerted by static m=2,n=1 external magnetic fields on a rigid rotating plasma. Vertical axis indicates the radial direction and the plasma rotation lies on the x-axis (a). Rotation threshold for the transition between both regimes of reconnection (b).

and overall positive plasma current, were continued both via numerical simulations in more demanding conditions and by further theoretical developments. In particular, numerical solutions were found for some profiles where the toroidal current density assumes negative values in a location sufficiently off-axis (Figure 8.4) which are strong enough in order to develop two distinct poloidal-field reversal (PFR) layers, where the poloidal magnetic field does vanish (Figure 8.5). Contrary to currently available GS solutions in toroidal-current reversal scenarios, the considered configuration does not yield a central channel containing the magnetic axis where the current flows in a direction opposite to the one in rest of the plasma. Instead, it results in an annular region of negative current enclosing a positive current channel and being surrounded by positive currents also. Toroidal current-density profiles of this type are usually found in nonlinear resistive MHD simulations of JET plasmas with strongly reversed magnetic shear, but no GS equilibria was yet available for them. Besides showing the robustness of the scheme previously proposed to solve the GS equation for equilibria with toroidal current reversal, these are

expected to help understand the physics behind the current-hole problem.

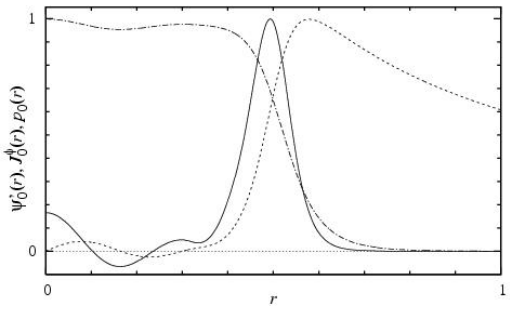

Figure 8.4 - Zeroth-order profiles $J^{\phi}_0(r)$ (solid line), $\psi'_0(r)$ (dashed line), and $p(r)=p_0(1+\alpha\, r)\, exp(-\gamma\, r)$ for $\alpha=5.55$ and $\gamma=10$ (dot-dashed line), normalized to their maximum values.

Following some previous work, a rigorous and consistent framework to describe *the topological features of reversed equilibria (nested and non-nested)* was developed by extending some fundamental concepts of Catastrophe Theory. This involved finding a suitable definition for nested equilibria, along with a systematic derivation of its most significant properties in current reversal scenarios. In general, these are extensions of results already established for isolated singularities of finite multiplicity, to manifolds of non-isolated singularities (such as the PFR layer) of infinite multiplicity. By rigorously showing that nested equilibria, on which most of the current knowledge is based, are non-typical and isolated elements, these results are expected to lead into a new paradigm when discussing GS solutions with toroidal current reversal.

In addition, it was noted that non-static configurations with non-vanishing poloidal and toroidal plasma flow could, at least in principle, force the toroidal current-density profile to display negative values. This led to efforts aiming to include finite plasma-flow effects in GS equilibria computations in order to assess their role in leading to reversed configurations.

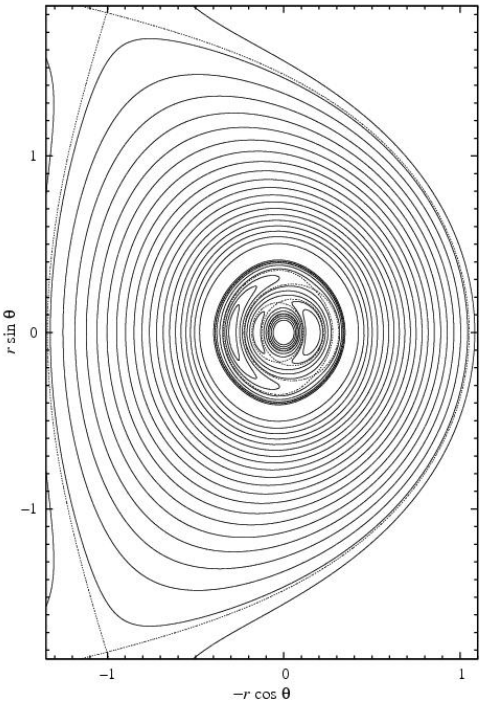

Figure 8.5 - Flux surfaces for typical JET parameters and the profiles depicted in Figure 8.4.

9. OTHER ACTIVITIES ON CONTROL DATA ACQUISITION AND SIGNAL PROCESSING

J. Sousa (Head), H. Fernandes, B.B. Carvalho, A. Batista, A. Combo, C. Correia, M. Correia, N. Cruz, R. Pereira, P. Ricardo.

9.1. INTRODUCTION

This project concerns the activities on control, data acquisition and signal processing that are not included in the previous projects. The 2005 work programme has been essentially focused in four main working lines:

- Development of a data acquisition system for the ETE tokamak;
- Participation in the CASTOR programme on data acquisition;
- Development of a low-cost, fully integrated, event-driven real-time control and data acquisition system for fusion experiments;
- Development of a time digitizer and transient recorder hybrid module for the enhanced neutron diagnostics data acquisition system

Concerning the *development of a complete data acquisition system for ETE*[1], the system architecture has been designed, including 64 transient recorder channels, a timing module and a CORBA based control and signal visualization software. Eight transient recorder modules were assembled and tested in 2005.

The *participation in the CASTOR*[2] *programme on data acquisition* has included the development of a complete data acquisition system, including 72 transient recorder channels as well as a CORBA based control and signal visualization software. Nine transient recorder modules, each one providing eight galvanic isolated channels, have been designed, assembled, mounted on an industry standard ATAC rack and functionally tested.

The overall architecture of *a low-cost, fully integrated, event-driven real-time control and data acquisition system for fusion experiments* was planned.

Regarding the *time digitizer and transient recorder hybrid module for the enhanced neutron diagnostics data acquisition system*, the module architecture has been defined accordingly to the specificities of the diagnostics, the acquisition module has been designed and the adequate software, firmware and hardware platforms have been identified.

[1] ETE is a tokamak of the 'Laboratório Associado de Plasma do Instituto Nacional de Pesquisas Espaciais', de São José dos Campos, Brazil.

[2] CASTOR is a tokamak of the Association Euratom/ IPP.CR (Institute of Plasma Physics), Prague.

9.2. PCI TRANSIENT RECORDER MODULE WITH GALVANIC ISOLATION

This module (Figure 9.1) has eight differential acquisition channels, performing a sampling rate up to 2 MSPS with 14-bit resolution. Each channel is galvanicly isolated by means of a magneto-coupler device. The input dynamic range is settable to ±10V, ±5V, ±2.5V, ±2V, ±0.5V. Data from each channel is serialized by a local PLD.

The main component of this module is its TMS320C6415™ DSP, which interfaces with the PCI bus, handles data processing tasks, and performs control of onboard memory. The use of state-of-the-art Field Programmable Gate Array (FPGA). (Xilinx Spartan 3 series) allows the implementation of data de-serialization, data synchronism and buffering and even the integration of digital data filters. A maximum storage of 512 MWords is available, in SDRAMM DIMM format.

The module has both internal and external clock and trigger capabilities, configurable to either TTL or RS-485 standards. A dedicated bus permits the synchronization of a maximum of 8 units within the same host.

9.3. LOW-COST, FULLY INTEGRATED, EVENT-DRIVEN REAL-TIME CONTROL AND DATA ACQUISITION SYSTEM

The overall architecture of this system (Figure 9.2) was designed based on the PCI Express, Advanced Switching Interconnect (ASI) and Advanced Telecommunications Computer Architecture (ATCA) standards, to be scalable both in performance and number of input signals, to permit the transport of signals and events in real-time (< 1 μs), to have all nodes synchronized over the gigabit data interconnections (clock, time, triggers), include Ethernet, ATM, PCI-X bridges and to provide automatic recognition of each node features through a XML description for easy integration on existing platforms.

Initially the following modules will be implemented: (i) an ATCA ix86-based controller; (ii) a digitizer/generator/processing card with 16 analogue input channels sampling at a rate up to 50 MSPS@12-bit, 4 analogue output channels, 8 digital IO channels and a state-of-the-art DSP and FPGA for real-time signal processing, and data flow control; (iii) a spectroscopy transient recorders with 4(2) channels sampling at a rate up to 200(400) MSPS@12-bit, 100(200) MSPS@14-bit and 1(2) GSPS@8-bit; and (iv) an ASI switch-fabric interconnection module and an ASI to ATM bridge.

Figure 9.1 – View of the TCA transient recorder module with galvanic isolation.

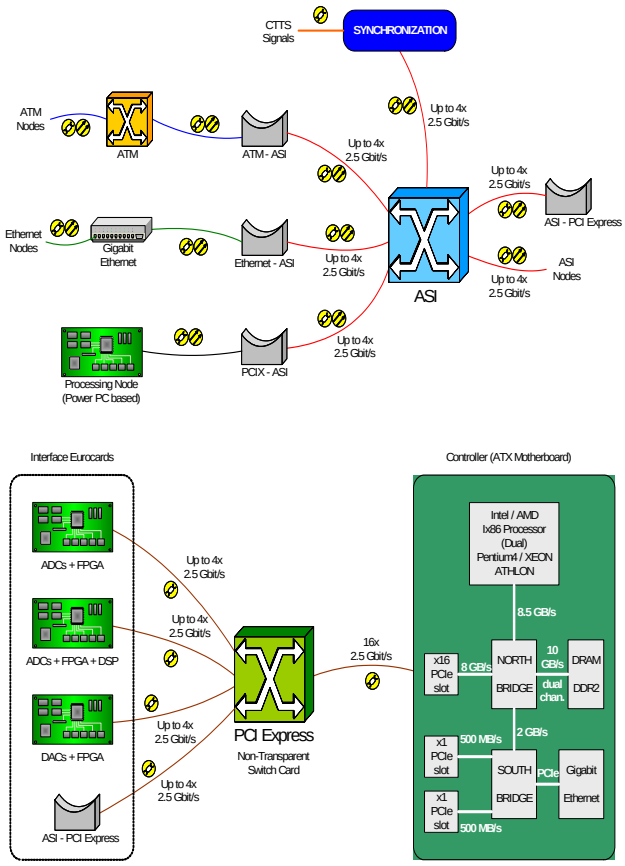

Figure 9.2 - Overall architecture of the system and of one node.

9.4. TIME DIGITIZER AND TRANSIENT RECORDER HYBRID MODULE

This module aims at: (i) implementing digital pulse processing (DPP) functions such as pulse height analysis (PHA) and pulse shape discrimination (PSD) for data reduction and real-time rough assessment of plasma parameters; (ii) fulfilling the requirements of the experiment diagnostics; (iii) having a high number of channels per board and consequently decreasing the cost per channel; and (iv) having an architecture designed for upgradeability and scalability. The module was designed for the ATAC bus with eight 12-bit resolution ADCs, providing eight analogue channels at 200 MSPS or, using a pair of digitizing channels shifted in phase (180º), four channels at 400 MSPS. Circuitry for using four ADCs to provide one channel at 800 MSPS is also included.

The module contains two FPGAs, each controlling a memory bank of 1 GB and four acquisition channels and providing a gigabit communications interface, thereby reducing circuit complexity and cost by acting as a system-on-chip device, (Figure 9.3).

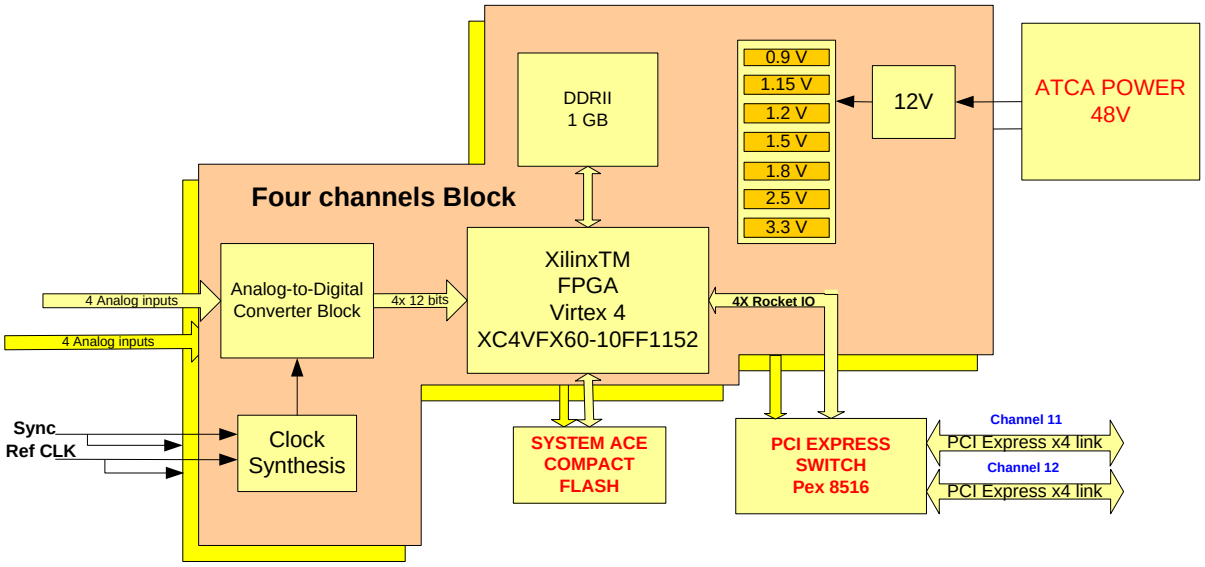

Figure 9.3 – Simplified module block diagram

Only raw data (array of sampled pulses) is stored in memory. A continuous stream of processed data is sent to the ATCA controller for further processing and subsequent use for monitoring and control.

10. KEEP-IN-TOUCH ACTIVITIES IN INERTIAL FUSION ENERGY[1]

J. T. Mendonça, (Head), J. Davies, J. M. Dias, M. Fajardo, R. A. Fonseca, D. Resendes, J. A. Rodrigues, L. O. Silva, G. Sorasio, P. T. Abreu, L. Cardoso, M. Fiore, L. Gargaté, M. Marti, I. Vieira, J. Vieira, C. Leitão, N. Lemos, F. Wahaia, E. Abreu, B. Brandão, N. Brites, F. Fiúza, J. L. Martins, S. Martins, S. Mota, J. Sampaio, J. Santos, A. Smith, F. Viola

10.1. INTRODUCTION

The keep-in-touch activities in inertial confinement fusion (ICF) dealt with some of the critical problems facing the new developments in ICF, in particular the issues associates with fast ignition fusion targets. The highlights of research associated with ICF were:

- Project HiPER;
- Fast ignition and ICF physics;
- OPCPA laser technology and development of diagnostics of ultra intense lasers;
- Development of simulation infrastructure for multi-scale fast ignition experiments.

10.2. PROJECT HIPER

GoLP has been involved in the planning almost since its inception of HiPER (High Power Experimental Research Facility) (Figure 10.1), a proposal for a European Large Scale Facility for direct drive inertial confinement fusion, fast ignition and laser-plasma experiments in general. It is planned to have 200 kJ in multiple, nanosecond laser beams, intended to achieve compression in a cone, and 70 kJ in a picosecond ignition beam. The energy in the ignition beam could also be channelled into the compression beams for experiments in "conventional" ignition. It will also provide a unique facility for straightforward laser-plasma experiments at high laser powers and for other experiments that require a combination of long and short pulse beams, such as X-ray lasers and experiments relevant to astrophysics. The estimated cost is of the order of 109 M€, compared to 1010 M€ for NIF and LMJ, making it by far the cheapest facility capable of achieving ignition.

10.3. FAST IGNITION AND ICF PHYSICS

10.3.1. A new diagnostic for very high magnetic fields in expanding plasmas

Strong magnetic fields can be generated by intense laser plasma interaction. Magnetic fields of 700(±100) Mega-Gauss were inferred from polarization shifts of low order VUV harmonics induced by the Cotton-Mouton effect. We have proposed *a new diagnostic method for the magnetic field value inside the plasma*, based on the idea of photon acceleration, or photon frequency shift. The frequency shift is also polarization dependent, which means that, by comparing the observed frequency shifts for the two orthogonal polarization states, for photons propagating along a given direction with respect to the magnetic field, we will be able to measure the magnetic field amplitude, as well as the expanding velocity, if the plasma frequency is known.

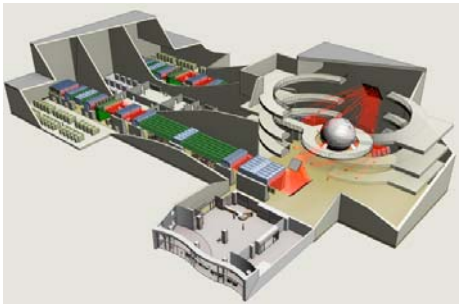

Figure 10.1 - Sketch of the HiPER laser system

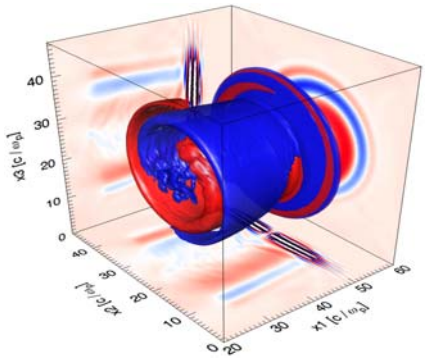

Figure 10.2 - The three-dimensional structure of the longitudinal magnetic field by a circularly polarized laser (blue represents positive and red represents negative), obtained from a 3D PIC simulation. The laser propagates from left tp right along x1, in a moving window (@ c)

10.3.2. A coupled two-step plasma instability in PW laser plasma interaction

One of the most recent, and remarkable, experimental results was the measurement of thermonuclear neutrons from deuterated plastic targets irradiated by the Vulcan

[1] This project has been carried out by "Grupo de Lasers e Plasmas" (GoLP) of "Centro de Física de Plasmas".

PetaWatt laser at the Rutherford Appleton Laboratory. These results indicated temperatures in excess of 100 keV, whereas all other diagnostics indicated target temperatures that did not exceed 1 keV. We explained this in terms *of an ion instability driven by perturbations in the density of the target electrons.* This instability can convert the energy given to the target electrons into ion energy more rapidly than it is converted into electron heating, if the electron collision frequency is small enough. The collision frequency can be reduced sufficiently by a high drift velocity or by the initial heating. The theory reproduced the observed intensity threshold for thermonuclear neutron emission.

10.4. OPCPA LASER TECHNOLOGY AND LASER AMPLIFIER CHAIN

10.4.1. Broadband non-collinear optical parametric chirped pulse amplification

Recent advances in high intensity laser technology, such as the optical parametric chirped pulse amplification technique, allow the amplification of broadband pulses to high energies, by parametric interaction in a non-linear crystal. We have applied the technique developed by GoLP last year to the *comparative study of three non-linear crystals, BBO, LBO and KDP*, in order to evaluate their suitability for ultra-broadband parametric amplification. Although the maximum bandwidth of KDP does not broaden, we show how to avoid its severe narrowing below the degeneracy wavelength. The results show that the OPCPA technique can benefit enormously from this novel geometry, extending further its broadband capability.

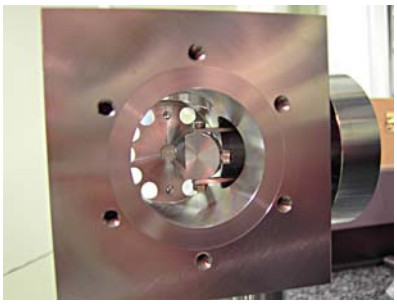

10.3 - Experimental set-up, with the nonlinear crystal in the centre of the optical mount

10.4.2. Development of the L2I laser amplifier chain

The MIRO code was used to simulate all the active components of the amplifier section, together with the vacuum spatial filters. A gaussian beam was the injected into the simulated chain and its output amplitude distribution was evaluated as a function of the pumping energy in both amplifiers. This allowed a definition of the optimum input beam diameter for the first amplifier and the magnification ration between the two amplifiers in order to obtain an approximately top-hat output beam. These results will now be confirmed and implemented in the laser chain.

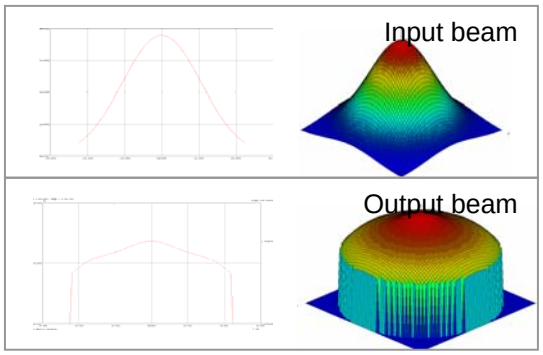

10.4 - Results of the MIRO code, comparing the transverse profile of the input beam with the shape of the beam after the amplification chain

10.5. DEVELOPMENT OF SIMULATION INFRASTRUCTURE FOR MULTISCALE FAST IGNITION EXPERIMENTS

Based on the highly nonlinear and kinetic processes that occur during high-intensity particle and laser beam-plasma interactions, we use *particle-in-cell codes, which are a subset of the particle-mesh techniques, for the modeling of these physical problems.* In these codes the full set of Maxwell's equations are solved on a grid using currents and charge densities calculated by weighting discrete particles onto the grid. Each particle is pushed to a new position and momentum via self-consistently calculated fields. The main code behind our simulation effort is the OSIRIS framework. These codes capture the relevant physics but are also computationally demanding. For problems involving multiple time and length scales, such as fast ignition, standard PIC codes cannot, with the available computing power, perform an accurate modeling. During 2005, we have performed several developments in OSIRIS including further physics (such as ionization, binary collisions), algorithm optimization (higher order deposition schemes), and performance optimization (dynamic load balancing). At the same time, we have started to develop *the set of diagnostics and output information required to couple a PIC code, such as OSIRIS, to other reduced codes,* thus opening the way for a full scale modeling of a fast ignition target.

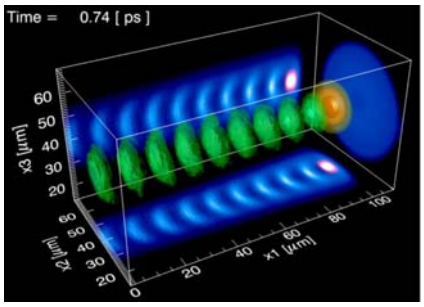

Figure 10.5 - Tunnel ionization of a gas target by an ultra intense laser, demonstrating the formation of the wakefield structure (green) behind the laser pulse (in orange)

11. PARTICIPATION IN THE FUSION TECHNOLOGY PROGRAMME[1]

E. Alves (Head), A. Paúl, L.C. Alves, M.R. da Silva, N. Franco

11.1. INTRODUCTION

The Portuguese participation in the Fusion Technology Program was focused in 2005 on the *micro-structure characterisation of ODS-RAFM steels and titanium beryllide samples*, both candidate materials for the ITER and DEMO nuclear fusion reactors.

Three different Eurofer-ODS samples have been characterized: 5 and 10 mm thick plate fabricated by CEA and 12 mm disk fabricated by CRPP. Samples were analysed before and after annealing experiments and data comparison was carried out.

Two titanium beryllide alloys with a nominal composition of Be-5 at % Ti and Be-7 at % Ti were produced at JAERI, Japan, and its structural stability and oxidation behaviour under air annealing was followed.

11.2. TW5-TTMS-006: HIGH PERFORMANCE STEELS DELIVERABLE D2: CHARACTERIZATION OF REFERENCE EU ODS-EUROFER BATCH.

Small pieces were cut from the as received material and analysed before and after the annealing conditions. The samples were initially heated at 700 ºC during several hours in a He/0.1% H gas mixture followed by long-term annealing also, at 700 ºC, in an oxidizing atmosphere (dry air). The total annealing time was of 5000 h. Before and after the aging procedure the samples where characterized by means of SEM, TEM, XRD and nuclear microprobe techniques in order to detect changes in the microstructure.

The elemental distribution maps obtained after the heat treatment at the edge of the samples are shown in Figure 11.1. For the CRPP sample the oxidation altered the surface layer to an extension of 30 µm and presents a bilayered structure with very sharp interfaces (Figure 11.1a)). The layer in the oxide/atmosphere interface has an extension of ~15 µm where Cr is the major metal component. This layer also indicates the diffusion of Mn (~3 wt.%) and strong Fe depletion (~2 wt.%). The innermost layer in the metal/oxide interface also has ~15 µm thickness and a main metal composition of Cr and Mn with a strong increment in the Mn content, reaching a 2:1 ratio for the Cr/Mn amount. In this layer there is also depletion on Fe, W and Y. The oxidized layer of the 5 mm thick CEA sample has a much larger and irregular extension than the one observed for the CRPP sample, reaching 120 µm (Figure 11.1b)). The scale formed in this sample doesn't have the same multilayer structure seen in the CRPP specimen and the interface separating the scale and bulk has an irregular shape. Mainly Cr forms the outer region but there is presence of Fe in the inner parts of the scale. Besides, Y has an uneven spatial distribution with some Y segregation to the mid scale.

Although the studied alloys have the same nominal composition, fabrication route and heat treatment, SEM, TEM and XRD analysis also reveal that the samples present different microstructures and appreciable differences in the ferritic-martensitic phase transformation temperatures as well as on the distribution of the yttria dispersion.

11.3. MATERIAL CHARACTERIZATION USING NUCLEAR TECHNIQUES: STRUCTURAL AND OXIDATION STUDIES OF BERYLLIUM ALLOYS.

Small pieces (about 2 mm^3) were cut from the as-cast material and studied before and after annealing at 600 and 800 ^oC in dry air. Both high resolution x-ray diffraction and micro-beam techniques were used to follow the evolution of the composition and crystalline phases as well as the microstructure. The impurity content and oxide layer were monitored with Rutherford Backscattering Spectrometry (RBS) and Particle Induce X-ray Emission (PIXE) techniques. The image shown in Figure 11.2 for the Be-5at%Ti alloy shows a granular distribution of the beryllide phase surrounded by a beryllium rich region containing several impurities as revealed by PIXE. The Be-7at%Ti is more homogeneous as shown by the titanium distribution map (Figure 11.2) and the impurity content is significantly lower compared to the other alloy. On the other hand the presence of uranium in both types of compounds needs to be taken into account when applications are foreseen.

The identification of the beryllide phases present in the samples was done using high resolution X-ray diffraction. The $Be_{12}Ti$ intermetallic compound is present in both Be-5at%Ti and Be-7at%Ti alloys whereas the $Be_{10}Ti$ compound could only be detected in the Be-7at%Ti alloy.

[1] Work carried out by "Instituto Tecnológico e Nuclear" (ITN).

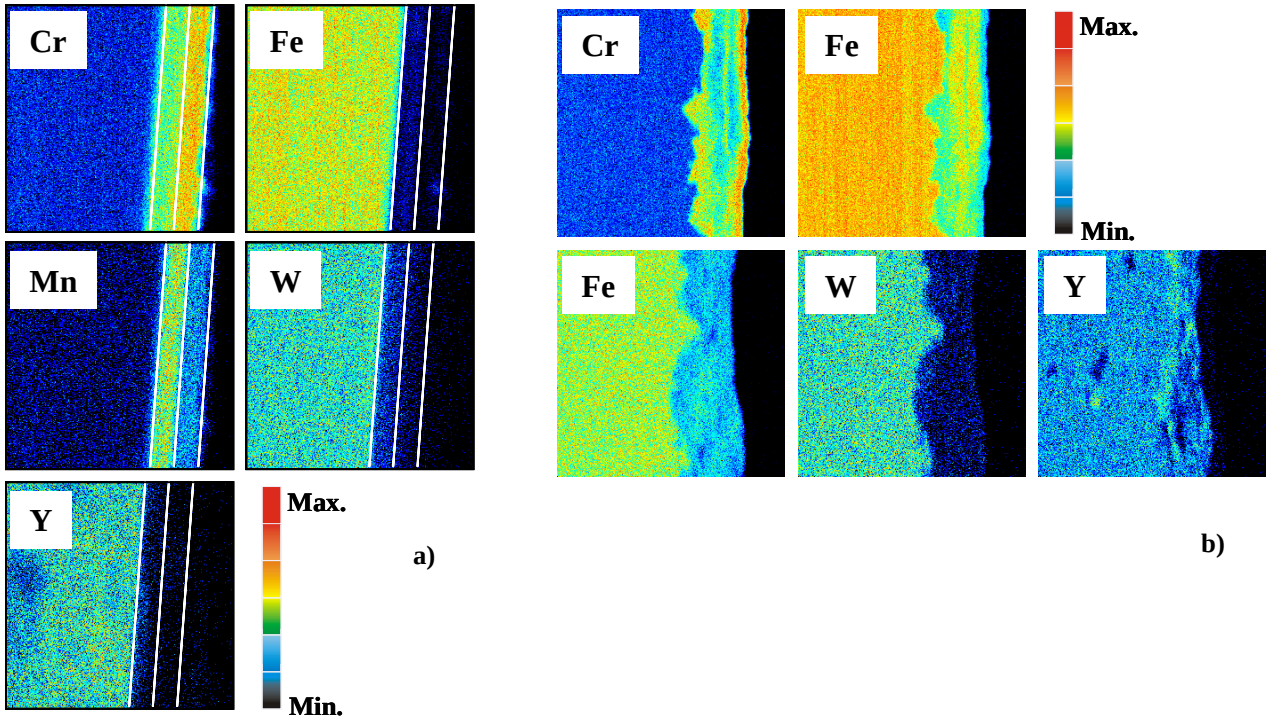

Figure 11.1 - Elemental distribution maps obtained for the CRPP sample after the thermal treatment, in a cross section near the sample surface. The maps have dimension of 130x130 μm^2. The white lines shown in all the elemental distribution maps indicate the layers referred in the text and are used to guide the eye; b) - Elemental distribution maps obtained for the 5 mm thick CEA sample after the thermal treatment, in a cross section near the sample surface. The maps have dimension of 530x530 μm^2. The elemental maps at the bottom row of the figure 10.1b) were obtained in a position different from the one used to obtain the maps shown in the top row. In both rows the Fe map is shown as a reference

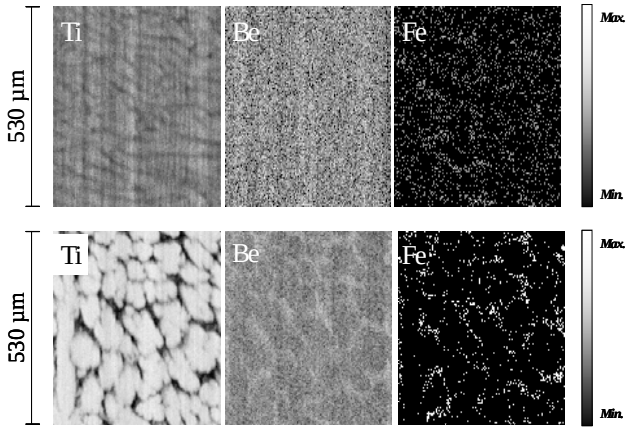

Figure 11.2 - 530×530 μm^2 Ti, Be and Fe elemental maps obtained from as cast Be-7at % Ti (top) and Be-5at % Ti (bottom) compounds.

The thermal stability of the intermetallic beryllides was studied after annealing at 800 ^{o}C in a tubular furnace with a dry-air atmosphere and in-situ up to 750 ^{o}C in vacuum. The changes were not pronounced and only for the Be-7 at % Ti compound the presence of the $Be_{17}Ti_2$ could not be excluded.

The oxidation of the beryllides was studied in the range of 600 to 800 ^{o}C in dry air atmosphere but only BeO could be identified.

Ion beam RBS technique was also used to extract information on the oxygen profile. We observe that before annealing only a small peak indicating the presence of oxygen was found in the beryllium rich regions of the samples. The oxygen profiles after the annealing are shown in Figure 11.3; Figure 11.3a shows the profile obtained in a Ti rich region for the Be-5 at % Ti alloy. As expected the oxidation process starts at low temperature and a pronounced oxygen peak at the surface region is visible immediately after 1h annealing at 600 ^{o}C. Further annealing at 800 ^{o}C almost doubles the peak intensity and a broadening into deeper regions. Extending the annealing for longer time the height of the peak remains constant but the profile continues to widen, indicating the diffusion of oxygen into the bulk. The analysis in the Ti depleted region (Figure 11.3b) indicates higher oxygen content concentration.

These results suggest an enhancement of the oxidation rate in the Be rich region. For the Be-7 at % Ti the oxidation is clearly inhibited in the Ti rich regions of the sample (Figure 11.3c). The difference in the oxidation rate for the Be-5 at % Ti and Be-7 at % Ti is most probably related with the different microstructure of these alloys.

The more homogeneous distribution of Ti in Be-7 at % Ti could retard or prevent the oxidation. On the contrary the intra grain Be rich regions in Be-5 at % Ti could enhance the oxygen diffusion.

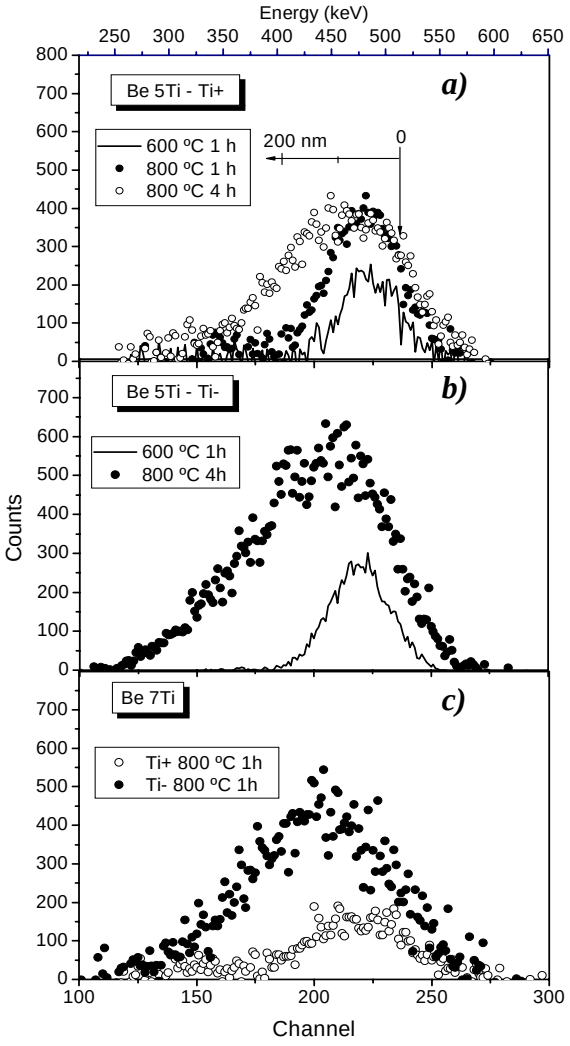

Figure 11.3 – RBS oxygen profiles obtained from a Be_{12} Ti region (Ti+) (a) and a Ti depleted region (Ti-) (beryllium rich) (b) for the Be-5 % Ti alloy after annealing. The oxygen profiles for the Be-7% Ti alloy are shown in (c).

12. OTHER FUSION-RELATED ACTIVITIES

12.1. Collaboration with Brazilian Institutions

IST/CFN has proceeded with the collaboration on nuclear fusion with two Brazilian Institutions:

- Laboratório de Plasmas (LP), do Instituto de Física, da Universidade de São Paulo;
- Laboratório Associado de Plasmas (LAP), do Instituto Nacional de Pesquisas Espaciais, de São José dos Campos.

The 2005 working programme included the development of *data acquisition boards* for TCA/Br[1] and ETE[2], the design of a *microwave reflectometer* for TCA/Br, the development of a *high spatial resolution Thomson scattering diagnostic* for ETE and *experiments on edge physics* on TCA/Br.

12.2. Collaboration with IPP.CR

IST starts in 2005 a new collaboration with Institute of Plasma Physics, (IPP.CR) related with the re-commissioning in Prague of the COMPASS-D tokamak. The areas of joint work are *control and data acquisition, microwave reflectometry and edge plasma diagnostics and physics.*

12.3. Participation in the management of Fusion Programmes

- Some members of the Association EURATOM/IST are delegates to Committees of the European Fusion Programme and of the European Fusion Development Agreement (Table 11.1).
- Prof. Carlos Varandas is/was:
  - Chairman of the EFDA Steering Committee;
  - Member of the European Union Delegation to the ITER negotiations;
  - Member of the Steering Committees of the Bilateral Agreements of EURATOM with Russia, Japan and USA;
  - Member of the Ad-Hoc Group on ELE/EFEDO and related issues;
  - Chairman of the Ad-Hoc Group on the new European Fusion Development Agreement and the Contracts of Association.
- Prof. Fernando Serra is/was a member of:
  - Ad-Hoc Group from STAC for the "Monitoring of W7-X Project";
  - Member of the ITPA (International Tokamak Physics Activity) Topical Group on Diagnostics.
- Profª Maria Emília Manso was:
  - Member of the Programme Committee of the ASDEX-Upgrade Project;
  - Chairperson of the International Advisory Board on Reflectometry.

12.4. Organization of scientific meetings

Two members of the CFN staff have been involved in the organization of scientific meetings:

- Dr. Carlos Silva was member of the Programme Committee of the "Workshop on the Role of Electric Field in Plasma Confinement and Exhaust".
- Prof. Carlos Varandas was:
  - Chairman of the Organizing Committee of the Workshop on "Energies of the Present and Future", Lisboa, 21 and 22 November 2005;
  - Member of the International Organizing Committee of the "XI Latin-American Workshop on Plasma Physics", Mexico, 1-5 December 2005.

12.5. Collaboration with Portuguese Universities

CFN has proceeded with the collaboration in graduation and post-graduation universitary programmes:

- CFN has been responsible by experimental teaching in tokamak physics and engineering;
- Seventh students have been performing Master and Ph.D. programmes at CFN in fusion plasma physics and engineering.

12.6. Public information

CFN has proceeded with activities aiming at increasing the public understanding on fusion energy:

- Six seminaries have been given in secondary schools;
- A film about fusion and ITER has been translated to Portuguese;
- Prof. Carlos Varandas has participated in television programmes about the ITER Project;
- Several articles have been published in Portuguese newspapers with the direct or indirect participation of members of the IST/CFN staff.

[1] TCA/Br is a tokamak of the University of São Paulo
[2] ETE is a tokamak of LAP.

Name	Member of
Carlos Varandas	CCE-FU
	EFDA Steering Committee
	GoC[3]
	CFI[4]
	STC[5]
	EFDA Technology Sub-Committee
Maria Emília Manso	CCE-FU
	EFDA Steering Committee
	EFDA Public Information Sub-Committee
Fernando Serra	STAC[6]
	EFDA/PIG[7]
J.P. Bizarro	STAC
P. Silva	STC
	EFDA Technology Sub-Committee
Carlos Silva	AFAC[8]
J.T. Mendonça	IFEC[9]

Table 12.1 – Participation of members of the Association EURATOM/IST on the management of the European Fusion Programme and of the European Fusion Development Agreement

[3] GoC means "Group of Chairmen"
[4] CFI means "Committee Fusion Industry"
[5] STC means "Scientific and Technical Committee"
[6] STAC means "Scientific and Technical Advisory Committee"
[7] PIG means "Public Information Group"
[8] AFAC means "Administrative and Financial Advisory Committee"
[9] IFEC means "Inertial Fusion Energy Committee"

13. THEORY AND SIMULATIONS ON HIGH ENERGY DENSITY SCIENCE AND ASTROPHYSICAL AND SPACE PLASMA PHYSICS

J. T. Mendonça (Head), D. Resendes, L. O. Silva, J. Davies, J. M. Dias, M. Fajardo, R. A. Fonseca, A. Martins, Y. Omar, P. K. Shukla, G. Sorasio, P. T. Abreu, M. Fiore, L. Gargaté, M. Marti, I. Vieira, J. Vieira, B. Brandão, F. Fiúza, J. L. Martins, S. Martins, S. Mota, J. Santos

13.1. INTRODUCTION

Research in theory and simulation at GoLP/CFP was focused on some of the outstanding problems in laser-plasma interactions, basic plasma physics, exploring the connection between laboratory and astrophysical scenarios. The key aspects of research in 2005 dealt with:

- Fast ignition and ICF physics, and laser-solid interactions;
- Ultra intense laser plasma interactions and plasma based accelerators;
- Development of simulation infrastructure for e-Science;
- Relativistic Astrophysics and space plasma physics.

13.2. FAST IGNITION AND ICF PHYSICS, AND LASER-SOLID INTERACTIONS

13.2.1. A coupled two-step plasma instability in PW laser plasma interaction[1]

There is now a growing body of evidence for anomalous ion bulk heating in laser plasma interaction experiments, when the laser power approaches the Peta-Watt (PW) regime, both from experiments and from hybrid code simulations.

We have proposed a possible *explanation for the observed anomalous resistivity*. Our model is based on the existence of two coupled processes. First, the fast electrons created by the laser pulse interact with the resulting return current and produce an intense electrostatic field, by means of a two stream instability. Second, the resulting electrostatic waves become modulationally unstable and decay resonantly into ion-acoustic waves. This mechanism is not efficient for electron heating but leads to an efficient ion heating which could explain the observations.

13.2.2. Laser-Solid Interactions and Fast Ignition Inertial Confinement Fusion

The Vulcan TeraWatt and PetaWatt lasers have produced a vast quantity of data from laser-solid experiments using numerous diagnostics and target materials. We have been able to provide a *coherent interpretation* of much of this data *based on our theoretical work on ion instabilities and magnetic field generation.* Our work on magnetic field generation has been able to explain the increase in the divergence of the electrons accelerated into the target with increasing laser power and the associated appearance of a hollow plasma at the back of the target, in experiments with both the TeraWatt and PetaWatt lasers using both plastic and metal targets (Figure 13.1). We have also worked on magnetic inhibition of electron flow in layered targets.

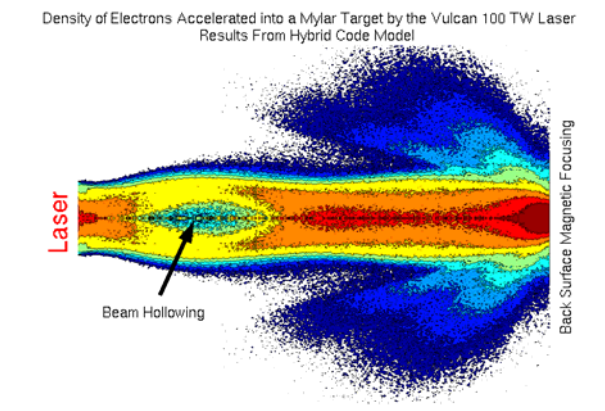

Figure 13.1 - Results from hybrid code modelling of experiments on the Vulcan 100 TW laser with solid, plastic targets (Mylar) that reproduces the electron beam hollowing.

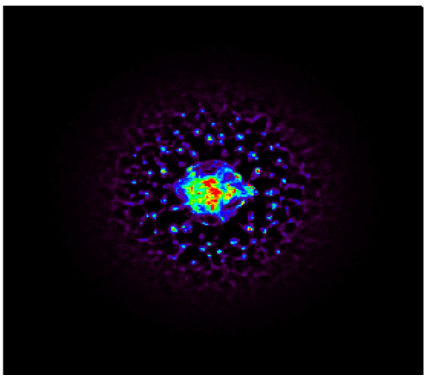

Figure 13.2 - "Finite width beam filamentation due to the Weibel instability"

[1] Work carried out in collaboration with R. Bingham, P. Norreys (RAL).

13.2.3. Weibel instability in fast ignition of fusion targets[2]

Using relativistic kinetic theory, a *theoretical model for the linear stage of the collisionless filamentation* (Weibel) *instability* has been worked out, analyzing the coronal region of the fuel pellet in fast ignition. We have shown that only at the edge of the compressed pellet, the filamentation instability can develop even at large beam temperature with a small but not negligible growth rate. This is due to the ion presence, which cancels the space charge effects and allows for the instability to occur on the ion time scale.

(i) Finite width beam filamentation due to the Weibel instability

These aspects have been also numerically explored with a very large 2D simulation dealing with both the interaction of a picosecond-long ignition pulse with high-density (40 times critical density) pellet and the pulse driven electron beam propagation. Beam filamentation due to the Weibel instability as well as the role played by ions of neutralizing the space charge effects have been observed.

The propagation of finite width beams through a background plasma has been studied numerically, performing 2D simulations (Figure 13.2). When the simulation plane is perpendicular to the propagation direction, the Weibel instability shows up, filamenting the beam. When the simulation plane is parallel to the propagation direction, evidences of the two-stream instability and the hosing instability have been observed.

13.2.4. Very High Mach-Number Electrostatic Shocks in Collisionless Plasmas

The kinetic theory of *collisionless electrostatic shocks resulting from the collision of plasma slabs with different temperatures and densities* has been developed. The theoretical results are confirmed by self-consistent particle-in-cell simulations, revealing the formation and stable propagation of electrostatic shocks with very high Mach numbers (M >>10), well above the predictions of the classical theories for electrostatic shocks. The theory demonstrates that the shock properties are strongly influenced by Θ, the ratio of the electron temperatures in the two slabs, and by Y the ratio of the electron densities in the two slabs. The analysis shows that when the electron temperature of the downstream slab (R) is higher than the electron temperature of the upstream slab (L), the shock waves can have very large Mach numbers, which are otherwise not supported by isothermal plasmas. The model predicts that the maximum allowed Mach number increases with Θ, without an absolute upper limit.

The theoretical results have been confirmed by one-dimensional (1D) self-consistent particle-in-cell simulations, demonstrating the formation and the stable propagation of electrostatic shock waves with very large Mach numbers (M ~ 20) (Figure 13.3).

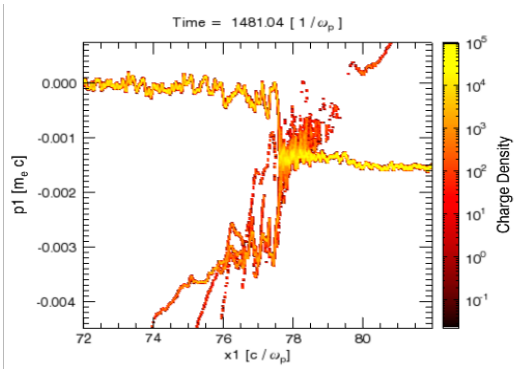

Figure 13.3 - Shock wave in the ion phase space p1x1.

13.2.5 White light parametric instabilities[3]

Parametric instabilities are pervasive in many fields of science with its importance stemming from their close connection to the onset of nonlinear and collective effects such as solitons, vortices, self-organization, and spontaneous ordering. We have employed a *generalized photon kinetics formalism,* directly inspired in the Wigner-Moyal formalism for Quantum Mechanics to establish the general dispersion relation for parametric instabilities driven by electromagnetic radiation, with arbitrary statistics, coupled to the electron collective dynamics in a unmagnetized plasma. The one-dimensional analysis for Stimulated Raman Scattering reveals a growth rate dependence with the coherence width σ of the radiation field scaling as $1/\sigma$ for backscattering, and $1/\sigma^{1/2}$ for forward scattering, and a significant dependence of the instability growth rate on the shape of the power spectrum of the radiation. The results open the way to a full multi-dimensional description of parametric instabilities driven by intense radiation sources, with arbitrary statistics, interacting with plasmas in laboratory and astrophysical scenarios.

13.3. ULTRA INTENSE LASER PLASMA INTERACTIONS AND PLASMA BASED ACCELERATORS

13.3.1 Shock shells driven by layered clusters and explosion of clusters driven by intense x-ray sources[4]

The interaction of ultra-short ultra-intense laser pulses with large deuterium clusters (>10^5 atoms) can lead to the removal of all (or most of) the electrons inducing a Coulomb explosion. During this phenomenon shock shells (multi-branch structures in the phase space) may be formed if ion overtaking occurs.

However, significantly thick shock shells are hard to produce in homonuclear clusters with a single laser pulse. Instead, the use of *heteronuclear layered clusters* has been proposed *as a means of driving shock shells*. This method is based on the fact that the initial ion acceleration profile is a critical issue for the shock formation. Both the number density and the mass profiles can be chosen so as to

[2] Work performed in collaboration with C. Ren (U. Rochester), M. Tzoufras, W B. Mori (UCLA).

[3] Work carried out in collaboration with R. Bingham (RAL)

[4] Work performed in collaboration with F. Peano (Poli Torino)

produce the desired acceleration profile, the latter being used in this case.

The explosion of layered clusters with light inner species and increasingly heavier species with radial distance was studied. PIC simulations of a three-layer cluster with step-like mass profile were performed with OSIRIS 2.0. It was found that ion overtaking of the outer heavy ions by the lighter inner ones occurs in both of the borders between the layers, even before the total removal of the electrons (Figure 13.4). Density peaks were observed where the overtaking occurs in an analogous manner to what is found in homonuclear clusters. As the core ions continued to expand the two density peaks eventually merged. However, the phase space structure observed in the case of the layered cluster differed from the homonuclear clusters shock shells in that only two branches appeared instead of the three branches seen in the latter.

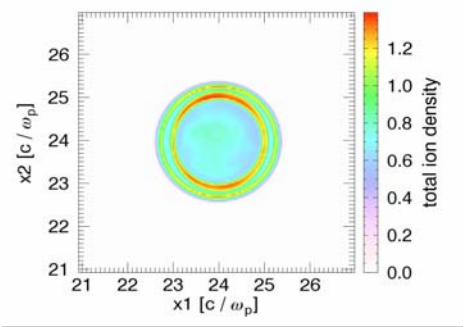

Figure 13.4 - Density peaks due to ion overtaking

In this way, the proper selection of a mass profile offers a method for controlling the phase space of the cluster explosion to induce shock shell formation. The characteristics of this structure can be selected "a priori" by varying the widths, composition and number of layers of the cluster.

The study of the possibility of *producing shock shells in clusters in the x-ray regime* was also initiated. Simulations were made of homonuclear clusters with two pairs of ion and electron populations. These electron populations were initiated at different times and with different energies, representing the two ionization stages expected if the cluster were to be irradiated by two x-ray laser pulses with distinct intensities and frequencies. It was observed that by choosing the laser parameters properly it was possible to induce ion overtaking with the appearance of shock shells in the phase space.

13.3.2 Blowout regime of the laser wakefield accelerator [5]

Studies of electron acceleration in parabolic plasma channels have been carried out. Plasma is a very good medium for accelerating electrons, both injected externally, or self injected from the plasma itself, since the accelerating gradients are orders of magnitude greater than in conventional accelerators. *The primary focus* of the work *is* focused *on the plasma self injected electrons*.

There has been a considerate effort in achieving GeV electrons with this technique, as current experiments place the maximum energy gain of self-injected electrons on a few hundreds of MeV. These experiments operated in the blowout regime, where an intense laser pulse radially expels nearly all plasma electrons. An ion column is left behind the laser pulse and electrons are attracted inwards to the axis, forming an electron void cavity. This cavity is spherical and resembles a bubble that gave its name to the bucket (Figure 13.5).

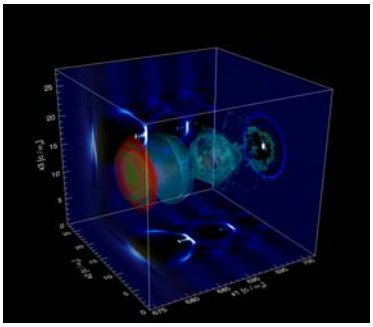

Figure 13.5 - Contour plot of the bubble excited by an ultraintense laser pulse. Blue contours are the plasma density. Red-Green contours are the laser pulse

13.3.3. Wigner diagnostic for photon acceleration [6]

A short intense laser pulse propagating through a gas can generate plasma waves, due to electron density modulation. This mechanism can upshift photons riding the waves, whether they are from a driver pulse or from a trailing low intensity pulse. Such phenomena provide important information about relativistic structures, as well as a novel way to tune radiation (Figure 13.6).

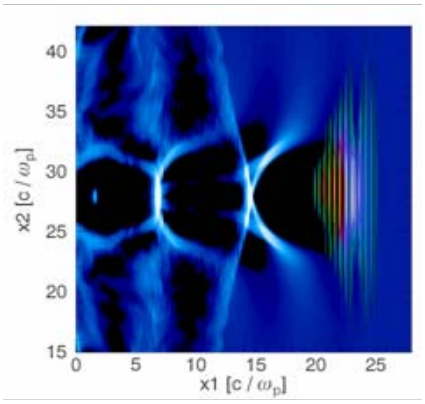

Figure 13.6 - Wakefield generated by an ultra short intense laser pulse (laser pulse in red/green).

[5] Work carried out in collaboration with W. Lu, M. Tzoufras, C. Joshi, W. B. Mori (UCLA)

[6] Work performed in collaboration with J. P. Bizarro, A. Figueiredo (CFN), R. Trines, and R. Bingham (RAL)

Several kinds of *Wigner transforms* were implemented *to analyze photon acceleration.* PIC simulations were preformed with OSIRIS 2.0, revealing that in 1D simulations, where the interaction length is comparable/longer than photon dephasing length in wake (regime achievable for very long Rayleigh lengths), different initial delays between the driver and probe pulses do not lead to different signatures in Wigner distribution (Figure 13.7). However, in 2D simulations, a tight focus leads to short interaction time with wake, thus different probe displacements lead to different final conditions. On the other hand, the FFT failed to reveal detailed internal dynamics of laser pulse.

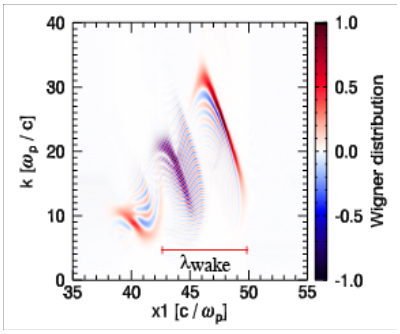

Figure 13.7 - Wigner transform of ultra short laser pulse riding a laser wakefield.

13.4. DEVELOPMENT OF THE SIMULATION INFRASTRUCTURE FOR E-SCIENCE

13.4.1 osiris 2.0 development[7]

The OSIRIS 2.0 framework is an integrated framework for particle-in-cell (PIC) simulations. This framework is based on a three-dimensional, fully relativistic, massively parallel, object oriented particle-in-cell code, that has successfully been applied to a number of problems, ranging from laser-plasma interaction and inertial fusion to plasma shell collisions in astrophysical scenarios.

The main development milestone achieved in 2005 was the *full implementation of the dynamic load balancing algorithm in OSIRIS.* A binary tree algorithm for finding best problem partition solution was implemented to this end. During runtime, OSIRIS will dynamically analyze the load of each computing node, and reshape the parallel partition whenever needed to maintain an evenly balanced node.

The OSIRIS code structure was also updated, with significant changes to the object hierarchy, and new current deposition modules are under development that will result in a significant performance boost.

Standard PIC "collisions" occur between finite sized particles. It is an inherent property of the PIC algorithm that collisional effects therefore are not properly reproduced in a standard PIC algorithm, due to limitations in grid size possible with available computing power. In order to fully deal with collisional effects the standard PIC algorithm must be extended. Several extensions were proposed. For osiris, we follow the approach of binary collisions [Takizuka and Abe 1977, Nanbu 1997], generalized for the fully relativistic scenario.

As is the rest of OSIRIS the implemented algorithm is fully relativistic. Osiris uses different weights for different particles. The collision algorithm is able to deal with this circumstance without violating any of the conservation laws (i.e. energy- and momentum- conservation) [Nanbu and Yonemura 1998].

13.4.2 dHybrid[8]

A hybrid code called dHybrid has been used in the study of space plasma interactions. Hybrid codes, due to the use of kinetic ions and fluid electrons, allow an intermediate step between full particle codes and fluid codes. The applicability of such codes ranges from low density plasmas like space plasmas to denser plasmas like the ones found in tokamaks.

The first massively parallel version of dHybrid is now ready to completion. This code, originally written to study the solar wind interaction with an artificially created plasma cloud (AMPTE release experiments) has now new important features that broaden its applications (Figure 13.8). Studies such as solar wind interactions with artificial magnetospheres and coronal mass ejection interactions with the solar wind are now possible.

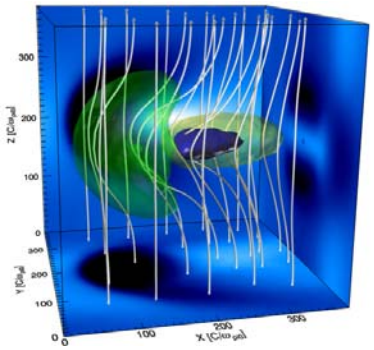

Figure 13.8 - Magnetic field isosurfaces and field lines of the artificial magnetosphere at time 72 (simulation units). The solar wind flowing from the left exerts pressure on the system and creates asymmetry.

The new version of the code allows better results due to improved statistics in these runs, which is possible only due to the use of massively parallel machines. New problems like the solar wind interaction with planetary exospheres (e.g. Mars, Venus) and planetary magnetospheres (eg. Earth) can now be considered.

[7] Work carried out in collaboration with F. Tsung and W. B. Mori (UCLA)

[8] In collaboration with R. Bingham (RAL)

13.4.3 Visualization infrastructure

Visualization is an essential part of any numerical laboratory. The data being produced by our simulations is both large and complex, and requires an appropriate set of tools for the adequate understanding of the results obtained. We therefore developed a custom visualization and analysis infrastructure for our needs, that has been successfully used with several simulation and experimental data sources, most notably the OSIRIS code, the QUICKPIC code and the dHybrid code.

The development of this infrastructure continued over 2005, and as a result of user feedback led to the development of new visualization tools, Significant work also went into the development of the new version of the visualization and data analysis routines, that will allow for better user-data interaction, and also provide a unified interface for representing data and metadata in encapsulated objects (Figure 13.9).

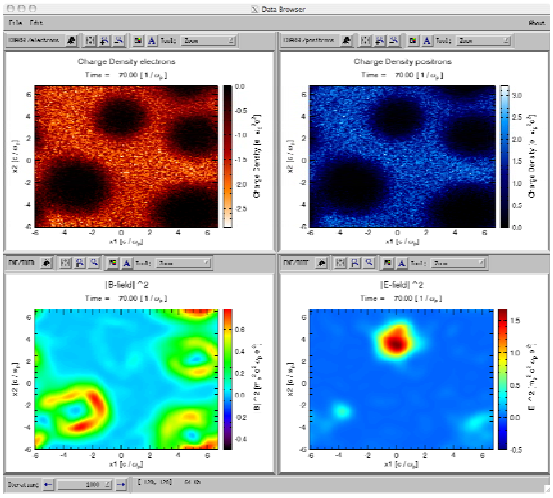

Figure 13.9 - Simulation Browser. This simulation tools allows for quick access to multiple diagnostics for the same time step. The navigation tools (zoom/pan) for all the plots are linked.

Different new visualization software for very large datasets was evaluated (VTK, OpenDX, SciRun), and finally VisIt was chosen (a visualization program from Lawrence Livermore National Laboratory, USA), because it was the only one to offer all the features needed: parallel data processing and rendering (distributed and shared memory), scriptable, expandable, high performance and scalability, multi platform, uses VTK and it is Open Source (Figure 13.10).

A database plugin was developed for VisIt, that allows the full exploration and rendering, in parallel, of Osiris and dHybrid simulation results, in particular of very large datasets of 3D vectorial data (Figure 13.11).

Research has been done in *the development of general purpose algorithms for the modern graphics processor* (GPGPU). Simulation algorithms can be accelerated by passing some of them to the shader unit of the GPU and taking advantage of its vectorial capabilities. A development system has been set up on the visualization cluster that allows for general research on this kind of algorithms and for research on parallel versions (distributed memory) of GPGPU.

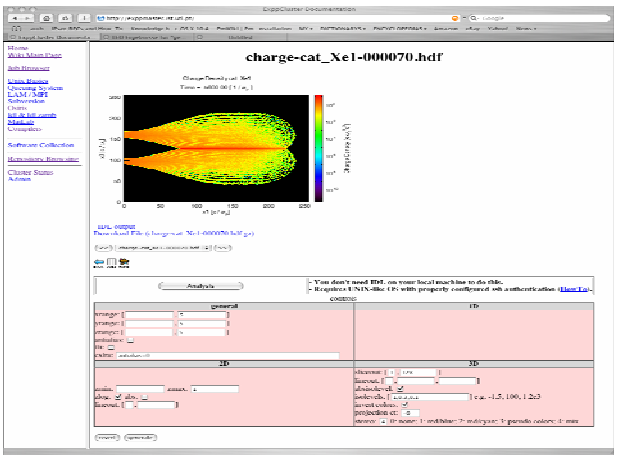

Figure 13.10 - Data visualization and users interface as seen in a web browser.

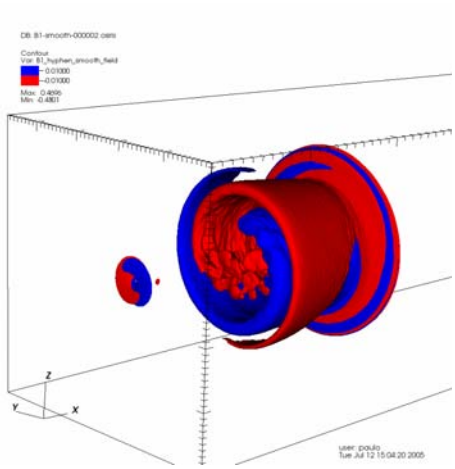

Figure 13. 11 - Visualizing the inverse Faraday effect in VisIt.

13.5. ASTROPHYSICS AND SPACE PLASMA PHYSICS

13.5.1 Plasma thruster dynamics and charge exchange collisions

With the goal of *understanding the full kinetic dynamics of the charge exchange back flow originating from the plume injected from a spacecraft,* and to understand how relevant the electron dynamics is in such scenario (in particular, to understand if a Boltzmann equilibrium for the electrons can be assumed in such configurations) several multi-dimensional particle in cell simulations have been performed in osiris 2.0 (Figure 13.12). In these scenarios charge exchange (cex) collisions play an important role, as they are responsible for the slowing down and thermalization of the fast ions originating from the thruster plume. Consequently a cex-module has been written and

tested for osiris 2.0. This module is an extension of the existent neutral module and allows for cex collisions to occur between multiple neutral and multiple charged species. Different models for the cross-section of interaction are available and fully parameterized. Proper accounting for the charge and mass transfer between the collision partners is conducted.

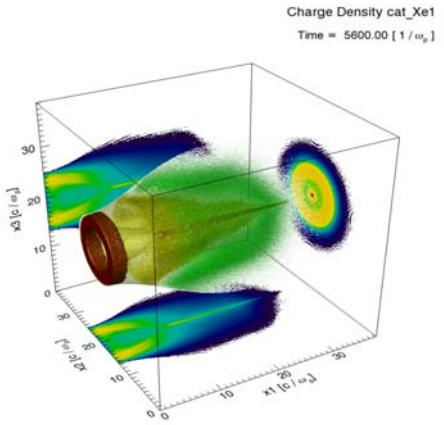

Figure 13.12 - Xe+ ions originating from the thruster. The thruster plum pinches after a stage of free expansion leading to higher flow velocity. Densities [e ω03c3]: red 1, yellow 0.3 and green 0.1.

13.5.2 Development of Plasma Reflectometry for In-Flight Aerothermodynamic Research[9]

The reflectometry for in-flight aerothermodynamic research project is a new comprehensive project involving theory development, instrument design and prototype development. The principal objective of this project is *the measurement of plasma density profiles surrounding a re-entry vehicle* as it comes into the atmosphere. Use of electromagnetic waves constitutes a powerful plasma diagnostic method. Due to the large electron to ion charge to mass ratio, it is primarily the electron properties of the plasma which can be obtained at microwave and higher frequencies.

The physical parameters of relevance to plasma reflectometry in the shock layer of a re-entry vehicle, are the plasma density, neutral density and temperature. These are characterized on the basis of computational fluid dynamics (CFD), in order to define a reference environment and to set up an optimum measurement strategy.

A typical case is the European Experimental Reentry Testbed (EXPERT) vehicle scenario. For this vehicle, the ionization shocked layer and the plasma sheath is thin, roughly at most 20 cm thick on the side and 1/3 of that in the nose region. The expected plasma frequencies for a 6.8 km/s re-entry speeds appears in the figure 13.13. The plasma distribution along a normal line to the vehicle surface is approximately parabolic. The electron density goes to zero at the surface, in the catalytic case, while it is the electron density gradient that goes to zero in the non-catalytic case. Plasma gradients can be very high with 1 GHz frequency change over a 1 cm distance fairly common.

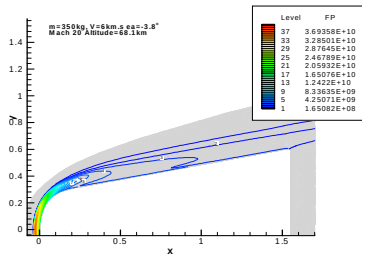

Figure 13.13 - Predicted plasma characteristics for a 6 km/s re-entry speed for EXPERT.

13.5.3 Magnetic field generation in clusters of galaxies[10]

Magnetic fields are ubiquitous in cosmic objects, from stars and galaxies, to galaxy clusters, the largest gravitationally bound objects in the Universe. The origin of these fields, observed to be as strong as a few micro-Gauss in a number of clusters, remains one of the outstanding problems of modern cosmology. Conventional explanations involve the amplification of a very weak seed field of possibly primordial origin by turbulence and gas compression during the formation of the cluster. However, the origin of the nano-Gauss seed field that is required remains a mystery. We have *demonstrated that cluster magnetic fields could have been produced by shocks* propagating through galaxy clusters and in the intercluster (ICM) medium during the formation of large-scale structure. We have performed three-dimensional particle-in-cell simulations of a nonrelativistic shock in a electron-proton plasma that show that such shocks generate a magnetic field via the counter-streaming (Weibel) instability (Figure 13.14). The strengths of the shock-generated fields range from tens of nano-Gauss in the ICM through few micro-Gauss inside galaxy clusters. Thus, cluster magnetic fields may be explained without resorting to amplification of a primordial magnetic field.

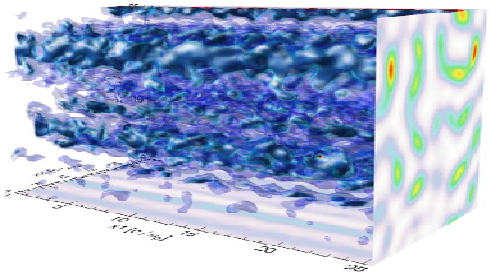

Figure 13.14 - The three-dimensional structure of the magnetic field generated at nonrelativistic collisionless shocks.

[9] Work carried out in collaboration with G. Vecchi, V. Lancelloti, R. Maggiora (Poli Torino), M.E. Manso, and L. Cupido (CFN)

[10] Work performed in collaboration with M. Medvedev and M. Kamionkowski (Caltech)

14. EXPERIMENTAL PHYSICS AND TECHNOLOGICAL DEVELOPMENTS ON ULTRA INTENSE LASERS, RADIATION SOURCES, PLASMA BASED ACCELERATORS AND BIOMEDICAL OPTICS

J. T. Mendonça (Head), J. M. Dias, M. Fajardo, G. Figueira, N. Lopes, R. A. Fonseca, J. A. Rodrigues, L. O. Silva, L. Cardoso, J. Wemans, C. Leitão, N. Lemos, F. Wahaia, E. Abreu, N. Brites, R. Macedo, J. Sampaio, A. Smith, F. Viola

14.1. INTRODUCTION

Research in experimental physics at GoLP/CFP covers fundamental and applied aspects of lasers, laser-plasma interactions, intense x-ray and vuv sources, biomedical optics, as well as technology developments for the support of these activities. A significant part of this work is associated with the activities of the Laboratory for Intense Lasers (L2I), the central experimental infrastructure maintained by GoLP. The key aspects of research in 2005 dealt with:

- Laser physics and laser technology;
- X-ray and VUV sources and their interaction with plasmas;
- Plasma channels for laser-plasma accelerators;
- Tunable radiation sources;
- Biomedical optics

14.2. LASER PHYSICS AND LASER TECHNOLOGY

14.2.1 Mirrorless tilted-pulse-front single-shot autocorrelator

Ultrashort pulses exhibiting angular dispersion have their pulse front tilted relative to the phase front. This leads to a serious degradation in the focused peak power, making the use of adequate diagnostics indispensable.

We have developed an upgrade to a previously demonstrated autocorrelator for ultrashort laser pulse-width measurements that extends its versatility, by making it suitable for detecting and correcting tilted pulse fronts. The device, called *a tilted-pulse-front single-shot autocorrelator* (TPF-SSAC) can be used to detect tilts in pulse fronts and perform pulse autocorrelation along any arbitrary direction.

The principle of the TPF-SSAC is to decouple the measurements of the autocorrelation shape and the amount of pulse-front tilt: One of the replicas is flipped in both planes, and the tilt is detected in each direction at a time by correlating the replicas in the orthogonal direction. In this fashion, the presence of a tilt will result in an oblique autocorrelation, as shown in the figure below.

Our modification consisted in introducing two orthogonal Dove prisms to provide horizontal and vertical flipping, converting this autocorrelator into a TPF-SSAC. The figure 14.1 shows this experimental arrangement.

We have used this modified TPF-SSAC to optimize the alignment of the grating compressor of our terawatt CPA laser. We found that initially there was a small pulse-front tilt present in our compressed pulse, which was easy to correct with the aid of this diagnostic. The resulting autocorrelation trace is shown in Figure 14.1.

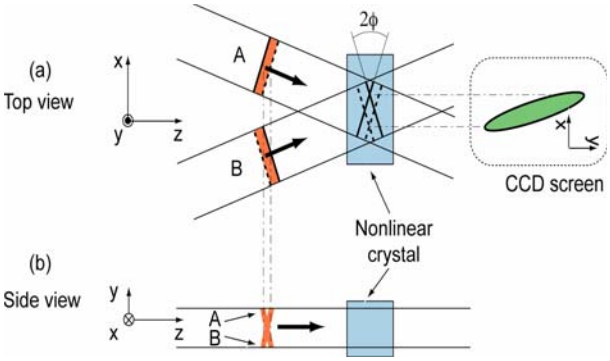

Figure 14.1 – Schematic of tilted pulse front autocorrelator geometry.

To illustrate the capability of the device, we have also acquired a trace of the autocorrelation for a large front tilt, introduced by deliberately deviating the grating pair from parallelism and correcting for the resulting change in their separation in order to obtain the shortest autocorrelation, also shown in the Figure 14.2. From this, we can appreciate that the actual trace width does not change significantly from the corrected version, which illustrates the necessity of using this kind of autocorrelator.

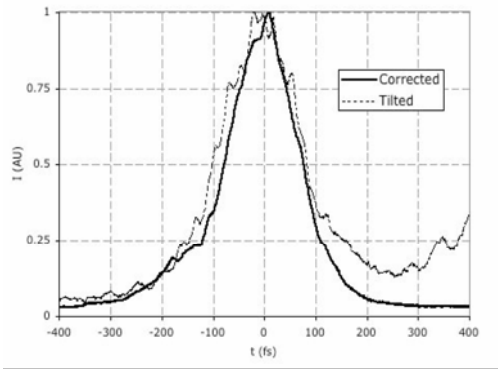

Figure 14.2 - Autocorrelation traces of corrected (solid line) and tilted (dashed line) pulse fronts

14.2.2 OPCPA at GoLP

Optical parametric processes are not new, but their application in laser amplification, especially in high power pulses, is quite recent. Optical parametric amplification can combine a very high gain per pass, tunability and a

broad bandwidth. Adding to it the chirped pulse amplification technique to avoid the inconvenience of excessive peak power inside the laser system, and we have a versatile and relatively efficient way to achieve short, high power laser pulses. Due to the short path needed inside the amplifying media (Figure 14.3), femtosecond pulses suffer little distortions and lengthening, enabling petawatt range pulses to be raised out of the energy of mere terawatt range pump beams.

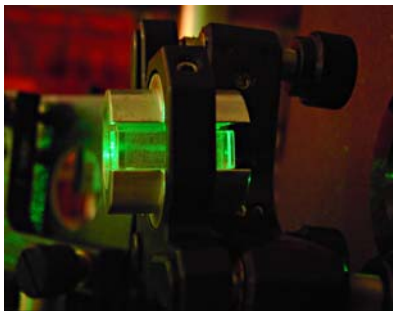

Figure 14.3 - BBO non-linear crystal: the amplifying media where the green pump beam transfers its energy to the infrared signal beam.

Presently we want to demonstrate we can master this promising technique by running mid power amplifiers and comparing the experimental against the expected theoretical results. The equipment in the current setup is likely to become part of some future secondary/probe beam, provided a new pump beam is made available.

Concurrently, there are plans to use OPCPA as an "upgrade" to L2I's multi terawatt laser system, whose beam, the whole or in part, would be used as a pump for a possible petawatt range system.

14.2.3 Ultra Broadband OPCPA – from the theory to the demonstration

The creation of a 3D compatible simulation code for the better understanding of the OPA process provided the conditions to find a new geometry allowing the amplification of ultra broadband pulses. Usually both signal and pump are input in the crystal propagating at given fixed directions which, in general, allows a quite limited gain bandwidth. But the optimum input angle actually varies rather smoothly and predictably with the signal wavelength. It is then possible to angularly disperse the broadband signal, with a grating for example, to interact with the pump beam at close to the optimum angle over a large bandwidth.

To demonstrate this concept we use a slightly modified version of our first OPCPA setup, but we also need to get a broadband signal. That is being arranged by a photonic crystal fibre tailored to generate white light supercontinuum out of our sub-20 nm wide, ~100 fs oscillator.

This technique will enable the simultaneous amplification of wavelengths spanning for almost one octave (Figure 14.4). This will allow *the construction of tuneless amplifiers for tunable narrow band oscillators* or, exploring its full potential, the support of sub-10 fs pulses with excellent contrast.

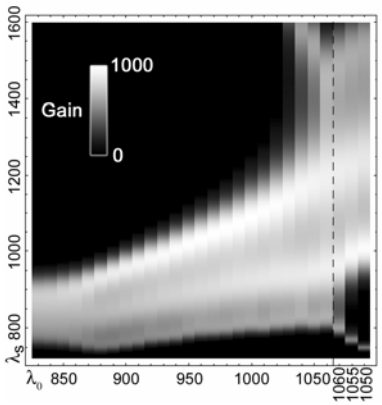

Figure 14.4 - Spectral gain profile (λS/nm) vs. reference signal wavelength (λ0/nm), when signal angular dispersion is optimised for the broadest bandwidth in BBO pumped with 532 nm.

14.2.4 Characterization of the dynamical behavior of diode pumping induced thermal lens on a Yb:phosphate glass[1]

We measured *the characteristic focal length of the thermal lens effect induced in a Yb:phosphate glass pumped by a high intensity diode laser pulse* (Figure 14.5). Because the glass is the active material of a laser amplifier setup its was necessary to define some special characteristics of the thermal effect: the ideal amplification section in the glass where the thermal lens effect is constant; the temporal dynamics of the effect during a single pump pulse and through the first warm-up pump cycles; the dependence of the effect with the pump intensity. The overall goal of the study was to provide vital information about the thermal effects that can be applied in improving the performance of laser amplifiers based on this active medium and pump setup.

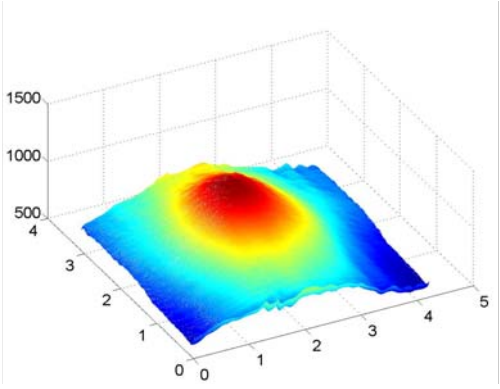

Figure 14.5 - 3D visualization of the wavefront distortion induce to the laser beam during one pass trough the glass at full pump.

[1] Work carried out collaboration with the Polaris group in the Institut für Optik und Quantenelektronik, Jena

The treatment of the interferometric data showed the presence of induce thermal lens with focal distances of 1.5 m at full pump power and uniform in a 1.5 mm diameter section of the glass. The temporal behaviour of the thermal lens was measured and the dependence with the pump intensity defined.

14.2.5 Dual Nd:glass rod amplifier operation of L2I's laser chain

The electronics and software at L2I was initially designed and assembled for firing a single Ø16 mm Nd:glass laser amplifier from Quantel, based on a synchronous handshake pattern between a main computer with Labview® software and the digital delay generator controlling the sequencing of the laser pre-amplifier. The signals were received and processed at L2I's main electronic console, and the firing event – involving charging the capacitor banks, receiving an end-of-charge confirmation, and providing a synchronous firing order – was transmitted via fibre optics to receiver boxes located inside the amplifier power units.
The addition of a new Ø45 mm amplifier, also from Quantel, required a *modification in the triggering electronics:* although coming from the same manufacturer, the two amplifiers were based on technologies that were a few years apart. The electronic upgrade was performed at the level of the amplifiers' receiver boxes, in order to trigger simultaneously both amplifiers and preserve the original handshake pattern. The use of two of these receiver boxes was found to cause electronic offset levels in the triggering signals; in order to solve this, new optical-to-electrical conversion circuits were designed and built, which produce a single control signal.

14.2.6 Setup, alignment and characterization of a high power CW Nd:YLF laser

In March 2005 we received two high power Neodymium:YLF laser oscillators donated by the Central Laser Facility (CLF) of the Rutherford Appleton Laboratory. Their high power (>10 Watts, continuous) allows the beam diameter to be expanded to several centimetres, which is ideal for aligning the high-energy stages of the L2I laser. In particular, the diffraction gratings used in the compressor must be aligned with a precise reference wavelength.

These high power lasers demanded considerable requirements in terms of three-phase power consumption and water cooling, which together with the physical size of their power supplies led to a remodelling of the laboratory room where they are housed.

The lasers required a number of replacement components and a detailed evaluation of their operating procedure.

The laser was further characterized in terms of the efficiency (Figure 14.6) and beam shape of the various modes. For the TEM00 mode, an evaluation of the role of the Fresnel number of the cavity in the efficiency was also performed, by adjusting an intra-cavity aperture. The measurement of the beam shapes for the several cases allowed us to determine the effective beam intensity.

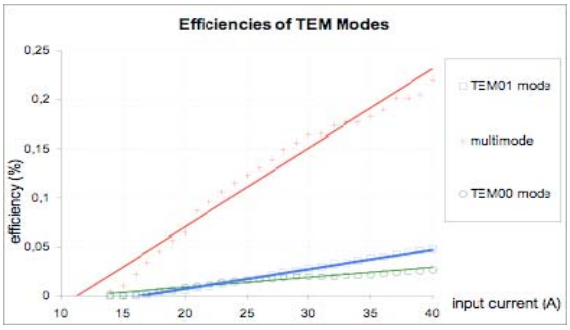

Figure 13.6 - Efficiency of the several lasing modes as a function of the input current.

14.3. X-RAY AND VUV SOURCES AND THEIR INTERACTION WITH PLASMAS

14.3.1 Novel XUV Sources: Second Generation X-ray Lasers

High Harmonic Amplification is shown in an Optical-Field Ionized X-ray laser. The 4d-4p X-ray line of Kr at 32.8 nm, which has a close match to the 25th harmonic of the infrared laser, was amplified up to 200 times. Energy extraction regime was also achieved, depending on the level of seeding. This *second-generation X-ray laser* is fully polarized, has low divergence and shows a high degree of coherence. The duration is also expected to be short, fulfilling the requirements for *an ultra-intense tabletop X-ray laser.* Conditions for higher energetic output are also suggested.

In the experiment shown (Figure 14.7), we have used, for this second generation X-ray laser, a well-characterized, short-pulse, coherent and polarized High Harmonic seed, an image relay to focus the harmonic pulse onto the amplifier plasma, and a low-density amplifier medium with a population inversion in the XUV, which keeps the perfect optical properties of the seed.

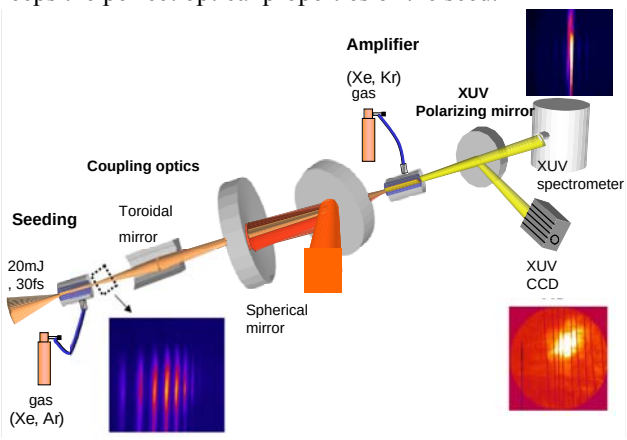

Figure 14.7 - Experimental setup for seeded optical field. ionization x-ray laser at Laboratoire d'Optique Appliquée

We have shown that tabletop X-ray lasers have reached a second generation by extending the concept of an optical laser chain to the XUV. The seeded X-ray laser is a new X-ray source, which may serve as a lower intensity complement to the forthcoming XUV-FELs. While further studies must be made to determine the amplified pulse duration, due to the high optical properties of the beam we may expect to reach unprecedented XUV intensities on a tabletop, allowing to bridge the gap between current X-ray sources and future ultra-bright XUV free electron lasers.

14.3.2 X-ray Optics: VUV FEL wavefront measurements

We have characterized for the first time the wavefront of an XUV Free Electon laser (Figure 14.8). The experiment was performed at DESY in November 2005.

A 30 nm VUV Free Electron Laser was focused using a grazing incidence toroidal mirror. The resulting divergent beam was propagated under vacuum onto a Hartmann plate followed by a back-thinned, cooled CCD. The full beam coming from the XUV toroidal mirror was then recorded. Several shots were made showing a beam fluctuation over 200mrad, incompatible with usage of the beam for high intensity focusing. As saturation of the laser was not achieved during the course of the experiment, a better performance is expected for future experiments.

The VUV-FEL mean energy was around 5μJ. Using a noble gas in the beam path as attenuator, we were able to record *single-shot measurements of the VUV FEL wavefront* for the first time.

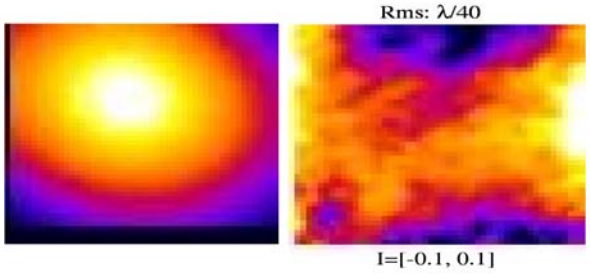

Figure 14.8 - Raw data for wavefront measurement using spherical wavefront (sensor calibration). Left: intensity on sensor; right: wavefront displacement in units of λ

14.4. PLASMA CHANNELS FOR LASER-PLASMA ACCELERATORS

14.4.1 Capillary plasma discharges for electron accelerators[2]

The development of compact laser-plasma electron accelerators in the GeV range is an important step in the accelerator research after the recent demonstration of the capability of these accelerators to produce monochromatic electron bunches in recent experiments. These energies can be obtained by extending the acceleration length well beyond of the Rayleigh length, using some type of guiding.

A new set of *guiding devices for ultra intense lasers* was designed, built and tested (Figure 14.9). These devices use a set of glass capillaries (aligned to a common axis) about 2.5 mm long separated by 0.8 mm gaps and located between two conic-shaped metallic electrodes with a hole on the apex. The distance between the electrodes and the first and last capillary surfaces is 0.2 mm. The plasma in the gaps between the capillaries can be imaged to outside and probed by a laser beam orthogonal to the device axis (Figure 14.10).

These guiding devices need an extensive dynamic characterization using different high-voltage pulses, hydrogen pressures and filling times. However, this preliminary results show guiding for distances up to 1 cm at plasma densities compatible with GeV energy gains. The use of these devices for high-intensity laser propagation are the objectives of 2006 research.

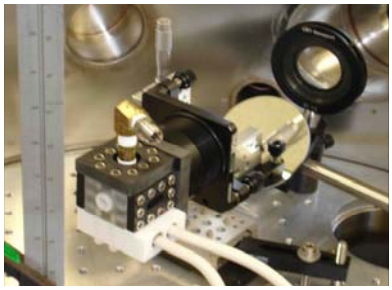

Figure 14.9 - Picture of a 1 cm plasma channel prototype mounted in the target chamber

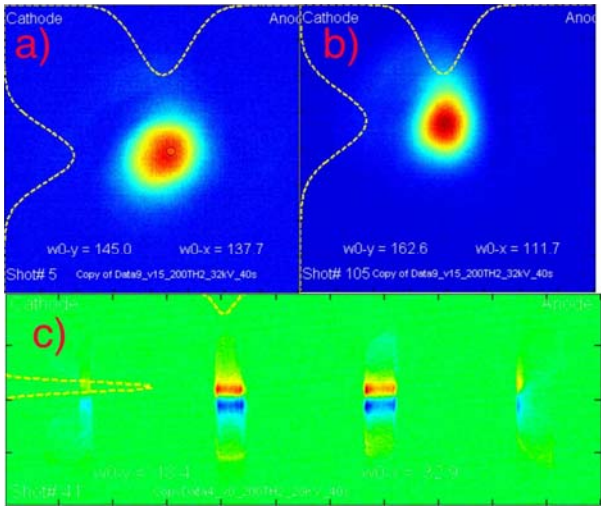

Figure 14.10 - a) image of f/50 focal spot taken at capillary entrance; b) image of laser beam taken at exit of capillary showing light focusing due to interaction with plasma; c) Schlieren image of plasma capillary obtained by propagating a probe beam through the capillary gaps perpendicularly to the plasma channel axis.

[2] Work performed in collaboration with F. Fang, and C. Clayton (UCLA).

14.4.2 Development of a short pulse high-voltage source for plasma channels[3]

The goal of the project described here is the development of a device to generate *ultra-short high-voltage (HV) pulses to produce plasma channels.* A functional discharge-based plasma channel requires a high-voltage pulse in excess of 30 KV/cm with steep rising and low jitter. Our goal is to develop the channel in two stages: first, a high voltage (50KV), high impedance (400Ω) and short (10ns) pulse will ionize the plasma and secondly, a high current (≥200A) capacitive discharge will heat the plasma during up to 150 ns, creating a suitable plasma density profile for guiding high intensity laser light.

The system is composed of 4 main parts: an HV source (off-the-shelf), a pulse forming switch, which has to be fast and low in resistance, a transmission-line transformer (TLT), which increases the amplitude of the pulse to the final voltage and a shockline which shapes the pulse, shortening its risetime (Figure 14.11).

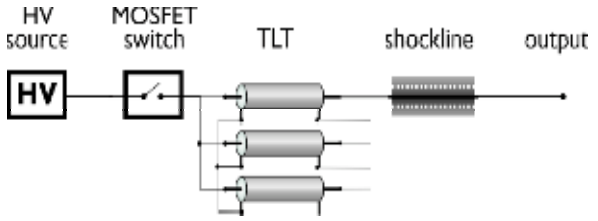

Figure 14.11 - General arrangement of the several components of the device

Although several HV switch technologies can be used, the use of MOSFET technology is considered the most promising for our parameters. In comparison to the thyratron technology it presents shorter risetime, lower jitter and allows to control the opening of the switch and therefore the discharge duration.

Figure 14.12 - MOSFET switch module, showing 7 MOSFET units. The main MOSFET is seen on top, and part of the protection and driving circuitry is directly below

The first prototype devices were built at UCLA. They were used to study the behavior and operational limitations of the several components and to test the device as a whole.

Two switch prototypes were built. The first, conceived only to test the feasibility of the design, consisted of only 4 MOSFET switches in series and its respective triggering and protection system. The second switch was composed by 14 MOSFETs in series, capable of a stand-off voltage of 10KV (Figure 14.12).

A HV ultrashort electric pulse generator was conceived and a first prototype was built. This has allowed for the demonstration of this technology as possibility for current experiments on the generation of plasma channels.

14.5. TUNABLE RADIATION SOURCES

14.5.1 Relativistic Mirror for THz Radiation Sources[4]

The Strathclyde Terahertz to Optical Pulse Source (TOPS) at the Scottish University of Strathclyde in Glasgow, is one of the few facilities in Europe that provides high power few-cycle visible and near-infrared laser sources, together with sub-cycle electromagnetic pulses in the far infrared (mm-wave or terahertz spectral region). We have started this collaboration in order to perform experiments on the production of *relativistic mirrors generated by ionization fronts, for sub-cycle terahertz radiation pulses.* The aim of those experiments is to obtain sub-cycle visible radiation by the double Doppler relativistic effect.

During this year we have installed the experimental setup for generating the ionization fronts (Figure 14.13). The ionization fronts were produced in a pulsed supersonic gas jet (Mach 3) of Argon inside a vacuum chamber. In order to characterize the generated plasma a Mach-Zehnder interferometer was installed in the diagnostic beam. The spectral contents of the ionization pulse were also recorded using a spectrometer. Several plasma profiles and spectra were obtained. In parallel we have started preliminary simulations in the EPP cluster using the Osiris 2.0 code reproducing the experimental conditions.

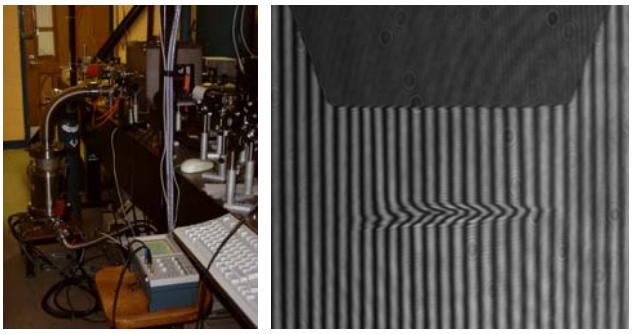

Figure 14.13 - Experimental setup (left) and interferogram of the plasma in the gas jet (right)

14.5.2 Design and characterization of gas jets for laser-plasma interactions

Experiments on high intensity laser-gas interaction require the use of sharp edge and well-defined pulsed gas jets in order to avoid ionization induced refraction and achieve the maximum intensity on the focal spot. *Supersonic Laval nozzles* can produce sharp gas jets in vacuum with uniform gas density and are suitable for many applications.

[3] Work carried out in collaboration with C. Clayton (UCLA)

[4] Work performed in collaboration with D. Jarozinsky's group (U. Strathclyde)

To analyse the interferograms obtained from the Mach-Zehnder interferometer it was developed an automatic fringe-pattern analysis code.

Observing the density profiles for different initial pressures applied to the nozzles, it was possible to see three different nozzle flows (overexpanded, ideal, underexpanded). As predicted by the theory, the ideal and the underexpanded flows were the ones that had less shock waves.

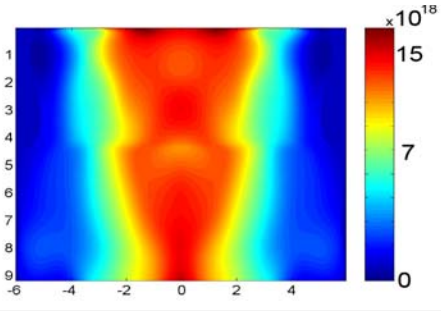

Figure 14.14 - Density profile of a Laval nozzle (8mm exit diameter)

14.6. BIOMEDICAL OPTICS

14.6.1 Axial myopia reduces laser dose in the photodynamic therapy[5]

Pathologic myopia is diagnosed when axial length of the eye is greater than 26,5 mm and when distance acuity is greater then 6 diopters. This rare type of myopia, in which the eyeball continues to elongate, has been reported to be a major cause of blindness in young patients. Nowadays the most popular treatment to CNV is photodynamic therapy (PDT). The PDT therapeutic standard protocol consists in administrating Visudyne® by intravenous injection, followed by application of a non-thermal red laser light (λ=689 nm) with an irradiance of 600 mW/cm2 (Figure 14.15).

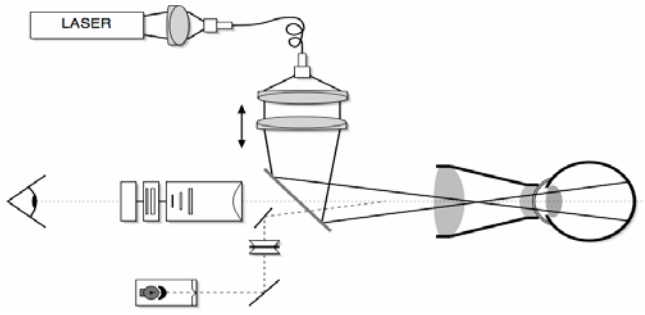

Figure 14.15 - Schematic diagram representing the output laser system, the slit lamp, the accessory Mainster lens and the patient's eye in the PDT treatment.

As the refractive eye's power is one of the main factors that determine the size of laser spot in the retina and its irradiance power, it should be taken in consideration, especially in pathologic myopic eyes. Moreover the eyes that had been corrected with intraocular lens implants, had also suffered significantly changes in their refractive power. One important question that arises is how these changes can affect the laser spot size and irradiance in the PDT treatment. In this work we evaluate not only the *influence of eye's axial length in laser spot size in retina and variation in laser irradiance in PDT in high myopia, but also to study the influence of intraocular lenses in induction of laser dose reduction in this treatment.*

For the optical model we have used Liou and Brennan model, among other corrections to match our problem. These models were integrated using Oslo-LT Edition 6.1 optical design software (Lambda Research Corporation).
The increase of eye's axial length implies an increase in laser spot size in retina with a linear correlation. Consequently, for the same output laser power, the irradiance changes inversely with the square of the projection size of the laser spot in the retina. For operated eyes with the corrective pseudophakic implantation will increases even more the retinal laser spot dimension, and consequently will aggravate the induced irradiation reduction.

This study demonstrate that axial length of the eye reduces progressively the light dose in photodynamic therapy. The axial length is an important factor to take in consideration for ensuring, safety, reproducibility of clinical results and optimization of photodynamic therapy in high myopics eyes. Therefore the axial length is an important parameter that should be taken in to account for the elaboration of future Visudyne treatment protocols in pathologic myopia.

14.6.2 Diffraction enhanced imaging

Point-source X-ray radiography is a well established technique for probing dense objects, and laser-produced Kα sources, with time resolution down to 2 ps, have been used for X-ray imaging of biological objects [1] or dense plasmas [2]. The incident radiation is partially absorbed by the object, and the transmitted image depends on the object's thickness and constitution. However, these images lack definition, namely at the borders of the object, due to poor contrast of X-ray absorption far from absorption edges.

Our aim is to achieve the same *enhancement in contrast* on the object's structure, *by means of a Bragg crystal.* A numerical analysis of the imaging experience was made, using a 7 Å x-ray plasma as light source, and a TLAP crystal (d = 25.8 Å) for the phase shift enhancement. Two objects were considered: a simple cylinder (made of SiO2, with a 5μm radius) and an empty cylinder (made of SiO2, with a 5μm outside radius and a 2μm inside radius). For these two objects it was possible to compare absorption and phase contrast images (Figure 14.16).

The results obtained for the simple cylinder were equivalent to the ones shown above with a capillary. The

[5] Work carried out in collaboration with António Castanheira Dinis (CECV-FML), João Nascimento (Instituto Gama Pinto), Pedro Reis (ALM)

enhanced phase contrast technique clearly represents a gain in definition for the borders and the details inside the object. Moreover, these results correspond to 78 photon/pixel or 97 photon/pixel maximum photon densities on the detector, for the simple and empty cylinder respectively, meaning this experience could be made with a single shot.

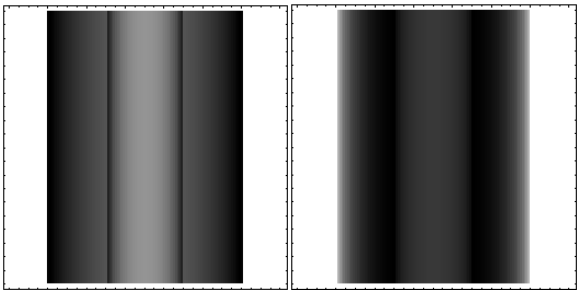

Figure 14.16 - Image of an empty cylinder: left) with absorption alone; right) with absorption and enhanced phase contrast

14.6.3 Optical aberrations: wavefront reconstruction and simulation of visual acuity[6]

All optical systems suffer from aberrations that limit the quality of the image produced. The human eye, besides its complex and exquisitely designed optical system, is no exception. Surprisingly, our visual system has a poor image quality by comparison to man-made optical systems. Visual acuity is defined as the spatial resolving capacity of the visual system. This may be thought of as the ability of the eye to see fine detail. Visual acuity is limited by aberrations, diffraction, and photoreceptor density in the eye. Previous studies have concluded that human optical aberrations can be influenced by the pupil size, age and the refractive surfaces of the eye.

The aberration map can be reconstructed from measures of the eye's wavefront. Typically the measures are taken using a wavefront aberrometer. The outputs of the majority of the devices are aberrations maps and several metrics, as pupil diameter and the zernike coefficients. Normally these maps and metrics are not sufficient to predict visual acuity (Figure 14.17).

In order to predict visual acuity we implemented *an algorithm that reconstructs the eye's wavefront by fitting the zernike coefficients to the zernike polynomials.*

The computational simulation was tested using both synthetic data and real data from examinations performed with a ZywaveTM wavefront aberrometer from ALM – Oftalmolaser Medical Center.

By studying optical aberrations we can estimate not only visual acuity, but also plan ways to correct it. It is also possible to compare different lenses and different surgery techniques.

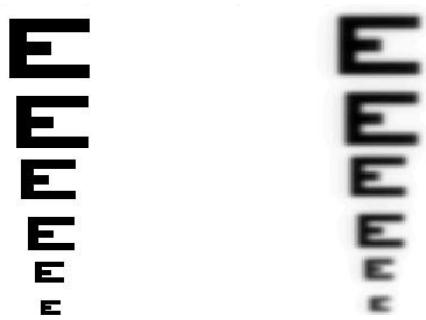

Figure 14.17 - Left: original image – Snellen Chart; Right: the same image degradated due aberration plotted in the left eye of a woman. Metric 36/6 means that the eye is able to see at 6 meters what the "standard eye" sees at 36 meters.

[6] Work performed in collaboration with António Castanheira Dinis (CECV-FML), João Nascimento (Instituto Gama Pinto), Pedro Reis (ALM).

15. SPACE PLASMA PHYSICS

A. L. Brinca (Head), F. J. Romeiras and M. H. Marçal

15.1. INTRODUCTION

The research work carried out by the Space Plasma Group in 2005 falls into the following main fields of investigation:

- Totem Pole emissions;
- Effects of large-amplitude waves on linear instabilities;
- Nonlinear wave equations: integrability and exact solutions.

15.2. TOTEM POLE EMISSIONS

15.2.1 Introduction[1]

Totem Pole emissions were first observed near the dayside magnetopause by the Geotail spacecraft in 1997. They are electrostatic electron Bernstein waves whose characteristics are not fully explained by the standard model invoked for the generation of this type of wave activity. In particular, the occurrence of harmonic branches above the upper hybrid frequency and the fine spectral structure of the lower frequency emissions could not be interpreted in the context of the model adopted to study Bernstein waves in the magnetosphere.

The classical paradigm associated with electron Bernstein emissions uses an admixture of cold and hot electron populations neutralized by a background of immobile ions, with the perpendicular velocity distribution of the hot species providing the free energy, and the emphasis placed on modes propagating slightly away from the perpendicular (with respect to the background magnetic field).

We adopted *an alternative source of free energy to stimulate electron Bernstein waves:* the almost *monoenergetic ion (AMI) beams* recently observed by the Interball 1 spacecraft. The success of this model led to its utilization in the context of the Totem Pole emissions where it was demonstrated that AMI beams could generate electron Bernstein emissions both below and above the upper hybrid frequency (as observed by the Geotail spacecraft) and provided a simple means of accounting for the fine spectral structure found in the lower harmonic bands (Figures 15.1 and 15.2).

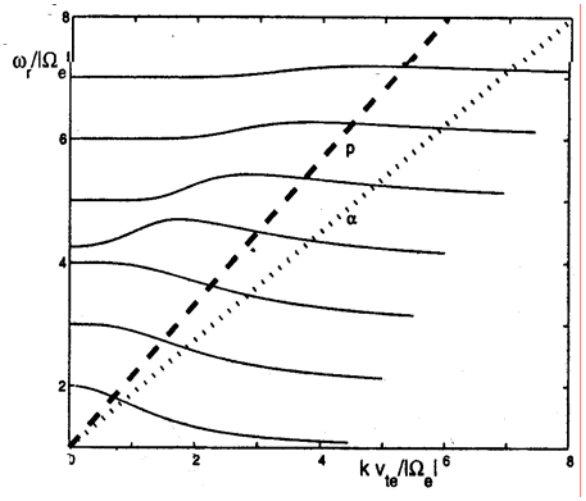

Figure 15.1 – Dispersion of the first seven electron Bernstein flute modes in a hydrogen maxwellian plasma with B_0=55 nT, T=30 eV and N_0=0.5 cm^{-3}. The straight lines indicate the perpendicular drift velocities of the proton (dashed) and alpha particle (dotted) beams.

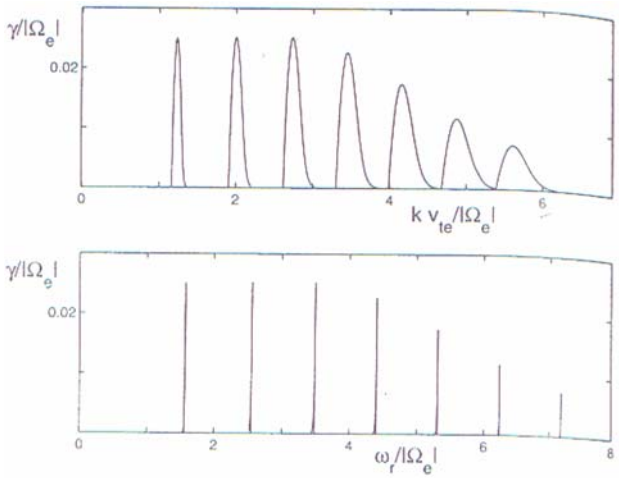

Figure 15.2 – Temporal growth rates of the first seven electron Bernstein flute modes stimulated by a perpendicular proton beam as a function of the wavenumber (upper panel) and the real frequency (lower panel).

15.2.2 Ongoing research

The previous work led to an original mechanism that offers a consistent interpretation of the main features encountered in the observations of Totem Pole emissions, relying on the properties of linear instabilities. Understanding of finer details displayed in the emissions spectrograms could benefit from the analysis of the nonlinear evolution of the

[1] This research line has been carried out in collaboration with Prof. Luis Gomberoff, Physics Department, University of Chile at Santiago and partially funded by FONDECYT (Chilean Institute).

growth associated with the identified linear instabilities. To pursue this goal, we are assessing the possibility of adapting a numerical kinetic (particle in cell) code developed in Kyoto University (Kempo1) to simulate the proposed model underlying the emissions and thus follow the nonlinear regime of the instabilities.

15.3. LARGE AMPLITUDE WAVES AND INSTABILITIES

15.3.1. Introduction[2]

Electrostatic ion-acoustic instabilities have been observed in space environments (e.g., in the solar wind) where both the nature of the free energy source and the inexistence of the condition for small Landau damping (Te >> Tp) are not encountered and thus defy the standard theory of these instabilities.

15.3.2 Research results

To contribute to the interpretation of the above observations, we looked into the generation of electrostatic waves by *parametric decays of large-amplitude left-hand and right-hand waves propagating in the direction of the background magnetic field.* It is shown that the forward propagating ion acoustic waves involved in the parametric decay of the circularly polarized waves experience negligible Landau damping and can thus account for the puzzling observations of electrostatic ion-acoustic wave activity.

15.4. NONLINEAR WAVE EQUATIONS

15.4.1 Introduction

The study of nonlinear wave equations is a problem of considerable theoretical importance and with applications to several branches of Physics. In the case of Plasma Physics, it is relevant to the study of the interaction of pulsars and high power laser radiation with plasmas. It is the purpose of this research to give a contribution to the theoretical understanding of such waves. We address the question of integrability and the construction of exact solutions, in particular solitons, of certain nonlinear wave equations.

15.4.2 Ongoing research

We resort to the Painlevé method (for determining the type of movable singularities of the solutions) and the Hirota method (for determining if multisoliton solutions exist) to investigate the integrability of the following nonlinear equations: (i) the system of four partial differential equations that describe the evolution in time and one space dimension of the complex amplitudes of four waves constituting two resonant triplets; (ii) the partial differential equation in l+1 dimensions that appears in the analysis of the consistency error of the second-order Runge-Kutta method for the numerical integration of ordinary differential equations.

[2] This research line has been carried out in collaboration with Prof. Luis Gomberoff, Physics Department, University of Chile at Santiago, and partially funded by FONDECYT (Chilean Institute).

16. ENVIRONMENTAL ENGINEERING PLASMA LABORATORY

C. M. Ferreira (Head), F. M. Dias (Deputy Head), E. Tatarova, J. Henriques

16. 1. INTRODUCTION

The research work carried out by this team in 2005 falls into the following main fields of investigation:

- Spatial structure and radiation of microwave plasma sources;
- Surface wave induced N2 – Ar plasma torch;
- Flowing N2 and N2-O2 discharges and post-discharges;
- Improved Langmuir Probe Techniques for Plasma Diagnostics.

16.2. SPATIAL STRUCTURE OF MICROWAVE N_2-AR PLASMA SOURCE[1]

A theoretical model for *a large-scale, slot-antenna excited surface wave plasma source operating in N_2-Ar mixtures* was developed. The model incorporates the description of both the discharge plasma, sustained by a pure TM_{140} surface mode, and the remote "electric field free" plasma. Maxwell's equations and the rate balance equations for the most important species – vibrationally

$$N_2(X^1\Sigma_g^+, v), \tag{16.1}$$

electronically excited molecules

$$N_2(A^3\Sigma_u^+, B^3\Pi_g, C^3\Pi_u, a'^1\Sigma_u^-, a^1\Pi_g, w\,'\Delta\,u), \tag{16.2}$$

$Ar(3p^5 4s)$ and $Ar(3p^5 4p)$ atomic states,

$$N^+, N_2^+, N_4^+, Ar^+, Ar_2^+ \tag{16.3}$$

ions, and nitrogen atoms $N(^4S,^2P,^2D)$ are consistently solved to yield the species spatial distributions. The model further determines the three-dimensional discharge structure, i.e., the radial, azimuthal and axial variations of the main plasma quantities. Strong correlation is shown to exist between the density distributions of plasma electrons and electronically excited states of molecules and atoms and the electric field intensity distribution in the discharge zone of the source. This indicates that electron driven processes play a dominant role in the discharge workings.

The transition from the source discharge to the remote plasma was analysed in detail. The pumping of the higher vth levels as a result of near-resonant V-V energy-exchanges between vibrationally excited $N_2(X^1\Sigma_g^+, v)$ was shown to be very effective, and to influence strongly the remote plasma kinetics. In fact, the pumping of the vibrational distribution function "tail" strongly influences the axial evolution of the EEDF and the number density of electrons and electronically excited states of molecules in the remote plasma zone. Collisions of

$$N_2(X^1\Sigma_g^+, v) \tag{16.4}$$

molecules in highly vibrational levels with ground $N(^4S)$ atoms are responsible for the formation of

$$N_2(A^3\Sigma_u^+, B^3\Pi_g, C^3\Pi_u, a'^1\Sigma_u^-) \tag{16.5}$$

electronically excited states. As a result, the number densities of electrons and electronically excited states

$$N_2(A^3\Sigma_u^+, B^3\Pi_g, C^3\Pi_u, a'^1\Sigma_u^-) \tag{16.6}$$

increase in the "late" remote plasma zone, at axial distances $\Delta z > 35$ cm (Figure 16.1).

An *experimental validation of the model* predictions was achieved *using optical emission spectroscopy.* The spatial variations of the emission intensities of the lines belonging to the 1st negative and 2nd positive systems of nitrogen have been detected and compared with the theoretical results. The agreement obtained between experimental and theoretical results is satisfactory, taking into account the numerous uncertainties in collisional data still existing.

The results obtained clearly demonstrate that the remote "electric field free" plasma zone of the present source is a big reservoir of excited species in metastable and vibrational states and of charged particles. By changing the mixture composition, and thus the dissociation degree of N_2 molecules, it is possible to control the processes of excited species production in the remote plasma zone of this microwave source.

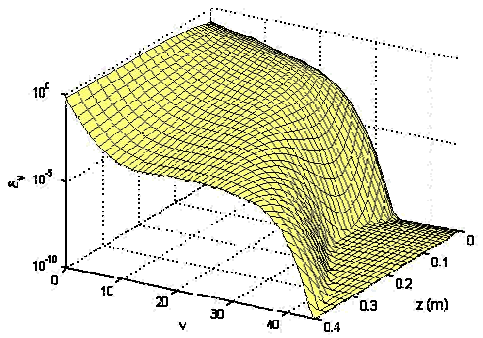

Figure 16.1 - Axial variation of the vibrational distribution function (80%N_2 – 20% Ar, p = 0.9 mbar, r = cm, φ = 162).

[1] Colaborators: Prof. H. Sugai and Dr. I. Ganachev (Nagoya University, Japan)

16.3. HYDROGEN BALMER LINE BROADENIBNG IN A MICROWAVE PLASMA SOURCE[2]

Emission spectroscopy (Doppler broadening technique and molecular rotational bands measurements) was used *for the diagnostic of gas particle temperatures in a large-scale,* slot-antenna excited *microwave plasma source* operating in pure hydrogen, helium-hydrogen and argon-hydrogen mixtures at low-pressures (p = 0.3 Torr). The measured profiles of H_α and H_β lines are well fitted by a Gaussian profile, (Figure 16.4 (a,b)). For the purposes of comparison, the normalized profiles of the 6678.8 Aº helium line [transition $3^1D \rightarrow 2^1P$] (shifted along the scale of wavelengths) are also shown (Figure 16.2). The helium line profiles are also well fitted by a Gaussian one. The emission profile of the Balmer-α line shows larger broadening than that of the Balmer-β and helium singlet line at 6678.8 Aº [transition $3^1D \rightarrow 2^1P$]. The line profiles do not present wings and we could not find any evidence of fast hydrogen atoms in the discharge zone of the plasma source. The Doppler temperatures corresponding to the helium singlet line at 6678.8 Aº (400 – 900 K) are close to the rotational temperatures (300 – 800 K) calculated from the Q-branch of the Fulcher-α band [$d^3\Pi_u\,(v{=}0) \rightarrow a^3\Sigma_g^+\,(v{=}0)$] under the same conditions. Therefore these temperatures can be assumed to be indicative of the gas temperature. The measured Doppler temperatures of hydrogen atoms range from 3100 K to 3700 K (Figure 16.5b) in a 95% He-5% H_2 mixture (P = 900 W) and from 2700 K to 3600 K in a 95% Ar- 5% H_2 mixture (P = 600 W) while in pure hydrogen (P = 600 W) the minimum and maximum temperatures are 2500 K and 3400 K, respectively. Thus, there is a "separation" of the excited hydrogen atom temperature from the gas temperature. The reason for such "separation" are connected to the processes leading to the creation of excited atoms such as electron impact dissociation and ion conversion.

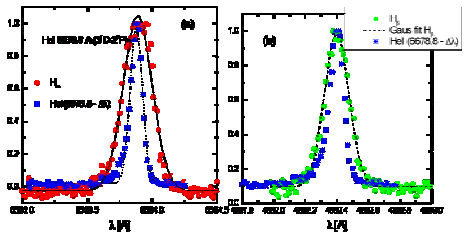

Figure 16.2 - H_α (a) and H_β (b) profiles compared with 6678 A He line profile.

16.4. SURFACE WAVE INDUCED N_2 – AR PLASMA TORCH[3]

Theoretical investigation on surface wave driven N_2-Ar microwave plasma torch at atmospheric pressure conditions is presented. The main plasma and wave characteristics are obtained in the framework of self-consistent 1D theoretical model which describes the axial structure, including overdense discharge plasma sustained by an azimuthally symmetric TM surface mode and post-discharge plasma arising due to the axial gas transport.

The system of equations (in the framework of fluid approach) considered to describe the plasma source includes: Maxwell´s equations; The rate balance equations for the vibrationally excited states of electronic ground state molecules

$$N_2(X^1\Sigma_g^+, v);\quad N_2(A^3\Sigma_u^+, B^3\Pi_g, C^3\Pi_u, a'^1\Sigma_u^-, a^1\Pi_g, w'\Delta u)$$

and $Ar(3p^5 4s)$, $Ar(3p^5 4p)$ excited states of molecules and atoms, positive

$$N_2^+, N_4^+, N^+, Ar^+, Ar_2^+$$

ions and electrons, ground state $N(^4S)$ and excited $N(^2P, ^2D)$ atoms. Further on, the gas thermal balance equation and the equation of mass conservation for the fluid as a whole are incorporated in the model.

The results show high values of the gas temperature (up to 12 000 and very strong population in vibrational levels of the electronic ground state

$$N_2(X^1\Sigma_g^+, v)$$

molecules in the discharge part of the, close to the microwave source (Figure 16.3).

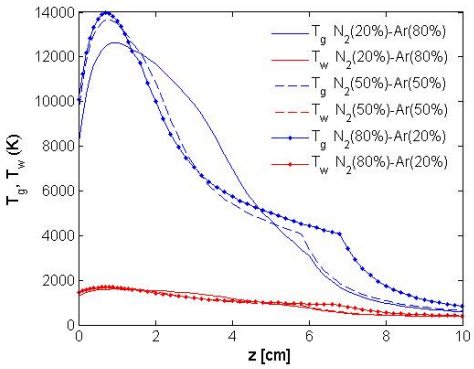

Figure 16.3 - Axial variation of T_g at different Ar percentages (P=2000 W, Q=1000 sccm).

16.5. EXPERIMENTAL AND THEORETICAL STUDY OF FLOWING N_2 AND N_2-O_2 DISCHARGES AND POST-DISCHARGES[4]

A complex experimental and theoretical investigation on a strong afterglow formed in the post-discharge region of a microwave plasma source is performed (Figure 16.4). The objective of this work was to investigate the concentration of various active species, such as O and N – atoms, N_2^+ ions, and $N_2(A^3S_u^+)$ and $NO(A^2S_u^+)$ molecules, as a function of the spatial position and the mixture composition. Emission spectroscopy was used to measure

[2] Work carried out in collaboration with Dr. N. Puac (Belgrade University, Serbia) and Dr. A. Ricard (CPAT, Université Paul Sabatier, France)

[3] Work performed in collaboration with Prof. Dr. B. Gordiets (Institute of Physics, Academy of Sciencies, Russia).

[4] Work carried out in collaboration with André Ricard (CPAT, Université Paul Sabatier, France)

the $N_2(1^+,2^+,1)$ and NO(g,b) band intensities in the discharge and in early post-discharge (see pictures below). The densities of N and O – atoms were measured using an actinometry method in the plasma region and NO titration in the post-discharge. The titration technique that provides absolute densities was used to calibrate the actinometry method in the early post-discharge, close to the discharge end. The experimental results are interpreted using kinetic theory in the discharge and in the late afterglow. The post-discharge region is of particular interest due to the formation of a strong afterglow and this extended "field free region" is rich in active species such as nitrogen and oxygen atoms, vibrationally and electronically excited nitrogen molecules and ions as the results show. The obtained results have *direct application for cold plasma sterilization of surgical material and other medical devices.*

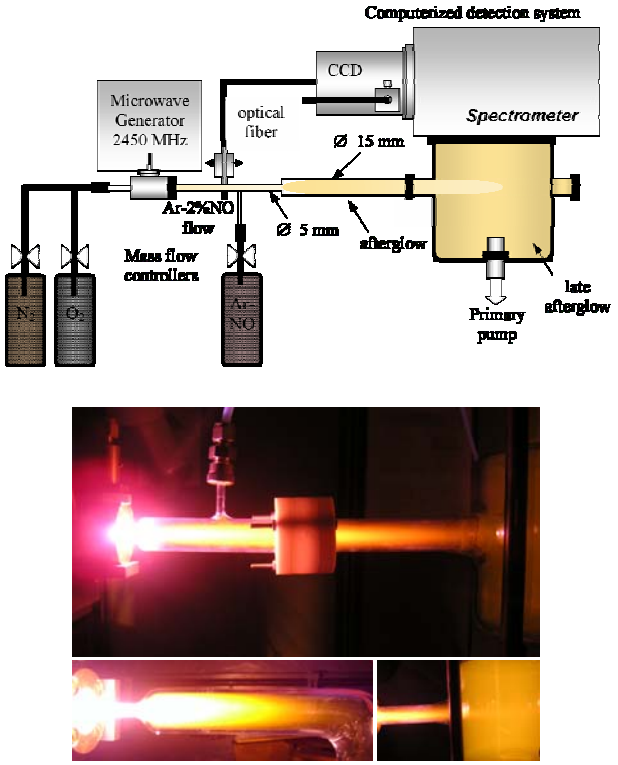

Figure 16.4 - Experimental setup showing the discharge and post-discharge reactor.

16.6. IMPROVED LANGMUIR PROBE TECHNIQUES FOR PLASMA DIAGNOSTICS[5]

16.6.1. Restoration of Time-averaged Probe Characteristics

We developed three simple methods that enable restoring time-averaged Langmuir probe characteristics measured under time-varying plasmas, in the sense that plasma parameters, *i.e.*, electron density and average energy, electron energy distribution function (EEDF), and plasma potential, are deduced more accurately than what otherwise could be retrieved from averaged data.

The first method (SAM) is based on analytic expressions of the first and second derivatives of the probe characteristic, and only requires the standard deviation of the measured current, *i.e.*, the probe characteristic itself is not needed. The other two methods assume that the probe characteristic experiences either an anamorphic deformation (ADM) or a linear deformation of the low-energy part of the EEDF (BDM), which from our experience are the most simple, acceptable assumptions (Figure 16.5).

Although our motivation were probe diagnostics, the above techniques are of general interest since all kinds of data acquisition have to deal with the problem of a finite integration time, and the output is always the result of some kind of average.

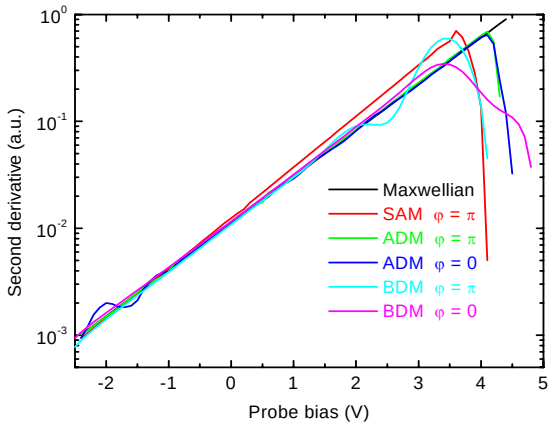

Figure 16.5 - Model test of the three restoration methods (Maxwellian EEDF)

16.6.2 Improved Probe Differentiation Techniques

A combination of the *harmonic and numerical differentiation techniques* is being developed *in order to measure the electron energy distribution function* (EEDF) with an error of the order of the 8th derivative instead of the order of the 4th derivative, which is typical in standard methods. In addition to the increased accuracy, instrument functions are adaptively adjusted in such a way that the error and the noise levels are continuously kept at similar levels, which is possible because the overall system has the ability to evaluate the noise as well as the error levels of the differentiators at measuring time.

The superior differentiation performance is achieved using a redundant approach, which enables keeping the noise from individual differentiators uncorrelated, and signals are combined in such a way that the resulting signal-to-noise ratio is the maximum possible.

[5] Work carried out in collaboration with Tsv. Popov, and M. Dimitrova (St. Kliment Ohridski University of Sofia, Faculty of Physics, Bulgaria)

17. NONEQUILIBRIUM KINETICS AND SIMULATION OF DISCHARGES, AFTERGLOW PLASMAS AND HIGH-SPEED PLANETARY ENTRIES

C.M. Ferreira (Head), J. Loureiro (Deputy Head), V. Guerra, P. A. Sá, C. D. Pintassilgo, M. L. Silva and K. Kutasi

17.1. INTRODUCTION

The research work carried out by this team in 2005 falls into the following main fields of investigation:

- Kinetics of the nitrogen afterglow;
- Plasma sterilization at reduced gas pressure and low temperature;
- Nonequilibrium processes and plasma radiation in high-speed spacecraft planetary entries;
- Microwave discharges in N2-CH4 for metal nitrocarburizing and chemistry studies of Titan's atmosphere;
- Modeling of surface atomic recombination

17.2. KINETICS OF THE NITROGEN AFTERGLOW[1]

The study of the electron and heavy-particle kinetics in nitrogen post-discharges has been continued. The theoretical study involves two separate modules, one for the discharge (I) and another for the post-discharge (II). The stationary solutions from I are the initial conditions for module II. The electron energy distribution function (EEDF), the vibrational distribution function (VDF) of ground-state $N_2(X,v)$ molecules, and the concentrations of the most important neutral and ionic species are obtained from the coupled solutions to the electron Boltzmann equation and a system of rate-balance equations for the heavy-particles.

The purpose of this investigation is *to understand the behavior of the pink afterglow,* characterized by a raise in the emission of the first negative system bands, corresponding to transitions between the ionic states $N_2^+(B\rightarrow X)$, after a dark zone downstream from the end of a flowing discharge. The concentration of several other species, both radiative and metastable, exhibit a similar profile. In particular, it is very striking to verify an increase in the population of $N_2(A)$ and $N_2(a)$ metastables, taking place in the field-free post-discharge.

It has been shown that an equilibrium between the vibrational distribution of ground-stated $N_2(X,v)$ molecules is established and that collisions of highly vibrationally excited molecules with N atoms are in the origin of a maximum in the electron density, occurring downstream from the discharge. It is concluded that there must be a local production of $N_2(A)$ molecules, which has been shown to be due to near resonant vibration-vibration (V-V) energy exchanges, followed by electronic-vibration (V-E) exchanges. The later can be induced by collisions of highly vibrationally excited $N_2(X,v)$ molecules with both N atoms and electrons. Once the $N_2(A)$ state is created, it starts transferring energy to other states and to ionization. Therefore, many other excited states, as well as electrons and positive ions, have a similar profile during the afterglow (Figure 17.1).

In spite of the general good agreement between the available experimental results and the theoretical predictions, a global explanation for the ionization processes taking place in the nitrogen afterglow is still missing. As a matter of fact, recent experiments made in Grenoble, France, show that the role of singlet metastables in the ionization during the afterglow has been overestimated. That being so, the present-day description of the afterglow underestimates ionization, and new ionization mechanisms have to be investigated.

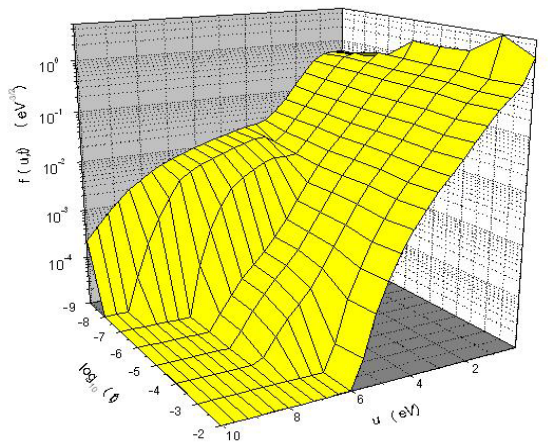

Figure 17.1 - Time evolution of the EEDF in the nitrogen afterglow.

17.3. PLASMA STERILIZATION AT REDUCED GAS PRESSURE AND LOW TEMPERATURE[2]

Gas plasma sterilization in hospitals has appeared a very promising alternative to conventional sterilization processes. Because of materials that are thermosensitive are increasingly being used in the composition of medical

[1] Work carried out in collaboration with Université des Sciences et Technologies de Lille (France) and Université Joseph Fourier de Grenoble (France).

[2] Work performed in collaboration with the Physics Department of the University of Montreal (Canada), the Laboratoire de Science et Génie des Surfaces de l' École des Mines de Nancy (France), the Department of Physical Electronics of the Faculty of Science of the Masaryk University of Brno (Czech Republic), and Prof. P.J. Coelho (Department of Mechanical Engineering, IST).

and dental devices, the possibility of the various active species created in a plasma medium may be used for sterilization has been considered. Further, this possibility should be also explored due to the necessity of inactivating new types of pathogenic agents. *Plasma sterilization reactors operating in the afterglow of a gas discharge* is the most interesting new device to be used, since it fulfill the two conditions of much lower gas temperature than in the discharge itself and the absence of charged species which could damage the material to be sterilized.

Investigations realized by the group of Plasma Physics in the Physics Department of the University of Montreal has shown that almost total inactivation of an initial prion spore population can be achieved using the afterglow of a microwave N_2-O_2 discharge, with small O_2 addition of the order of 0.2-2%, as a result of a synergistic effect between UV photons emitted by $NO(B^2\Pi)$ molecules and $O(^3P)$ atoms. With the aim of giving an insight into the the kinetics of a low pressure microwave flowing post-discharge in N_2-O_2, and thus determining the optimal operating conditions, investigations have been conducted in CFP by developing a fully self-consistent model for the kinetics of electrons and heavy-neutral and charged species in a flowing microwave discharge. Once the concentrations of active species produced in the discharge are determined, the afterglow is modeled by considering both a short-lived afterglow, at the end of the discharge, and the long-lived afterglow in the sterilization vessel of much larger dimension, where the objects to be sterilized will be placed. In the afterglow a complex interplay kinetics between active neutral species still continues to take place leading to the creation of some species and to the destruction of others.

Work has been performed on the kinetics of charged and heavy-species in a N_2-O_2 microwave discharge, with a model for the short-lived afterglow downstream from the discharge tube. Furthermore, a comparison between measured and predicted populations in the afterglow of a N_2-O_2 microwave discharge was also conducted.

This work has been pursued by considering a 3-D Navier-Stokes model for the post-discharge chamber, based on the coupled solutions to the set of equations for mass conservation of different species, total mass conservation, momentum transfer, and energy conservation. With this hydrodynamic model the concentrations of the various species, such as the molecules responsible by UV emission and oxygen atoms, may be followed up to the farthest remote zones of the reactor (Figure 17.2).

Finally, the study of O_2 and O_2-N_2 microwave discharges and post-discharges has been also conducted with the purpose of application to surface treatments, namely in the study of the oxygen plasma surface interaction in treatments of polyolefines and of the modification of hexatriacontane by O_2-N_2 microwave post-discharges (Figure 17.3).

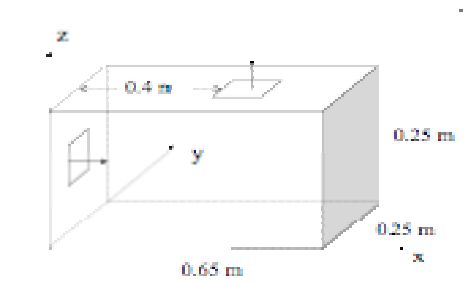

Figure 17.2 - The post-discharge chamber used in the modulation is shown in this figure. The active species created in a N_2-O_2 flowing microwave discharge after passing through a short afterglow region are introduced into the large vessel. The entrance and the outlet have a length and width of 2.6 cm and are situated in the middle of the planes giving symmetry to the chamber.

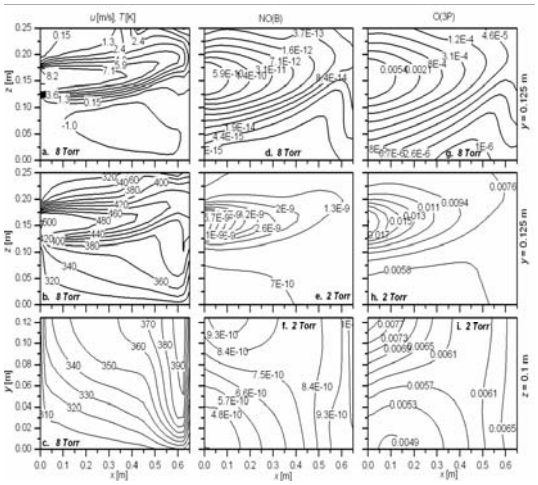

Figure 17.3 - Distribution of velocity (a), temperature (b, c), relative mass density of $NO(B^2\Pi)$ molecules (d, e, f) and of $O(^3P)$ atoms (g, h, i), in the entrance plane y = 0.125 m (figures a, b, d, e, g, h) and in the x-y plane at z = 0.1 m height (figures c, f, i). The results are presented for two discharge conditions: (i) p = 8 Torr, f = 915 MHz (figures a, b, c, d, g); and (ii) p = 2 Torr, f = 2.45 GHz (figures e, f, h, i). Here, the results are for a N_2-2%O_2 mixture composition and gas flow of 2×10^3 sccm but the influence of these parameters is investigated. The gas temperature at the inlet and in the wall is assumed to be 500 K and 300 K, respectively.

17.4. NONEQUILIBRIUM PROCESSES AND PLASMA RADIATION IN HIGH-SPEED SPACECRAFT PLANETARY ENTRIES

During an atmospheric entry of a space vehicle at hypersonic speeds (>5 km/s), a strong shock-wave is created in front of the spacecraft forebody. Immediately behind the shock-wave, the translational temperature of the flow reaches temperatures usually in large excess of 10,000 K. For interplanetary missions, the flight pattern is hyperbolic, and the entry velocities and translational temperatures may exceed 10 km/s and 100,000 K

respectively. After the excitation of the flow translational mode through the shock front, excitation of vibrational levels of the gas then follows through redistribution of energy from the translational mode to the vibrational mode. Dissociation and ionization of the gas species then follow until a plasma state is reached. Two issues arise in this case. The dissociation and ionization channels need to be known, in order to accurately describe the evolution of the flow macroscopic parameters (species concentrations and temperatures). This has a large impact on the determination of the convective heat transfer endured by the spacecraft thermal protections. Moreover, nonequilibrium excitation processes of neutral and ionised flow species need to be accurately known in order to determine the radiation from the plasma and to evaluate the radiative fluxes endured by the spacecraft thermal protections.

17.4.1. Analysis of shock-induced dissociation processes

A numerical model based on the Forced Harmonic Oscillator (FHO) theory has been developed for the *simulation of atom-diatom and diatom-diatom Vibration-Translation (V-T) processes.* This model is advantageous compared to First Order Perturbation Theory (SSH models) as it allows the simulation of multiquantum transitions and provides accurate results at very high temperatures (up to 100,000 K). Good agreement has been reached between this model and quasi-classical calculations for N_2 and O_2 molecules. The influence of multiquantum transitions on the global dissociation rates of molecular nitrogen has also been evidenced.

Currently, the influence of molecular rotation on V-T processes is being studied through the development of additional models. Vibration-Electronic (V-E) transfer processes are scheduled to being studied shortly. Future studies will also focus on ionization processes such as associative ionization ($A+B \rightarrow AB^+ + e^-$) or Penning ionization ($AB^*+AB^* \rightarrow AB^+ + e^-$). Long term objectives include the development of a full collisonal-radiative model for Earth, Mars and Titan high speed atmospheric entries.

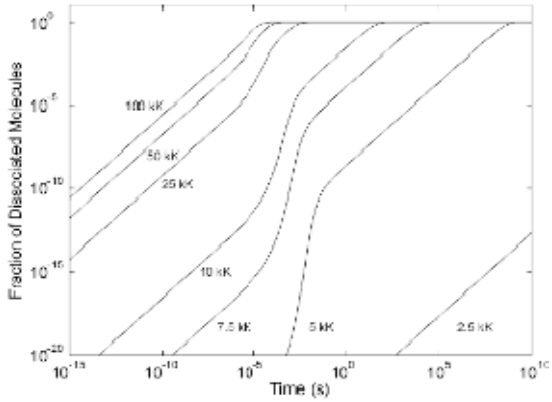

Figure 17.4 - Dissociation times for different post-shock translational temperatures, at a 76 km altitude, and for a pre-shock temperature of 195 K.

A collaboration program has also been established with the Université de Provence in Marseilles, France, where the shock-tube TCM2 is located. This facility is operated in the frame of the ESA-sponsored AURORA program for the simulation of shock-waves typical of Earth, Mars, and Titan atmospheric entries. The established working plan has scheduled a series of visits from researchers from the two institutions, in order to carry an interpretation and a numerical reproduction of spectra measured in Titan and Martian-type mixtures.

17.4.2. Analysis of atmospheric entry radiative processes

A detailed investigation of the *high temperature radiative processes encountered during an atmospheric entry* is also carried in the research group. Currently, two different numerical tools have been developed and made available to the atmospheric entry research community:

i) The line-by-line code SPARTAN (**S**imulation of **P**lasma **R**adiation in **T**hermodyn**A**mic **N**onequilibrium) for the simulation of plasma radiation from air and CO_2-N_2 plasmas has been developped and is freely made available to the general scientific community. The numerical code is capable of simulating over 50 different bound, bound-free, and free transitions (Figure 17.5). More informations on the numerical code can be found in the following electronic adress: http://cfp.ist.utl.pt/geg/radiation/SPARTAN/. Currently, the code is being used by three different european research teams (two in France and one in Italy).

ii) An electronic database gathering factual information on radiative transitions of diatomic molecules of interest for planetary atmospheric entries has been developed and put online at the following electronic adress: http://cfp.ist.utl.pt/geg/radiation/GPRD/. Future versions of this database are scheduled to be added to the electronic databases provided by the European Space Agency, acting as the database of reference for providing spectral coefficients for the calculation of atmospheric entries radiation.

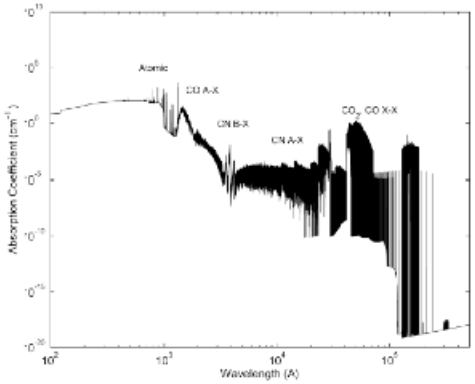

Figure 17.5 - Sample calculation of the spectral-dependent absorption coefficient for a 97% CO_2 – 3% N_2 plasma at 1bar, 5000K, and in thermodynamic equilibrium

The group maintains a collaboration with the Laboratoire Arc Electrique et Plasmas Thermiques in Clermont-Ferrand, France. An analysis of the thermodynamics and radiative properties of a Martian-type CO_2-N_2 plasma produced in a Inductively Coupled Plasma torch at atmospheric pressure is being carried in the scope of this collaboration. Also, the group is currently involved in the expertise and further development of the ESA line-by-line code PARADE (Fluid Gravity Eng. Contract with M. Dudeck, U. Paris VI).

17.4.3. Analysis of Born-Oppenheimer hypothesis in polyatomic molecules

A working group has been recently set-up to focus on the Born-Oppenheimer hypothesis breakdown and it's impact on aerothermodynamics. We are participating in this working group whose task is to meet at regular schedules and to analyse the consequences of using the Born-Oppenheimer hypothesis in the majority of all the classical to quantum molecular models developped by the scientific community. The working group task also includes examining the possibility of developping further methods who do not require this assumption, and defining a roadmap for future investigations.

.

17.5. MICROWAVE DISCHARGES IN N2-CH4 FOR METAL NITROCARBURIZING AND CHEMISTRY STUDIES OF TITAN'S ATMOSPHERE[3]

The study of a N_2-CH_4 afterglow has an actual interest due to the large number of applications in different fields, such as the detoxification of gases, metal surface nitrocarburizing and the study of the atmospheric chemistry of Titan.

In the case nitrocarburizing, the afterglow resulting from a nitrogen-methane flowing microwave discharge can be very efficient in metal surface treatments, due to the importance of the presence of N and C atoms in the formation of carbonitrides ε-Fe_{2-3} (C, N) and γ-Fe_4(C,N) in metal nitrocarburizing processes. Further, this treatment can be improved with the presence of H atoms.

Two situations have been investigated in a flowing N_2-CH_4 afterglow of a microwave discharge: i) methane is added to N_2 in the downstream afterglow; ii) methane is added to the discharge. In both cases the CH_4 addition is always smaller than ~ 0.5-1%. The discharge is produced using a surfatron device connected to a microwave generator at 2.45 GHz and the post-discharge is analysed at about 200 mm downstream from the discharge. Optical Emission Spectroscopy (OES) is carried out in the post-discharge. The densities of N and C atoms in the late post-discharge can be inferred from OES measurements of the first positive system of N_2 , emission of the $N_2(B^3\Pi_g,11) \rightarrow N_2(A^3\Sigma_u^+,7)$ transition, and of the CN violet band $CN(B^2\Sigma,7) \rightarrow CN(X^2\Sigma,7)$, respectively, by assuming simple kinetic models for the long-lived afterglow, and using absolute calibration by NO titration. On the other hand, the kinetic model considers the self-consistent determination of the active species concentrations in the discharge and consequent time-relaxation in the afterglow. In situation i), where a small methane percentage is introduced into the post-discharge at 250 mm downstream from the end of the discharge, methane dissociation (CH_3, CH_2, etc.) occurs in the afterglow in the presence of active nitrogen, together with several other reactions leading to formation of HCN, $CN(X^2\Sigma)$, $CN(B^2\Sigma)$, etc. The C atoms are then formed as a result of a complex kinetics.

Discharges in N_2-CH_4 have been also studied with the aim of understanding the organic chemistry of Titan's atmosphere, in particular the conditions for formation of organic aerosols, also termed "tholins", that are observed in Titan.

17.6. MODELING OF SURFACE ATOMIC RECOMBINATION:

The study of the surface kinetics of atomic species, such as N and O atoms, and in particular of the elementary processes leading to heterogeneous recombination, is nowadays an important subject of research in various problems of rarefied gas dynamics, such as the aerodynamics of space vehicles moving in rarefied gases. On the other hand, many of the characteristics of plasma reactors are in practice controlled by wall reactions. Therefore, there is a need to address the questions of the *role of surface processes in the overall behavior of different gas discharges.*

Many theoretical works have been done recently in order to investigate surface recombination of atoms. For instance, phenomenological models and Monte Carlo models have been developed. All these models provide important physical insight into the various elementary mechanisms occurring at the surface and, particularly for the case of the Monte Carlo, allow to perform quite complete and detailed simulations. The purpose of the present investigation is to follow a different approach, by obtaining asymptotic analytic solutions for the recombination probability. It is shown that the approximate analytic solutions describe the system with very high accuracy (Figure 17.6). Thus, for the system under analysis, the recombination probability can be readily evaluated from a simple expression, with no need for any numeric treatment. As a consequence, the dependence of the recombination probability on different surface parameters, such as the activation energies of the various processes and the wall temperature, can be fully understood.

The probability for surface atomic recombination of a single gas is theoretically investigated, for a system that takes into account atomic adsorption in physisorption and chemisorption sites, surface desorption, surface diffusion,

[3] Work carried out in collaboration with the Laboratoire de Science et Génie des Surfaces de l' École des Mines de Nancy (France) and the Service d' Aéronomie de l' Université de Paris VII and Versailles/Saint Quentin (France).

and both Eley-Rideal (E-R) and Langmuir-Hinshelwood (L-H) recombination mechanisms.

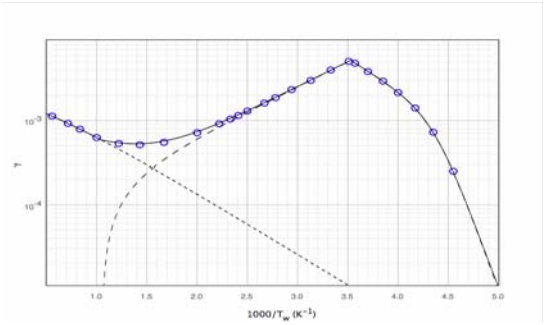

Figure 17.6 - Numerical (blue circles) and asymptotic analytical solutions (full line) for the recombination probability of nitrogen in silica. The contribution of L-H (dashed line) and E-R (dotted line) recombination mechanisms to the total recombination probability is also shown.

18. MODELLING OF PLASMA REACTORS

C.M. Ferreira (Head), L. L. Alves (Deputy Head), R. Alvarez, L. Marques, S. Letout

18. 1. INTRODUCTION

The research activity in 2005 was fully focused onto the modeling of several configurations of Plasma Reactors (PR), used in different types of industrial chains with electronics, photovoltaic, optics, food industry, or surface modification.

The main objective with this research program is the development of sophisticated simulation tools, to optimize the operation conditions of different PRs, according to the specific needs with each application. The validation of such tools requires a strong interplay between modeling and experiment, without which it is not possible to improve the understanding of the main mechanisms controlling discharge operation.

Several projects have been initiated, pursued or concluded, in the following main fields of investigation:

- Inductively-coupled plasma reactors;
- Microwave plasmas sustained by an Axial Injection Torch;
- Microwave plasma reactor with coaxial geometry at 2.45GHz frequency in argon;
- Capacitively-coupled radio-frequency discharges in hydrogen.

18.2. INDUCTIVELY-COUPLED PLASMA REACTOR FOR THE ETCHING OF METAL OXIDES[1]

We have started the modeling of an inductively-coupled plasma reactor (ICP-R), for the etching of metal oxides by fluorocarbon plasmas.

Standard fabrication techniques of CMOS-base electronic devices generally apply deep etching processes to silicon oxide (with low-dielectric constant). Usually, this plasma processing technique is carried out within ICP-R's, which present the advantage of operating at very low pressures (~mTorr) and high plasma densities (~10^{13} cm^{-3}), thus ensuring both the effectiveness of the etching mechanism and a reduced contamination. The *full description of etching processes within an ICP-R* can significantly contribute to their control and optimization. However, the development of such a global simulation program constitutes a very hard task due to the complex and diverse nature of the phenomena involved: electromagnetic, chemical (either in gas or in surface phases) and transport. The development of such a simulation tool will bring together complementary competences in the domains of Plasma Physics and Engineering, Surface Physics and Material Science. We intend to develop *a multi-scale model of an ICP-R* (Figure 18.1) *for the etching of metal oxides, by fluorocarbon plasmas.*

In 2005, we have concentrated onto the description of the excitation source part of the reactor, by developing a two-dimensional simulation tool that calculates the electromagnetic field distribution therein.

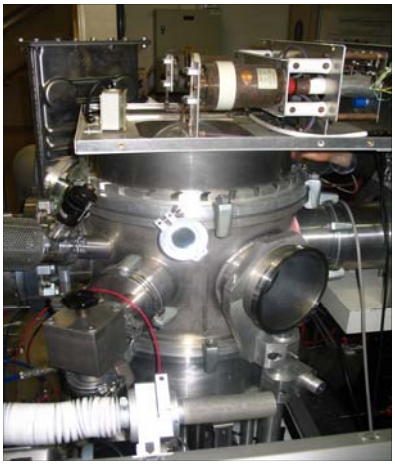

Figure 18.1 - ICP reactor with the LPCM (Nantes, France)

18.3. MICROWAVE PLASMAS SUSTAINED BY AN AXIAL INJECTION TORCH (*TORCHE À INJECTION AXIALE*, TIA)[2]

The disposal of pollutants produced by industrial processes is a mandatory task to ensure an environmental protection within a sustained development framework. Recently, a *microwave plasma torch* was applied *in waste treatment,* to the destruction of dangerous chemical compounds (such as Volatile Organic Compounds (VOCs) and BEXT aromatic hydrocarbons), with great success. Results show that this is a non-expensive and efficient way of neutralizing dangerous products, yielding destruction rates above 99,999% when applied to trichloroethylene and carbon tetrachloride.

The microwave plasma under study is produced by a TIA inside a cylindrical reactor (5.5 cm radius and 15 cm high) – Spanish patents P200201328 and P200302980. The 2.45 GHz discharge runs in atomic (Ar, He) or molecular (N_2, air) gases at atmospheric pressure, for powers ranging from 300 to 3000 W and gas flow-rates between 0.5 and 13 L/min, which shows the versatility of the plasma. The

[1] Work carried out in collaboration with the *Laboratoire des Plasmas et des Couches Minces* (LPCM) of the *Institut des Matériaux de Nantes* (IMN, Nantes, France).

[2] Work performed in collaboration with the Physics Department of the University of Cordoba (Cordoba, Spain).

system is also very stable and resistant to the introduction of water-vapour-saturated gaseous samples, unlike the majority of microwave plasmas.

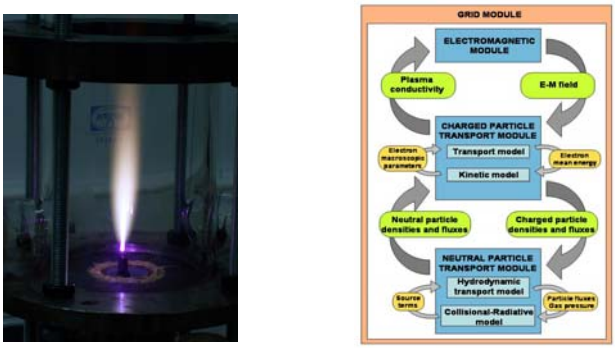

Figure 18.2 - Microwave torch with the Physics Department of the University of Cordoba, Spain (left), and schematic of the self-consistent model (right).

The project intends to develop a two-dimensional, self-consistent model for microwave helium plasmas, created by the TIA inside the reactor chamber. The model will be developed following a modular structure, each module addressing to a specific task (Figure 18.2). This clarifies model's structure, enhancing its versatility as a simulation tool.

The first two modules of the model have been successfully developed:

- *Grid Module.* The grid design follows the reactor geometry, being denser in regions where the plasma parameters are expected to present steep variations. For this two-dimensional model, variable grids have been defined along both axial and radial directions, with a higher point density at the tip of the torch and near the reactor walls. The number of grid points is high enough as to provide both numerical accuracy and a proper description of the plasma processes, while ensuring acceptable running times. These conditions were fulfilled adopting a non-uniform flexible grid, to discretize model equations (Figure 18.3).
- *Electromagnetic Module.* This module solves Maxwell's equations for the two-dimensional distribution of the electromagnetic (e-m) field within the reactor-TIA system, for a given spatial profile of the plasma conductivity. A DC-type description has been adopted to write the time dependence of the e-m field (and thus to calculate the transport features with charged particles), since the electron-neutral collision frequency at atmospheric pressure is higher than the microwave excitation frequency. Since both the TIA and the reactor chamber have axial symmetry, the e-m field components do not depend on the azimuthal angle. Moreover, the plasma dimensions and the coaxial nature of the TIA excitation device justify the assumption of a TM propagation mode, for the e-m field in the reactor-TIA system. Boundary conditions have been carefully chosen, particularly at the interface between the reactor chamber and the coaxial excitation waveguide, which acts as an open boundary. Absorbing boundary conditions have been considered to eliminate non-physical reflections coming from modelling the coaxial waveguide as a limited system.

Globally, a description of the electromagnetic field distribution with this microwave discharge has been successfully achieved.

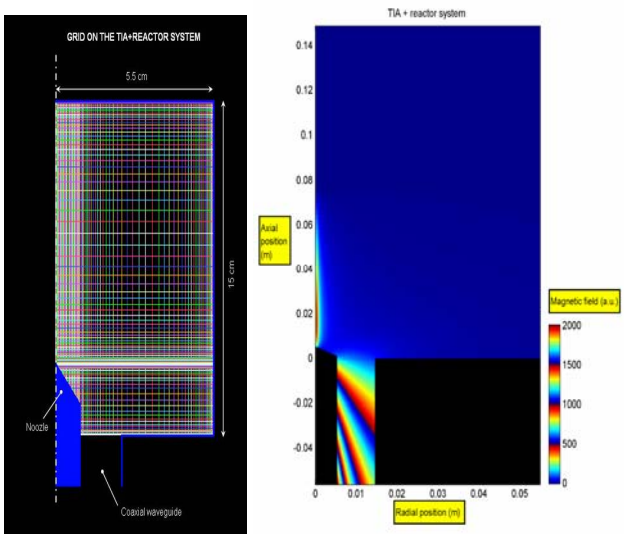

Figure 18.3 - Grid adopted (left) and magnetic field contour plot (right) with the reactor + TIA system.

18.4. MICROWAVE PLASMA REACTOR WITH COAXIAL GEOMETRY AT 2.45 GHZ FREQUENCY IN ARGON[3]

We have pursued the characterization (both experimental and theoretical) of a microwave plasma reactor with coaxial geometry (corresponding to the sequence metal-air-dielectric-plasma-metal of propagation media, within a ~1cm tube radius), operating at 2.45GHz frequency in argon, for 10-100mTorr pressures and 100-1000W coupled powers. The experimental analysis is essentially developed at the LPGP (Figure 18.4), whereas numerical simulations are carried out at the CFP.

A self-consistent one-dimensional (radial) fluid-type code has been used to demonstrate and to analyze the development of an electron-plasma resonance, associated with the strong density gradients that occur within space-charge sheath regions, at discharge boundaries. The code couples the transport equations (continuity and momentum transfer) for electron and ion particles and for the electron mean energy, Poisson's equation for the space-charge field associated with charge separation regions, and Maxwell equations for the adequate surface-wave (SW) propagating mode. Results reveal a strong increase in the SW electric

[3] Work carried out in collaboration with Dr. C. Boisse-Laporte (with the *Laboratoire de Physique des Gaz et des Plasmas* (LPGP), Orsay, France).

field, at positions where the plasma frequency equals the microwave excitation frequency (resonance effect), thus evidencing the strong plasma-wave coupling responsible for discharge maintenance.

In 2005, the work was focused mainly on the following topics.

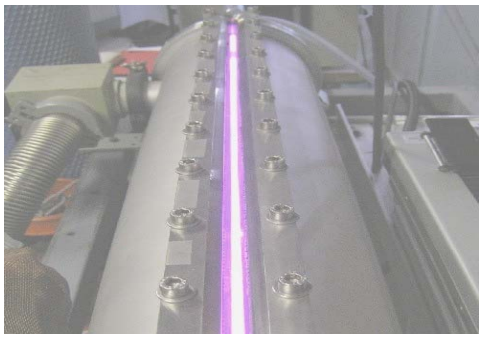

Figure 18.4 - Coaxial microwave plasma reactor with the LPGP (Orsay, France).

(i) Systematic runs of a numerical simulation code describing the microwave discharge, in view of characterizing the electron-plasma resonance as a function of the operating conditions (pressure and power coupled). The results obtained revealed that, at low pressures, there is a strong cross-linking between resonance and space-charge sheath, thus making impossible to separate the regions associated with these two phenomena.
It was also possible to define a similarity curve for the average power density deposition, for various electron densities, pressures and radial dimensions (Figure 18.5).

(ii) The experimental detection and characterization of the electron plasma-resonance, by means of directional measurements using a planar Langmuir probe. Results confirm the existence of strong deformations, associated with I-V characteristics obtained at different probe orientations. These deformations can be related to the presence of a supra-thermal flux of electrons, following their collisionless heating within resonance region.
Comparisons between calculated and measured values for the electron density and the wave attenuation constant were also carried out.

(iii) The analysis of the strong anisotropies associated with the presence of electron-plasma resonances, comparing model predictions with experimental measurements. For this study, the stationary fluid-type electron transport equations were updated, to include some extra non-linear wave-plasma coupling terms. The latter introduced an axial electron flux, hence perpendicular to the model's one-dimensional (radial) direction, which is to be compared to the relevant experimental information. In particular, the latter is to be obtained under stationary-wave conditions, for which the presence of extraordinary fluxes can be detected as perturbations to the electric field distribution.

Globally, an overall description of the microwave discharge under study was successfully achieved.

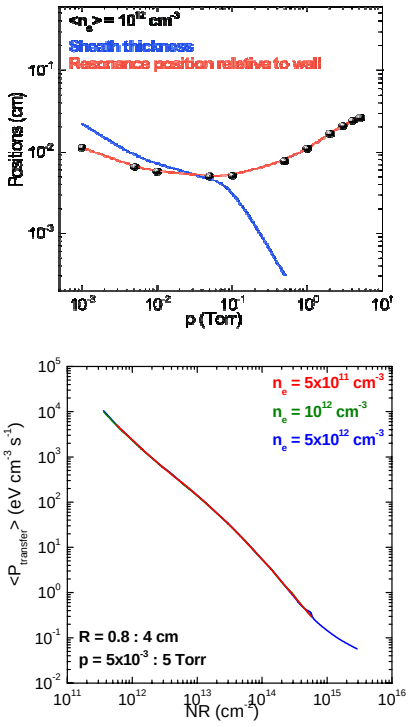

Figure 18.5 - Relative position of resonance and space charge sheath boundary (up) and similarity curve for the average power density (down).

18.5. CAPACITIVELY COUPLED RADIO-FREQUENCY DISCHARGES IN HYDROGEN[4]

We have concluded the *modelling and the characterization* of capacitively-coupled radio-frequency discharges in hydrogen, produced within a cylindrical parallel-plate reactor. These discharges are routinely used in plasma-assisted material processing applications. Model results were compared to experimental measurements (Figure 18.6).

The discharge characterization covered a wide range of excitation frequencies (13.56 – 80.0MHz), gas pressures (0.2 – 6Torr) and applied RF voltages (50 – 800V), and used a state of the art two-dimensional fluid model (to describe the dynamics of electrons, positive ions H^+ H_2^+ H_3^+ and negative ion H^- in the reactor), self-consistently coupled to a homogeneous collisional-radiative model for hydrogen (including a very complete kinetic scheme for $H_2(X_1\Sigma_g^+,v=0..14)$ vibrationally excited ground state molecules and H(n=1-5) electronically excited atoms).

[4] Work performed in collaboration with Dr. G. Gousset (with the *Laboratoire de Physique des Gaz et des Plasmas* (LPGP), Orsay, France), and with Dr. Jacques Jolly (with the *Laboratoire de Physique et Technologie des Plasmas* (LPTP), Palaiseau, France).

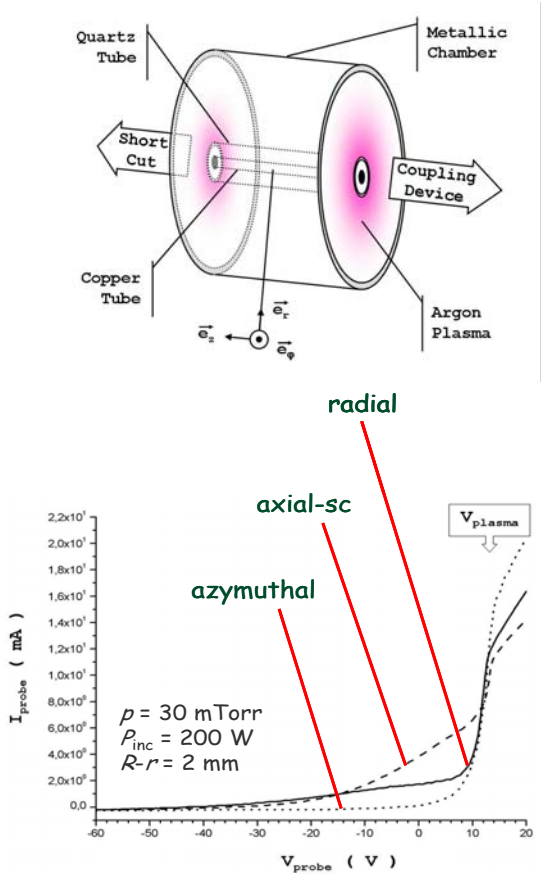

Figure 18.6 - (I,V) direction measurements using a planar Langmuir probe.

A good agreement was found between calculated results and experimental measurements for the self-bias voltage, the plasma potential and impedance and the electrical power coupled to the plasma. However, model predictions for the electron density and the self-bias voltage showed only a qualitative agreement with experiment, with calculated values underestimated with respect to measurements. This qualitative disagreement is only slightly dependent of the kinetic scheme adopted, and probably is a direct consequence of the homogenous model describing the transport of neutral species. To clarify this, *a two-dimensional, time-dependent, hydrodynamic gas model was developed, based on the Navier-Stokes / Saint-Venant equation system plus a multi-component reactive mass transport module.* This innovative model is the key piece of a powerful predictive tool yet under development, to be used in optimizing plasma reactors for material processing.

Calculations of the power absorbed by electrons W_e and the power spent on ion acceleration W_i showed that both these quantities increase with either V_{rf} and f, scaling as $W_e \sim V_{rf}^{1.2} f^{1.6}$ and $W_i \sim V_{rf}^{2.5} f^{1.6}$ at constant pressure. For applications, it is advantageous to operate at low applied voltages (regardless of frequency), in order to maximize the fractional power coupled to the electrons while minimizing that transferred to the ions. Moreover, W_e/W_i varies linearly with p at constant V_{rf}, thus showing that an increase in the pressure favors the transfer of power to the electrons.

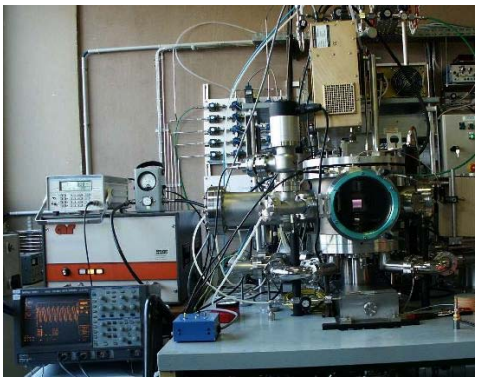

Figure 18.7 - Capacitively-coupled radio frequency reactor with the LPTP (Palaiseau, France)

A good agreement was also found between simulations and measurements (the latter obtained by LIF) for the density of H-atoms, at different discharge operating conditions (Figure 18.8). This corresponds to an improvement with respect to previous model results (failing to predict the correct features with the H-atoms density, even qualitatively), and it was achieved by using recent *in-situ* measurements of the wall-recombination coefficient for hydrogen atoms.

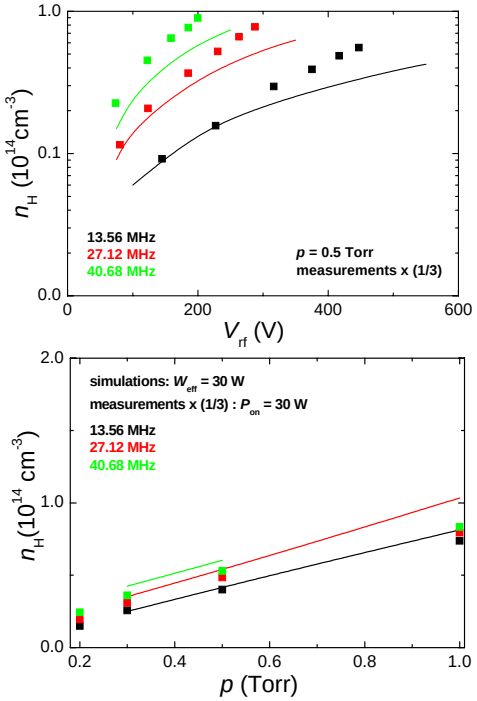

Figure 18.8 - H-atoms density as a function of applied voltage (up) and pressure (down)

19. PUBLICATIONS, LABORATORIAL PROTOTYPES, PRIZES AND AWARDS

19.1. MAGNETIC FUSION

19.1.1. Ph.D thesis

- *"Sistema de Multiprocessamento para Controlo em Tempo Real em Experiências de Fusão Nuclear"*
  António Pinto Rodrigues
  Universidade Técnica de Lisboa

- *"Turbulence Studies in the Scrape-Off Layer of Tokamak Plasmas by Three-Dimensional Gyrofluid Simulations"*
  Tiago Ribeiro
  Universidade Técnica de Lisboa

19.1.2. Articles in scientific journals

- *"Third-harmonic, top-launch, ECRH experiments on TCV tokamak"*
  Alberti, S., G. Arnoux, L. Porte, J.-P. Hogge, B. Marletaz, P. Marmillod, Y. Martin, S. Nowak and TCV Team.
  Nuclear Fusion, 45**,** (11), 1224, 2005

- *"Characterisation and Stability Studies of Titanium Beryllides"*
  Alves, E., L.C. Alves, N. Franco, M.R. da Silva, A. Paúl, J.B. Hegeman, F. Druyts
  Fusion Engineering and Design, 75-79, 759-763, 2005.

- *"Relationship between density peaking, particle thermodiffusion, Ohmic confinement and microinstabilities in ASDEX Upgrade L-mode plasmas"*
  Angioni, C., A. G. Peeters, F. Ryter, F. Jenko, G. D. Conway, T. Dannert, H. U. Fahrbach, L. Fattorini, M. Reich, W. Suttrop and the ASDEX Upgrade Team.
  Physics of Plasmas 12, 040701, 2005

- *"JETTO simulations of Te/Ti effects on plasma confinement"*
  Asp, E., J. Weiland, X. Garbet, P. Mantica, V. Parail, W. Suttrop and the EFDA-JET Contributors.
  Plasma Physics and Controlled Fusion, 47**,** (3), 505, 2005

- *"ITER-like PAM launcher for Tore Supra's LHCD system"*
  Belo, J.H., Ph. Bibet, M. Missirlian, J. Achard, B. Beaumont, B. Bertrand, M. Chantant, Ph. Chappuis, L. Doceul, A. Durocher, L. Gargiulo, A. Saille, F. Samaille, E. Villedieu.
  Fusion Engineering and Design, 74, 283, 2005

- *"Toward a LHCD system for ITER"*
  Bibet, Ph., Beaumont, B. Belo, J.H., Delpech, L., Ekedahl, A., Granucci, G., Kazarian, F., Litaudon, X., Mailloux, J., Mirizzi, F., Pericoli, V., Prou, M., Rantamäki, K.,Tuccillo, A.,
  Fusion Engineering and Design, 74, 419-423, 2005;

- *"An n-port error model and calibration procedure for measuring the scattering matrices of lower-hybrid multijunctions"*
  Bizarro, J.P.
  Fusion Engineering and Design, 74, 413, 2005

- *"Application of a stratified plasma model to microwave reflectometry of density fluctuations"*
  Bruskin, L.G., A. Mase, G.D. Conway, A. Silva, M.E. Manso, L. Fattorini, J. Santos, F. Serra and ASDEX Upgrade Team
  Plasma Physics and Controlled Fusion, 47**,** (9), 1379, 2005

- *"New millimeter-wave access for JET reflectometry and ECE"*
  Cupido, L., E. de la Luna, C. Antonucci, A. Guigon, F.J. van Amerongen, W.A. Bongers, A.J.H. Donné, M.F. Graswinckel, A. Bruschi, S. Cirant, A. Simonetto, C. Sozzi, D. Wagner, E. Manso, L. Meneses, F. Silva, P. Varela, N. Balshaw, J.M. Chareau, G. Conway, J. Fessey, S. Hanks, R. Pearce, V. Ricardo, D. Sands, D. Starky, T. Tisconia and JET-EFDA Contributers
  Fusion Engineering and Design, 74, 707, 2005

- *"Power deposition onto plasma facing components in poloidal divertor tokamaks during type-I ELMs and disruptions"*
  Eich,T., A. Herrmann, G. Pautasso, P. Andrew, N. Asakura, J.A. Boedo, Y. Corre, M.E. Fenstermacher, J.C. Fuchs, W. Fundamenski, G. Federici, E. Gauthier, B. Gonçalves, A.W. Leonard, A. Loarte, G.F. Matthews, R.A. Pitts, C. Silva, Journal of Nuclear Materials, 337-339, 669, 2005

- *"Type-I ELM substructure on the divertor target plates in ASDEX Upgrade"*
  Eich, T., A. Herrmann, J. Neuhauser, R. Dux, J.C. Fuchs, S. Günter, L.D. Horton, A. Kallenbach, P.T. Lang, C.F. Maggi, M. Maraschek, V. Rohde, W. Schneider and the ASDEX Upgrade Team
  Plasma Physics and Controlled Fusion, 47**,** (6), 815, 2005

- *"Long distance coupling of lower hybrid waves in JET plasmas with edge and core transport barriers"*
  Ekedahl, A., G. Granucci, J. Mailloux, Y. Baranov, S.K. Erents, E. Joffrin, X. Litaudon, A. Loarte, P.J. Lomas, D.C. McDonald, V. Petrzilka, K. Rantamäki, F.G. Rimini, C. Silva, M. Stamp, A.A. Tuccillo and JET EFDA Contributers.
  Nuclear Fusion, 45**,** (5) 351, 2005

- *"The fine structure of ELMs in the scrape-off layer"*
  Endler, M., I. Garcia-Cortés, C. Hidalgo, G.F. Matthews, ASDEX Team and JET Team.
  Plasma Physics and Controlled Fusion, 47**,** (2), 219, 2005

- *"Electron internal transport barriers, rationals and quasi-coherent oscillations in the stellarator TJ-II"*
  Estrada, T., A. Alonso, A.A. Chmyga, N. Dreval, L. Eliseev, C. Hidalgo, A.D. Komarov, A.S. Kozachok, L. Krupnik, A.V. Melnikov, I.S. Nedzelskiy, J.L. de Pablos, L.A. Pereira, Yu Tashev, V. Tereshin and I. Vargas
  Plasma Physics and Controlled Fusion, 47**,** (11), L57, 2005

- *"Real-time measurement and control at JET experiment control"*
  Felton, R., E. Joffrin, A. Murari, L. Zabeo, F. Sartori, F. Piccolo, J. Farthing, T. Budd, S. Dorling, P. McCullen, J. Harling, S. Dalley, A. Goodyear, A. Stephen, P. Card, M. Bright, R. Lucock, E. Jones, S. Griph, C. Hogben, M. Beldishevski, M. Buckley, J. Davis, I. Young, O. Hemming, M. Wheatley, P. Heesterman, G. Lloyd, M. Walters, R. Bridge, H. Leggate, D. Howell, K.-D Zastrow, C. Giroud, I. Coffey, N. Hawkes, M. Stamp, R. Barnsley, T. Edlington, K. Guenther, C. Gowers, S. Popovichef, A. Huber, C. Ingesson, D. Mazon, D. Moreau, D. Alves, J. Sousa, M. Riva, O. Barana, T. Bolzonella, M. Valisa, P. Innocente, M. Zerbini, K. Bosak, J. Blum, E. Vitale, F. Crisanti, E. de la Luna, J. Sanchez and EFDA-JET Contributers.
  Fusion Engineering and Design, 74, 561, 2005

- *"Real-time measurements and control at JET signal processing and physics analysis for diagnostics"*
  Felton, R., E. Joffrin, A. Murari and JET EFDA Contributers
  Fusion Engineering and Design, 74, 769, 2005

- *"Improved Time–Frequency Visualization of Chirping Mode Signals in Tokamak Plasmas Using the Choi-Williams Distribution"*
  Figueiredo, A. C. A., M. F. F. Nave, and EFDA-JET contributors
  IEEE Transactions on Plasma Science, 33, 2, 2005

- *"Statistical description of the radial structure of turbulence in the JET plasma boundary region"*
  Gonçalves, B., C. Hidalgo, C. Silva, M.A. Pedrosa and K. Erents,
  Journal of Nuclear Materials, 337-339, 376, 2005

- *"Safety factor profile requirements for electron ITB formation in TCV"*
  Goodman, T.P., R. Behn, Y. Camenen, S. Coda, E. Fable, M.A. Henderson, P. Nikkola, J. Rossel, O. Sauter, A. Scarabosio, C. Zucca, S. Alberti, P. Amorim, Y. Andrèbe, K. Appert, G. Arnoux, A. Bortolon, A. Bottino, R. Chavan, I. Condrea, E. Droz, B.P. Duval, P. Etienne, D. Fasel, A. Fasoli, B. Gulejová, J-P Hogge, J. Horacek, P-F Isoz, B. Joye, A. Karpushov, S.H. Kim, I. Klimanov, P. Lavanchy, J.B. Lister, X. Llobet, T. Madeira, J-C Magnin, A. Marinoni, J. Márki, B. Marlétaz, P. Marmillod, Y. Martin, An Martynov, M. Maslov, J-M Mayor, J-M Moret, A. Mück, P.J. Paris, I. Pavlov, A. Perez, R.A. Pitts, A. Pochelon, L. Porte, Ch Schlatter, K. Schombourg, H. Shidara, M. Siegrist, U. Siravo, A.V. Sushkov, G. Tonetti, M.Q. Tran, H. Weisen, M. Wischmeier, A. Zabolotsky, G. Zhuang and A. Zhuchkova.
  Plasma Physics and Controlled Fusion, 47**,** (12B), B107, 2005

- *"Sawtooth control in fusion plasmas"*
  Graves, J.P, C. Angioni, R.V. Budny, R.J. Buttery, S. Coda, L-G Eriksson, C.G. Gimblett, T.P. Goodman, R.J. Hastie, M.A. Henderson, H.R. Koslowski, M.J. Mantsinen, An Martynov, M-L Mayoral, A. Mück, M.F.F. Nave, O. Sauter, E. Westerhof, and JET-EFDA Contributers.
  Plasma Physics and Controlled Fusion, 47**,** (12B), B121, 2005

- *"Poloidal rotation dynamics, radial electric field, and neoclassical theory in the JET Internal-Transport-Barrier region"*
  Crombe, K., Y. Andrew, M. Brix, C. Giroud, S. Hacquin, N. Hawkes, A. Murari, F Nave, J. Ongena, V. Parail, G. Van Oost, I. Voitsekhovitch, K. Zastrow and EFDA-JET Contributors
  Physical Review Letters, 95, 155003, 2005

- *"ITER operation beyond its baseline scenario"*
  Gruber, O., J. Hobirk, C.F. Maggi, M. Maraschek, Y-S Na, A.C.C. Sips, A. Staebler, J. Stober, ASDEX Upgrade Team and ITPA TG on Steady-State Operation
  Plasma Physics and Controlled Fusion, 47**,** (12B), B135, 2005

- *"Development of an ITER relevant advanced scenario at ASDEX Upgrade"*
  Gruber, O., A.C.C. Sips, A. Staebler, R. Dux, J. Hobirk, L.D. Horton, C.F. Maggi, A. Manini, M. Maraschek, R. Neu and ASDEX Upgrade Team.
  Physics of Plasmas, 12**,** (5), 056127, 2005

- *"Joint research using small tokamaks"*
  Gryaznevich, M.P., E. Del Bosco, A. Malaquias, G. Mank, G. Van Oost, Yexi He, H. Hegazy, A. Hirose, M. Hron, B. Kuteev, G.O. Ludwig, I.C. Nascimento, C. Silva and G.M. Vorobyev
  Nuclear Fusion, 45**,** (10), S245, 2005

- *"Overview of ASDEX Upgrade results – development of integrated operating scenarios for ITER"*
  Günter, S., C. Angioni, M. Apostoliceanu, C. Atanasiu, M. Balden, G. Becker, W. Becker, K. Behler, K. Behringer, A. Bergmann, R. Bilato, I. Bizyukov, V. Bobkov, T. Bolzonella, D. Borba, K. Borras, M. Brambilla, F. Braun, A. Buhler, A. Carlson, A. Chankin, J. Chen, Y. Chen, S. Cirant, G. Conway, D. Coster, T. Dannert, K. Dimova, R. Drube, R. Dux, T. Eich, K. Engelhardt, H.-U. Fahrbach, U. Fantz, L. Fattorini, M. Foley, P. Franzen, J.C. Fuchs, J. Gafert, K. Gal, G. Gantenbein, M. Garcia Munoz, O. Gehre, A. Geier, L. Giannone, O. Gruber, G. Haas, D. Hartmann, B. Heger, B. Heinemann, A. Herrmann, J. Hobirk, H. Hohenöcker, L. Horton, M. Huart, V. Igochine, A. Jacchia, M. Jakobi, F. Jenko, A. Kallenbach, S. Kalvin, O. Kardaun, M. Kaufmann, A. Keller, A. Kendl, M. Kick, J.-W. Kim, K. Kirov, S. Klose, R. Kochergov, G. Kocsis, H. Kollotzek, C. Konz, W. Kraus, K. Krieger, T. Kurki-Suonio, B. Kurzan, K. Lackner, P.T. Lang, P. Lauber, M. Laux, F. Leuterer, J. Likonen, A. Lohs, A. Lorenz, R. Lorenzini, A. Lyssoivan, C. Maggi, H. Maier, K. Mank, A. Manini, M. E. Manso, P. Mantica, M. Maraschek, P. Martin, K.F. Mast, M. Mayer, P. McCarthy, H. Meyer, D. Meisel, H. Meister, S. Menmuir, F. Meo, P. Merkel, R. Merkel, D. Merkl, V. Mertens, F. Monaco, A. Mück, H.W. Müller, M. Münich, H. Murmann, Y.-S. Na, R. Narayanan, G. Neu, R. Neu, J. Neuhauser, D. Nishijima, Y. Nishimura, J.-M. Noterdaeme, I. Nunes, M. Pacco-Düchs, G. Pautasso, A.G. Peeters, G. Pereverzev, S. Pinches, E. Poli, E. Posthumus-Wolfrum,T. Pütterich, R. Pugno, E. Quigley, I. Radivojevic, G. Raupp, M. Reich, R. Riedl, T. Ribeiro, V. Rohde, J. Roth, F. Ryter, S. Saarelma, W. Sandmann, J.

Santos, G. Schall, H.-B. Schilling, J. Schirmer, W. Schneider, G. Schramm, J. Schweinzer, S. Schweizer, B. Scott, U. Seidel, F. Serra, C. Sihler, A. Silva, A. Sips, E. Speth, A. Stäbler, K.-H. Steuer, J. Stober, B. Streibl, D. Strintzi, E. Strumberger, W. Suttrop, G. Tardini, C. Tichmann, W. Treutterer, M. Troppmann, M. Tsalas, H. Urano, P. Varela, D. Wagner, F. Wesner, E. Würsching, M.Y. Ye, S.-W. Yoon, Q. Yu, B. Zaniol, D. Zasche, T. Zehetbauer, H.-P Zehrfeld, M. Zilker and H. Zohm.
Nuclear Fusion, 45**,** (10), S98, 2005

- *"Tritium fast ion distribution in JET current hole plasmas"*
Hawkes, N.C., V.A. Yavorskij, J.M. Adams, Yu F. Baranov, L. Bertalot, C.D. Challis, S. Conroy, V. Goloborod'ko, V. Kiptily, S. Popovichev, K. Schoepf, S.E. Sharapov, D. Stork, E. Surrey and EFDA-JET contributors
Plasma Physics and Controlled Fusion, 47**,** (9), 1475, 2005

- *"Rapid electron internal transport barrier formation during magnetic shear reversal in fully non-inductive TCV discharges"*
Henderson, M.A., Y. Camenen, S. Coda, E. Fable, T.P. Goodman, P. Nikkola, A. Pochelon, O. Sauter, C. Zucca and the TCV Team
Nuclear Fusion, 45**,** (12), 1642, 2005

- *"Overview of TJ-II experiments"*
Hidalgo, C., C. Alejaldre, A. Alonso, J. Alonso, L. Almoguera, F. de Aragón, E. Ascasíbar, A. Baciero, R. Balbín, E. Blanco, J. Botija, B. Brañas, E. Calderón, A. Cappa, J.A. Carmona, R. Carrasco, F. Castejón, J.R. Cepero, A.A. Chmyga, J. Doncel, N.B. Dreval, S. Eguilior, L. Eliseev, T. Estrada, J.A. Ferreira, A. Fernández, J.M. Fontdecaba, C. Fuentes, A. Garcia, I. García-Cortés, B. Gonçalves, J. Guasp, J. Herranz, A. Hidalgo, R. Jiménez, J.A. Jiménez, D. Jiménez-Rey, I. Kirpitchev, S.M. Khrebtov, A.D. Komarov, A.S. Kozachok, L. Krupnik, F. Lapayese, M. Liniers, D. López-Bruna, A. López-Fraguas, J. López-Rázola, A. López-Sánchez, E. de la Luna, G. Marcon, R. Martin, K.J. McCarthy, F. Medina, M. Medrano, A.V. Melnikov, P. Mendez, B. van Milligen, I.S. Nedzelskiy, M. Ochando, O. Orozco, J.L. de Pablos, L. Pacios, I. Pastor, M.A. Pedrosa, A. de la Peña, A. Pereira, A. Petrov, S. Petrov, A. Portas, D. Rapisarda, L. Rodriguez-Rodrigo, E. Rodriguez-Solano, J. Romero, A. Salas, E. Sanchez, J. Sanchez, M. Sanchez, K. Sarksian, C. Silva, S. Schchepetov, N. Skvortsova, F. Tabarés, D. Tafalla, A. Tolkachev, V. Tribaldos, I. Vargas, J. Vega, G. Wolfers and B. Zurro
Nuclear Fusion, 45**,** (10), S266, 2005

- *"Characterization of the H-mode edge barrier at ASDEX Upgrade"*
Horton, L.D., A.V. Chankin, Y.P. Chen, G.D. Conway, D.P. Coster, T. Eich, E. Kaveeva, C. Konz, B. Kurzan, J. Neuhauser, I. Nunes, M. Reich, V. Rozhansky, S. Saarelma, J. Schirmer, J. Schweinzer, S. Voskoboynikov, E. Wolfrum and the ASDEX Upgrade Team
Nuclear Fusion, 45**,** (8), 856, 2005

- *"Multi-machine transport analysis of hybrid discharges from the ITPA profile database"*
Imbeaux, F., J.F. Artaud, J. Kinsey, T.J.J. Tala, C. Bourdelle, T. Fujita, C. Greenfield, E. Joffrin, Y.S. Na, V.V. Parail, Y. Sakamoto, A.C.C. Sips, I. Voitsekovitch and contributers to the EFDA-JET Workprogramme, for the ITPA Topical Group on Transport Physics and the ITB Database Working Group
Plasma Physics and Controlled Fusion, 47**,** (12B), B179, 2005

- *"The 'hybrid' scenario in JET:towards its validation for ITER"*
Joffrin, E., A.C.C.Sips, J.F.Artaud, A.Becoulet, L.bertalot, R.Budny, P.Buratti, P.Belo, C.D.Challis, F.Crisanti, M.de Baar, P. De Vries, C.Gormezano, C.Giroud, O.Gruber, G.T.A.Huysmans, F.Imbeaux, A.Isayama, X.Litaudon, P.J.Lomas, D.C.McDonald, Y.S.Na, S.D.Pinches, A.Staebler, T.Tala, A.Tuccillo, K-D.Zastrow and JET-EFDA Contributors to the Work Programme,
Nuclear Fusion 45, 7, 626-634, 2005

- *"Comparison of TRANSP-evolved q-profiles with MSE constrained equilibrium fits on JET"*
Kelliher, D.J., N.C. Hawkes, P.J. Mc Carthy and contributors to the EFDA-JET Workprogramme
Plasma Physics and Controlled Fusion, 47**,** (9), 1459, 2005

- *"The spatial structure of type-I ELMs at the mid-plane in ASDEX Upgrade and a comparison with data from MAST"*
Kirk, A., T. Eich, A. Herrmann, H.W. Muller, L.D. Horton, G.F. Counsell, M. Price, V. Rohde, V. Bobkov, B. Kurzan, J. Neuhauser, H. Wilson and the ASDEX Upgrade and MAST Teams
Plasma Physics and Controlled Fusion, 47**,** (7), 995, 2005

- *"Observation of the palm tree mode, a new MHD mode excited by type-I ELMs on JET"*
Koslowski, H.R., B. Alper, D.N. Borba, T. Eich, S.E. Sharapov, C.P. Perez, E. Westerhof and JET-EFDA contributors.
Nuclear Fusion, 45**,** (3) 201, 2005

- *"Impact of a pulsed supersonic deuterium gas jet on the ELM behaviour in ASDEX Upgrade"*
Lang, P.T., J. Neuhauser, J. Bucalossi, A. Chankin, D.P. Coster, R. Drube, R. Dux, G. Haas, L.D. Horton, S. Kalvin, G. Kocsis, M. Maraschek, V. Mertens, V. Rohde, V. Rozhansky, R. Schneider, I. Senichenkov, I. Veselova, E. Wolfrum and ASDEX Upgrade Team
Plasma Physics and Controlled Fusion, 47**,** (9), 1495, 2005

- *"Integrated exhaust scenarios with actively controlled ELMs"*
Lang, P.T., A. Kallenbach, J. Bucalossi, G.D. Conway, A. Degeling, R. Dux, T. Eich, L. Fattorini, O. Gruber, S. Günter, A. Herrmann, J. Hobirk, L.D. Horton, S. Kalvin, G. Kocsis, J. Lister, M.E. Manso, Maraschek, Y. Martin, P.J. McCarthy, V. Mertens, R. Neu, J. Neuhauser, I. Nunes, T. Pütterich, V. Rozhansky, R. Schneider, W. Schneider, I. Senichenkov, A.C.C. Sips, W. Suttrop, W. Treutterer, I. Veselova, H. Zohm and the ASDEX Upgrade Team
Nuclear Fusion, 45**,** (6), 502, 2005

- *"The JET-enhanced performance programme: more heating power and diagnostic capabilities in preparation for ITER"*
  Lioure A., A. Kaye, A. Murari, J. Sanchez, T. Todd, C. Damiani, J. Pamela and JET-EFDA Contributors.
  Fusion Engineering and Design, 74, 141, 2005

- *"Fast ion distribution driven by polychromatic ICRF waves on JET"*
  Mantsinen, M.J., V. Kiptily, M. Laxaback, A. Salmi, Yu Baranov, R. Barnsley, P. Beaumont, S. Conroy, P. de Vries, C. Giroud, C. Gowers, T. Hellsten, L.C. Ingesson, T. Johnson, H. Leggate, M-L Mayoral, I. Monakhov, J-M Noterdaeme, S. Podda, S. Sharapov, A.A. Tuccillo, D. Van Eester and EFDA JET Contributers
  Plasma Physics and Controlled Fusion, 47**,** (9), 1439, 2005

- *"Active control of MHD instabilities by ECCD in ASDEX Upgrade"*
  Maraschek, M., G. Gantenbein, T.P. Goodman, S. Günter, D.F. Howell, F. Leuterer, A. Mück, O. Sauter, H. Zohm, contributers to the EFDA-JET workprogramme and the ASDEX Upgrade Team
  Nuclear Fusion, 45**,** (11), 1369, 2005

- *"Additional evidence for the universality of the probability distribution of turbulent fluctuations and fluxes in the scrape-off layer region of fusion plasmas"*
  Milligen, B. Ph. Van., R. Sánchez, B.A. Carreras, V.E. Lynch, B. LaBombard, M.A. Pedrosa, C. Hidalgo, B. Gonçalves, R. Balbín and the W7-AS Team.
  Physics of Plasmas, 12**,** (5), 052507, 2005

- *"Impurity-seeded ELMy H-modes in JET, with high density and reduced heat load"*
  Monier-Garbet, P., Ph. Andrew, P. Belo, G. Bonheure, Y. Corre, K. Crombe, P. Dumortier, T. Eich, R. Felton, J. Harling, J. Hogan, A. Huber, S. Jachmich, E. Joffrin, H.R. Koslowski, A. Kreter, G. Maddison, G.F. Matthews, A. Messiaen, M.F. Nave, J. Ongena, V. Parail, M.E. Puiatti, J. Rapp, R. Sartori, J. Stober, M.Z. Tokar, B. Unterberg, M. Valisa, I. Voitsekhovitch, M. von Hellermann and JET-EFDA contributers.
  Nuclear Fusion, 45**,** (11), 1404, 2005

- *"Sawtooth control experiments on ASDEX Upgrade"*
  Mück, A., T.P. Goodman, M. Maraschek, G. Pereverzev, F. Ryter, H. Zohm and ASDEX Upgrade Team
  Plasma Physics and Controlled Fusion, 47**,** (10), 1633, 2005

- *"New developments in JET neutron, γ-ray and particle diagnostics with relevance to ITER"*
  Murari, A., L. Bertalot, S. Conroy, G. Ericsson, V. Kiptily, S. Popovichev, H. Schuhmacher, J.M. Adams, V. Afanasyiev, M. Angelone, G. Bonheure, B. Esposito, J. Källne, M. Mironov, M. Pillon, M. Reginatto, D. Stork, A. Zimbal and JET-EFDA Contributers
  Nuclear Fusion, 45**,** (10), S195, 2005

- *"Fishbones in Joint European Torus plasmas with high ion-cyclotron-resonance-heated fast ions energy content"*
  Nabais, F., D. Borba, M. Mantsinen, M. F. F. Nave and S. E. Sharapov
  Physics of Plasmas, 12**,** 10, 102509, 2005

- *"Efficiency of plasma biasing by movable localized limiter in tokamak ISTTOK"*
  Nedzelskiy, I.S., C. Silva, H. Figueiredo, C.A.F. Varandas, J.A. Cabral,
  Chechoslovak Journal of Physics, 55, 3, 361, 2005.

- *"Tungsten: an option for divertor and main chamber plasma facing components in future fusion devices"*
  Neu, R., R. Dux, A. Kallenbach, T. Pütterich, M. Balden, J.C. Fuchs, A. Herrmann, C.F. Maggi, M.O'Mullane, R. Pugno, I. Radivojevic, V. Rohde, A.C.C. Sips, W. Suttrop, A. Whiteford and the ASDEX Upgrade team.
  Nuclear Fusion, 45**,** (3) 209, 2005

- *"Experimental studies of toroidal momentum transport in ASDEX Upgrade"*
  Nishijima, D., A. Kallenbach, S. Günter, M. Kaufmann, K. Lackner, C.F. Maggi, A.G. Peeters, G.V. Pereverzev, B. Zaniol and the ASDEX Upgrade Team.
  Plasma Physics and Controlled Fusion, 47**,** (1), 89, 2005

- *"Matching to ELMy plasmas in the ICRF domain"*
  Noterdaeme, J.-M., V.V. Bobkov, S. Brémond, A. Parisot, I. Monakhov, B. Beaumont, Ph. Lamalle, F. Durodié, M. Nightingale, the ASDEX Upgrade Team, the Tore Supra Team, and the JET-EFDA contributers.
  Fusion Engineering and Design, 74, 191, 2005

- *"Density profile analysis during an ELM event in ASDEX Upgrade H-modes"*
  Nunes, I., M. Manso, F. Serra, L.D. Horton, G.D. Conway, A. Loarte and the ASDEX Upgrade CFN Reflectometry Teams
  Nuclear Fusion, 45**,** (12), 1550, 2005

- *"Overview of JET results"*
  Pamela, J., J. Ongena and JET EFDA Contributers
  Nuclear Fusion, 45**,** (10), S63, 2005

- *"Overview of recent JET results in preparation for ITER operation: interplay between technical and scientific progress"*
  Pamela, J., J. Ongena, D. Borba, R. Buttery, G. Counsell, R. Felton, E. Joffrin, P. Lomas, A. Murari, J.-M. Noterdaeme, G. Piazza, V. Riccardo, R. Pitts, S. Rosanvallon, D. Stork, K.-D. Zastrow and JET-EFDA Contributors.
  Fusion Engineering and Design, 74, 17, 2005

- *"Microstructural Characterization on Eurofer/ODS RAFM Steel in the Normalized and Tempered Condition and after Thermal Aging in Simulated Fusion Conditions"*
  Paúl, A., E. Alves, L.C. Alves, C. Marques, R. Lindau, J.A. Odriozola,
  Fusion Engineering and Design, 75-79 (2005) 1061-1065.

- *"Threshold for sheared flow and turbulence development in the TJ-II stellarator"*
  Pedrosa, M.A., C. Hidalgo, E. Calderón, T. Estrada, A. Fernández, J. Herranz, I. Pastor and the TJ-II team

Plasma Physics and Controlled Fusion, 47**,** (6), 777, 2005

- *"Linear gyrokinetic stability calculations of electron heat dominated plasmas in ASDEX Upgrade"*
  Peeters, A.G., C. Angioni, M. Apostoliceanu, F. Jenko, F. Ryter and the ASDEX Upgrade Team.
  Physics of Plasmas, 12**,** (2), 022505, 2005

- *"Linear gyrokinetic calculations of toroidal momentum transport in a tokamak due to the ion temperature gradient mode"*
  Peeters, A.G., C. Angioni and the ASDEX Upgrade Team.
  Physics of Plasmas, 12**,** (7), 072515, 2005

- *"Understanding of the density profile shape, electron heat transport and internal transport barriers observed in ASDEX Upgrade"*
  Peeters, A.G., C. Angioni, M. Apostoliceanu, G.V. Pereverzev, E. Quigley, F. Ryter, D. Strintzi, F. Jenko, U. Fahrbach, C. Fuchs, O. Gehre, J. Hobirk, B. Kurzan, C.F. Maggi, A. Manini, P.J. McCarthy, H. Meister, J. Schweinzer, J. Stober, W. Suttrop, G. Tardini and the ASDEX Upgrade Team.
  Nuclear Fusion, 45**,** (9), 1140, 2005

- *"Edge and divertor physics with reversed toroidal field in JET"*
  Pitts, R.A., P. Andrew, X. Bonnin, A.V. Chankin, Y.Corre, G. Corrigan, D. Coster, I. Duran, T. Eich, S.K. Erents, W. Fundamenski, G. Kirnev, P.J. Lomas, A. Loate, G.F. Matthews, C. Silva, M.F. Stamp, J. Strachan,
  Journal of Nuclear Materials, 337-339, 146, 2005

- *"Bright spots generated by lower hybrid waves on JET"*
  Rantamäki, K.M., V. Petrzilka, P. Andrew, I. Coffey, A. Ekedahl, K. Erents, V. Fuchs, M Goniche, G. Granucci, E. Joffrin, S.J. Karttunen, P. Lomas, J. Mailloux, M. Mantsinen, M-L Mayoral, D.C. McDonald, J-M Noterdaeme, V. Parail, A.A. Tuccillo, F. Zacek and Contributers to the EFDA – JET Workprogramme
  Plasma Physics and Controlled Fusion, 47**,** (7), 1101, 2005

- *"Tokamak turbulence computations on closed and open magnetic flux surfaces"*
  Ribeiro, T.T., B. Scott
  Plasma Physics and Controlled Fusion, 47**,** (10), 1657, 2005

- *"Timescale and magnitude of plasma thermal energy loss before and during disruptions in JET"*
  Riccardo, V., A. Loarte and the JET EFDA Contributers
  Nuclear Fusion, 45**,** (11), 1427, 2005

- *"Development of internal transport barrier scenarios at ITER-relevant high triangularity in JET"*
  Rimini, F.G., M. Bécoulet, E. Giovannozzi, P.J. Lomas, O. Tudisco, B. Alper, F. Crisanti, M. de Baar, E. de La Luna, P. de Vries, A. Ekedahl, N. Hawkes, G. Huysmans, X. Litaudon, V. Parail, G. Saibene, A.A. Tuccillo, K.D. Zastrow and EFDA-JET Workprogramme Contributers
  Nuclear Fusion, 45**,** (12), 1481, 2005

- *"Grad-Shafranov equilibria with negative core toroidal current in tokamak plasmas"*
  Rodrigues, P. and J. P. S. Bizarro
  Phys. Rev. Lett., 95, 015001, 2005

- *"MHD stability analysis of diagnostic optimized configuration shots in JET"*
  Saarelma, S., V. Parail, Y. Andrew, E de la Luna, A. Kallenbach, M. Kempenaars, A. Korotkov, A. Loarte, J. Lonnroth, P. Monier-Garbet, J. Stober, W. Suttrop and Contributers to the EFDA-JET Workprogramme
  Plasma Physics and Controlled Fusion, 47**,** (5), 713, 2005

- *"On the energy transfer between flows and turbulence in the plasma boundary of fusion devices"*
  Sánchez, E., C. Hidalgo, B. Gonçalves, C. Silva, M.A. Pedrosa, M. Hron, K. Erents,
  Journal of Nuclear Materials, 337-339, 296, 2005

- *"Probe methods for direct measurements of the plasma potential"*
  Schrittwieser, R., C. Ioniță, P.C. Balan, C.A.F. Varandas, H.F.C. Figueiredo, C. Silva, H. Fernandes, J. Stöckel, J. Adámek, M. Hron, J. Ryszawy, M. Tichý, E. Martines, G. Van Oost, T. Klinger, R. Madani, R.M.O. Galvão,
  Romanian Journal of Physics, 50, No.7-8, 2005

- *"Experimental studies of instabilities and confinement of energetic particles on JET and MAST"*
  Sharapov, S.E., B. Alper, F. Andersson, Yu.F. Baranov, H.L. Berk, L. Bertalot, D. Borba, C. Boswell, B.N. Breizman, R. Buttery, C.D. Challis, M. de Baar, P. de Vries, L.-G. Eriksson, A. Fasoli, R. Galvão, V. Goloborod'ko, M.P. Gryaznevich, R.J. Hastie, N.C. Hawkes, P. Helander, V.G. Kiptily, G.J. Kramer, P.J. Lomas, J. Mailloux, M.J. Mantsinen, R. Martin, F. Nabais, M.F. Nave, R. Nazikian, J.-M. Noterdaeme, M.S. Pekker, S.D. Pinches, T. Pinfold, S.V. Popovichev, P. Sandquist, D. Stork, D. Testa, A. Tuccillo, I. Voitsekhovich, V. Yavorskij, N.P. Young, F. Zonca, JET-EFDA Contributers and the MAST Team
  Nuclear Fusion, 45**,** (9), 1168, 2005

- *"Determination of the particle and energy fluxes in the JET far SOL during ELMs using the reciprocating probe diagnostic"*
  Silva, C., B. Gonçalves, C. Hidalgo, K. Erents, A. Loarte, G. Matthews, M. Pedrosa
  Journal of Nuclear Materials, 337-339, 722, 2005

- *"Comparison of limiter and emissive electrode bias on the tokamak ISTTOK"*
  Silva, C., I. Nedzelskiy, H. Figueiredo, R.M.O. Galvão, J.A.C. Cabral, C.A.F. Varandas
  Journal of Nuclear Materials, 337-339, 415, 2005

- *"Transport and fluctuations during electrode biasing on TJ-II"*
  Silva, C., M.A. Pedrosa, C. Hidalgo, K. McCarthy, E. Calderón, B. Gonçalves, J. Herranz, I. Pastor, O. Orozco,
  Czechoslovak Journal of Physics, 55, 1589, 2005

- *"Unidirectional transparent signal injection in finite-difference time-domain electromagnetic codes – application to reflectometry simulations"*
  Silva, F. da, S. Heuraux, S. Hacquin and M. Manso
  Journal of Computational Physics, 203, 2, 467, 2005

- *"Small ELM regimes with good confinement on JET and comparison to those on ASDEX Upgrade, Alcator C-mod and JT-60U"*
  Stober, J., P.J. Lomas, G. Saibene, Y. Andrew, P. Belo, G.D. Conway, A. Herrmann, L.D. Horton, M. Kempenaars, H.-R. Koslowski, A. Loarte, G.P. Maddison, M. Maraschek, D.C. McDonald, A.G. Meigs, P. Monier-Garbet, D.A. Mossessian, M.F.F. Nave, N. Oyama, V. Parail, Ch. P. Perez, F. Rimini, R. Sartori, A.C.C. Sips, P.R. Thomas, Contributers to the EFDA-JET workprogramme and the ASDEX Upgrade Team
  Nuclear Fusion, 45**,** (11), 1213, 2005

- *"Overview of transport, fast particle and heating and current drive physics using tritium in JET plasmas"*
  Stork, D. Yu. Baranov, P. Belo, L. Bertalot, D. Borba, J.H. Brzozowski, C.D. Challis, D. Ciric, S. Conroy, M. de Baar, P. de Vries, P. Dumortier, L. Garzotti, N.C. Hawkes, T.C. Hender, E. Joffrin, T.T.C. Jones, V. Kiptily, P. Lamalle, J. Mailloux, M. Mantsinen, D.C. McDonald, M.F.F. Nave, R. Neu, M.O'Mullane, J. Ongena, R.J. Pearce, S. Popovichev, S.E. Sharapov, M. Stamp, J. Stober, E. Surrey, M. Valovic, I. Voitsekhovitch, H. Weisen, A.D. Whiteford, L. Worth, V. Yavorskij, K.-D. Zastrow and JET EFDA contributers.
  Nuclear Fusion, 45**,** (10), S181, 2005

- *"Studies of the 'Quiescent H-mode' regime in ASDEX Upgrade and JET"*
  Suttrop, W., V. Hynönen, T. Kurki-Suonio, P.T. Lang, M. Maraschek, R. Neu, A. Stäbler, G.D. Conway, S. Hacquin, M. Kempenaars, P.J. Lomas, M.F.F. Nave, R.A. Pitts, K.-D. Zastrow, the ASDEX Upgrade team and contributors to the JET-EFDA workprogramme
  Nuclear Fusion 45, 7, 721-730, 2005

- *"Predictive transport simulations of real-time profile control in JET advanced tokamak plasmas"*
  Tala, T., L. Laborde, D. Mazon, D. Moreau, G. Corrigan, F. Crisanti, X. Garbet, D. Heading, E. Joffrin, X, Litaudon, V. Parail, A. Salmi and contributers to the EFDA-JET workprogramme
  Nuclear Fusion, 45**,** (9), 1027, 2005

- *"Current losses induced by edge localized modes in JET tokamak plasmas"*
  Testa, D., M. Bigi and JET-EFDA contributers
  Plasma Physics and Controlled Fusion, 47**,** (6), 733, 2005

- *"Position dependence of the unstable vertical movement of JET plasmas triggered by ELMs"*
  Villone, F., V. Riccardo, F. Sartori and contributers to the EFDA-JET workprogramme
  Nuclear Fusion, 45**,** (11), 1328, 2005

- *"Effect of sawtooth activity on tritium and beam deuterium evolution in trace tritium experiments on JET"*
  Voitsekhovitch, I., K-D Zastrow, B. Alper, G. Bonheure, X. Garbet, V. Kiptily, E de la Luna, D.C. McDonald, S. Popovichev, S.E. Sharapov, D. Stork and JET EFDA Contributers
  Plasma Physics and Controlled Fusion, 47**,** (11), 1877, 2005

- *"Density dependence of trace tritium transport in H-mode Joint European Torus plasma"*
  Voitsekhovitch I., X. Garbet, D.C. McDonald, K.-D. Zastrow, M. Adams, Yu. Baranov, P. Belo, L. Bertalot, R. Budny, S. Conroy, J.G. Cordey, L. Garzotti, P. Mantica, D. McCune, J. Ongena, V. Parail, S. Popovichev, D. Stork, A.D. Whiteford and JET EFDA contributers
  Physics of Plasmas, 12**,** (5), 052508, 2005

- *"Simulation of environment effects on retroreflectors in ITER"*
  Voitsenya, V.S., A.J.H. Donné, A. F. Bardamid, A.I. Belyaeva, V.L. Berezhnyj, A.A. Galuza, Ch. Gil, V.G. Konovalov, M. Lipa, A. Malaquias, D.I. Naidenkova, V.I. Ryzhkov, B. Schunke, S.I. Solodovchenko and A.N. Topkov.
  Review of Scientific Instruments, 76**,** (8), 83502, 2005

- *"Effects of temperature ratio on JET transport in hot ion and hot electron regimes"*
  Weiland, J., E. Asp, X. Garbet, P. Mantica, V. Parail, P. Thomas, W. Suttrop, T. Tala and the EFDA-JET Contributors.
  Plasma Physics and Controlled Fusion, 47**,** (3), 441, 2005

- *"Collisionality and shear dependences of density peaking in JET and extrapolation to ITER"*
  Weisen, H., A. Zabolotsky, C. Angioni, I. Furno, X. Garbet, C. Giroud, H. Leggate, P. Mantica, D. Mazon, J. Weiland, L. Zabeo, K.-D Zastrow and JET-EFDA contributors.
  Nuclear Fusion, 45**,** (2) L1, 2005

- *"Edge stability of the ELM-free quiescent H-mode on DIII-D"*
  West, W.P., K.H. Burrell, T.A. Casper, E.J. Doyle, P.B. Snyder, P. Gohil, L.L. Lao, C.J. Lasnier, A.W. Leonard, M.F.F. Nave, T.H. Osborne, D.M. Thomas, G. Wang and L. Zeng
  Nuclear Fusion 45, 12, 1708-1714, 2005

- *"A cross-tokamak neural network disruption predictor for the JET and ASDEX Upgrade tokamaks"*
  Windsor, C.G., G. Pautasso, C. Tichmann, R.J. Buttery, T.C. Hender, JET EFDA Contributers and the ASDEX Upgrade Team
  Nuclear Fusion, 45**,** (5) 337, 2005

- *"Feedback and rotational stabilization of resistive wall modes in ITER"*
  Yueqiang Liu, A. Bondeson, M.S. Chu, J.-Y. Favez, Y. Gribov, M Gryaznevich, T.C. Hender, D.F. Howell, R.J. La Haye, J.B. Lister, P. de Vries and EFDA JET Contributers.
  Nuclear Fusion, 45**,** (9), 1131, 2005

- *"Helium exhaust experiments on JET with type I ELMs in H-mode and with Type III ELMs in ITB discharges"*
  Zastrow, K.-D., S.J. Cox, M.G. von Hellermann,

M.G.O'Mullane, D. Stork, M Brix, C.D. Callis, I.H. Coffey, R. Dux, K.H. Finken, C. Giroud, D. Hillis, J.T. Hogan, K.D. Lawson, T. Loarer, A.G. Meigs, P.D. Morgan, M.F. Stamp, A.D. Whiteford and JET-EFDA contributors.
Nuclear Fusion, 45**,** (3) 163, 2005

19.1.3. Papers in international conferences

- **Second IAEA Technical Meeting on the Theory of Plasma Instabilities: Transport, Stability and their Interaction, 2-4 de March, Trieste, Italy**

- *"Effect of Sheared Equilibrium Plasma Rotation on the Stability of Tearing Modes"*
  Coelho, R.

- **32nd Annual IoP Plasma Physics Group Conference, 21-24 of March, Oxford, England**

- *Reflectometry for Density Profile and Turbulence Measurement in Fusion Plasmas*
  Hacquin, S., on behalf of the "Electron Kinetics" Group, the JET Task Force D and the EFDA-JET Contributors

- **US-European transport task force Workshop, Napa, USA, April 6-9 2005**

- "*n=0 Energetic Particle Driven Oscillations in JET"*
  Berk, H.L., C. Boswell, T. Johnson, , M.F.F. Nave, S.D. Pinches, S.E. Sharapov, L. Zakharov and contributors to the EFDA-JET workprogramme

- *"Recent progress in diagnostics of energetic particle driven modes: new opportunities and challenges"*
  Sharapov, S., B. Alper, H. Berk, D. Borba, C. Boswell, B. Breizman, E. de la Luna, J. Fessey, S. Hacquin, G. Kramer, R. Nazikian, S. Pinches, J. Rapp, D. Testa, N. Young and JET-EFDA Contributors

- **7th International Reflectometry Workshop for Fusion Plasma Diagnostics, 9-12 of May, Garching, Germany**

- *"Profile Reflectometry on MAST"*
  Cunningham, G., T. Edlington, A. Silva and L. Meneses

- *"Frequency Hopping Millimeter-wave Reflectometry in ASDEX Upgrade"*
  Cupido, L., S. Graça, L. Meneses, J. Santos, M. Manso and F. Serra

- "*Identification of Local Alfvén Wave Resonances with Reflectometry as a Diagnostic Tool in Tokamaks"*
  Elfimov, A.G., R. M.O. Galvão, L. F. Ruchko, M.E.C.Manso and A.A.Ivanov

- "*Fluctuation Measurements in TJ-II using a Broadband Fast Frequency Hopping Reflectometer"*
  Estrada, T., E. Blanco, L. Cupido, M.E. Manso and J. Sánchez

- *"A New Spectral Analysis to Study Pellet Triggered ELMs from Broadband Reflectometry at ASDEX Upgrade"*
  Fattorini, L., M. E. Manso, P. T. Lang and the ASDEX Upgrade Team

- *"Nonlinear Effects in the Doppler Reflectometry (Analytical Theory and Numerical Simulations)"*
  Gusakov, E.Z., S. Heuraux, F. da Silva and A.V. Surkov

- *"Further Development of Reflectometry Diagnostics for Measurement of Alfvén Cascades on the JET Tokamak"*
  Hacquin, S., S. Sharapov, B. Alper, D. Borba, C. Boswell, J. Fessey, L. Meneses, M. Walsh and the JET EFDA Contributors

- *"Radial Behaviour of Density Fluctuations Deduced from FM-CW Tore Supra Reflectometry Data"*
  Heuraux, S., L. Vermare, F. Clairet, G. Leclert and F. da Silva

- *"JET Density Profile Reflectometer, New Design"*
  Meneses, L., L.Cupido, A.A. Ferreira, M. Manso and L. Guimarãis

- *"Experimental Studies of the Registration of Alfvén Wave Resonances in the TCABR Tokamak by the Frequency Scanning Reflectometry"*
  Ruchko, L. F., R. M. O. Galvão, A. G. Elfimov, J. I. Elizondo, E. Sanada, Yu. K. Kuznetsov, A. M. M. Fonseca, V. Bellintani Jr, A. N. Fagundes, I.C. Nascimento, W. P. de Sá, C.A.F. Varandas, M. Manso, P. Varela and A. Silva

- *"Doppler Reflectometry Spectra Simulations with Velocity Shear Layer"*
  Silva, F. da, S. Heuraux and M. Manso

- *"Automatic Electron Density Measurements with Microwave Reflectometry During High-Density H-mode Discharges on ASDEX Upgrade"*
  Silva, A., P. Varela, L. Cupido, M. Manso, L. Meneses, L.Guimarães, G. Conway, F. Serra and the ASDEX Upgrade Team

- *"Adaptive Window Calculation for Automatic Spectrogram Analysis of Broadband Reflectometry Data"*
  Varela, P., A. Silva, M. Manso and the ASDEX Upgrade Team

- *"Status and Plans for Reflectometry in ITER"*
  Vayakis, G., and C. Walker for the ITER International Team and Participant Teams with contributions from F. Clairet, R. Sabot, V. Tribaldos, T. Estrada, E. Blanco, J. Sánchez, G.G. Denisov, V.I. Belousov, F. Da Silva, P. Varela, M. E. Manso, L. Cupido, João Dias, Nuno Valverde, V.A. Vershkov, D.A. Shelukhin, S.V. Soldatov, A.O. Urazbaev, E.Yu. Frolov and S. Heuraux

- **14th IEEE-NPSS Real Time Conference, 4-11 of June, Stockholm, Sweden**

- *"A FPGA-Based Multi-Rate Interpolar with Real-Time Rate Change for a JET Test-Bench System"*
  Batista, A. J. N., D. Alves, N. Cruz, J. Sousa, C. A. F. Varandas, E. Joffrin, R. Felton, J. Farthing and JET-EFDA Contributors

- *"Upgrade of the Data Acquisition and Control System of the ASDEX Upgrade Microwave Reflectometer"*
  Combo, A., A. Silva, P. Varela, M. Manso, J. Sousa, C. Correia and C.A.F. Varandas

- *"Digital Control System for the TCV Tokamak"*
  Duval, B.P., J-M. Moret, A.P. Rodrigues, L.A. Pereira, C.A.F. Varandas

- *"A Cooperative JAVA Web-Start Environment for Shared Multi-User Remote Operation"*
  Neto, A., H. Fernandes, B. B. Carvalho, J. Sousa and C. A. F. Varandas

- *"Real-Time Multi-DSP Based VME System for Feedback Control on the TCV Tokamak"*
  Rodrigues, A.P., L. Pereira, T.I. Madeira, P. Amorim, C.A.F. Varandas and B. Duval

- *"Fast Feedback Control for Plasma Positioning with a PCI hybrid DSP/FPGA Board"*
  Valcárcel, D. F., I. S. Carvalho, B. B. Carvalho, H. Fernandes, J. Sousa and C. A. F. Varandas

- **32nd EPS Conference on Plasma Physics and Controlled Fusion, 27 of June to 1 of July of 2005, Tarragona, Spain**

- *"H-mode access in the low density regime on JET"*
  Andrew Y, Sartori R, Righi E, de la Luna E, Hacquin S, Hawkes N C, Horton L D, Huber A, Korotkov A, O'Mullane M G, JET-EFDA contributors

- *"Numerical Simulation of Impurity Screening in the SOL of JET Plasma by Localised Deuterium Gas Puffing"*
  Belo, P., V. Parail, G Corrigan, J Hogan, D. Heading, J. Spence, C. Giroud and JET EFDA contributors

- *"Experimental Observations of n = 0 Mode Driven by Energetic Particles on JET"*
  Boswell,C., H.L. Berk, T. Johnson, M.F.F. Nave, S.D. Pinches, S.E. Sharapov, L. Zakharov and EFDA-JET contributors

- *"Effect of Alfvén Resonances on the Penetration of Error Fields on a Rotating Viscous Plasma"*
  Coelho, R. and E. Lazzaro

- *"High Spatial and Temporal Resolution FM-CW Reflectometry to Study Pellet Triggered ELMs at ASDEX Upgrade"*
  Fattorini, L., P. T. Lang, M. E. Manso, S. Kalvin, G. Kocsis and the ASDEX Upgrade Team

- *"A tool for the Parallel Calculation and Ready Visualization of the Choi–Williams Distribution: Application to Fusion Plasma Signals"*
  Figueiredo, A.C.A., J.S. Ferreira, B.B. Carvalho and M.F.F. Nave

- *"Study of edge flows and transport during emissive electrode biased discharges on ISTTOK"*
  Figueiredo, H., C. Silva, I. Nedzelsky, B. Gonçalves, H. Fernandes, C.A.F. Varandas,

- *"Turbulence Experiments in Reversed and Standard-B Field Configurations in the JET Tokamak"*
  Gonçalves, B., C. Hidalgo, C. Silva, M.A. Pedrosa, M. Hron and JET EFDA contributors

- *"Sawtooth control in fusion plasmas"*
  Graves, J. P., R. V. Budny, R. J. Buttery, S. Coda, L.-G. Eriksson, C. G. Gimblett, R. J. Hastie, H. R. Koslowski, M. J. Mantsinen, M.-L. Mayoral, A. Mueck, M. F. F. Nave, O. Sauter, and JET-EFDA Contributors

- *"Electron transport barriers, rationals and fluctuations in the TJ-II"*
  Krupnik, L., J.A. Alonso, A. Cappa, A.A. Chmuga, N.B. Dreval, L. Eliseev, T. Estrada, A. Fernandez, C. Fuentes, C. Hidalgo, S.M. Khrebtov, A.D. Komarov, A.S. Kozachok, A.V. Melnikov, I.S. Nedzelskiy, M. Liniers, J.L. de Pablos, M.A. Pedrosa, Yu. Tashchev, V. Tereshin, E. Sanchez

- *"ELM mitigation by externally induced ELMs - Physics and Prospects"*
  Lang, P.T., J.Bucalossi, L.Fattorini, K.Gal, L.D.Horton, A.Kallenbach, J.Lister, S.Kalvin, G.Kocsis, M.E.Mansoy, M.Maraschek, Y.Martin, V.Mertens, R.Neu, J.Neuhauser, T.Pütterich, A.C.C.Sips, W.Suttrop, G.Veres and ASDEX Upgrade Team

- *"First Results Obtained with the Real-Time PHA Diagnostic on TCV"*
  Madeira, T.I., P.Amorim, B.P.Duval, A.P.Rodrigues, L.Pereira and C.A.F.Varandas

- *"Spatial Asymmetries in ELM induced Pedestal Density Collapse in ASDEX Upgrade H-modes"*
  Nunes, I., M. Manso, F. Serra, L. D. Horton, G. D. Conway, A. Loarte and the ASDEX Upgrade and CFN Reflectometry Teams

- *"Effect of the Plasmas Geometry Evolution on Runaway Electron Generation in Tokamak Disruptions"*
  Plyusnin, V.V.

- *"Gyrofluid Turbulence Computations in the Edge and SOL Regions of Tokamak Plasmas using Realistic Magnetic Field Geometry"*
  Ribeiro, T.T., B. Scott, D. Coster and F. Serra

- *"On the Momentum Re-distribution via Fluctuations in Fusion Plasmas"*
  Sanchez, E., C. Silva, M.A. Pedrosa, C. Hidalgo, K. McCarthy, E. Calderón, B. Gonçalves, J. Herranz, I. Pastor and O. Orozco

- *"Transport and fluctuations during electrode biasing on TJ-II"*
  Silva, C., M.A. Pedrosa, C. Hidalgo, K. McCarthy, E. Calderón, B. Gonçalves, J. Herranz, I. Pastor, O. Orozco,

- *"Relaxation phenomena during edge plasma biasing in the CASTOR tokamak"*
  Spolaore, M., J. Brotánková, P. Peleman, P. Devynck, H. Figueiredo, G. Kirnev, E. Martines, J. Stöckel, G. Van

Oost, J. Adamek, E. Dufková, I. Duran, M. Hron, V. Weinzettl

- **17th International Conference on Ion Beam Analysis, Sevilla, Spain, June 26 - July 1 2005**

- *"Ion Beam Characterisation of ODS Steel Samples after Long Term Annealing Conditions"*
  Alves, L. C., E. Alves, A. Paúl, M. R. da Silva, J. A. Odriozola

- **8th Workshop on the Electric Field, Structures and Relaxation in Edge Plasmas, 3-4 of July of 2005, Tarragona, Spain**

- *"Study of pellet triggered ELMs using high spatial and temporal resolution FM-CW reflectometry at ASDEX Upgrade"*
  Fattorini, L., P. T. Lang, M. E. Manso, S. Kalvin, G. Kocsis and the ASDEX Upgrade Team.

- *"Local 3D Perturbation Experiments for Probing the SLM stability"*
  Lang, P.T., J. Neuhauser, J. Bucalossi, L. Fattorini, L.D. Horton, S. Kalvin, G. Kocsis, M.E. Manso, M. Maraschek, G. Veres and the ASDEX Upgrade Team

- **5th IAEA Technical Meeting on Control, Data Acquisition and Remote Participation for Fusion Research, 12-15 of July of 2005, Budapest, Hungary**

- *"JET Real Time Project Test-Bench Software Structure"*
  Cruz, N., A.J.N. Batista, D. Alves, J. Sousa, C.A.F. Varandas, E. Joffrin, R. Felton, J.W. Farthing and JET-EFDA Contributors

- "Efficient use of VME modules in TCABR"
  Fagundes, A.N., B.B. Carvalho, M. Correia , J. Sousa

- *"A Generic Remote Method Invocation for Intensive Data Processing"*
  Neto, A., D. Alves, H. Fernandes, J. S. Ferreira and C.A.F. Varandas

- *"Control and Data Acquisition System for the Multiple Cell Array Detector of the TJ-II Heavy Ion Beam Diagnostic"*
  Pereira, L., I.S. Nedzelskiy, B. Gonçalves, J.L. de Pablos, A. Alonso, C. Hidalgo and C.A.F. Varandas

- *"The Software for the Real-Time DSP-Based VME System for Feedback Control on TCV using a PHA X-ray Diagnostic"*
  Pereira, L., A.P. Rodrigues, T.I. Madeira, P. Amorim, B. P. Duval and C.A.F.Varandas

- *"Enhanced Neutron Diagnostics Data Acquisition System based on a Time Digitizer and Transient Recorder Hybrid Module"*
  Pereira, R. C., A.Combo, N.Cruz, Jorge Sousa, C. Correia, C. Varandas, S. Conroy and J. Källne

- *"Real-Time Data Transfer in the TCV Advanced Plasma Control System"*
  Rodrigues, A.P., L. Pereira, J-M. Moret, B. P. Duval and C. A. F. Varandas

- *"A Unified Real-Time Control and Data Acquisition Hardware Platform"*
  Sousa, J., A. J. N. Batista, R. C. Pereira and C. Varandas

- **19th International Conference On Numerical Simulation of Plasmas, 12-15 of July of 2005, Nara, Japan**

- *"On the Computation of Tokamak Equilibria with Negative Core Toroidal Current"*
  Rodrigues, Paulo and João P. S. Bizarro

- *"Developments on Reflectometry Simulations for Fusion Plasmas: Application to ITER Position Reflectometers"*
  Silva, da F. S. Heuraux and M. Manso

- **6th International Workshop "Strong Microwaves in Plasmas", July 25 – August 1 of 2005, Nizhny Novgorod – Saint Petersburg, Russia**

- "*JET Passive Active Multijunction Lower Hybrid Launcher*"
  Bibet, Ph., Belo, J., Bertrand, B., Bizarro, J.P.S., Cesario, R., Kaye, A.,Leguern, F.,Lioure, A.,Mailloux, J., Mirizzi, F., Portafaix, C., Testoni, P., Tuccillo, A.A., Vallet, J.C., Walton, B.,

- **10th IAEA Technical Meeting on H–mode Physics and Transport Barriers, St. Petersburg (Russia), September 2005.**

- *"The quiescent H-mode regime in ASDEX Upgrade"*
  Suttrop, W., V. Hynönen, T. Kurki-Suonio, G. D. Conway, L. Fattorini, P. T. Lang, M. Maraschek, R. Neu, J. Schirmer, A. Stäbler and ASDEX Upgrade Team.

- **RIVA V - 5th Iberian Vacuum Meeting, 18-21 of September of 2005, Guimarães, Portugal**

- *"Redesign of the tokamak ISTTOK hydrogen injection system"*
  Correia, J. Nunes, A. Soares, H. Fernandes

- *"Aluminium Vacuum Deposition Coatings for Dielectric Substrate Microwave Antennas Production"*
  Figueiredo, J., H. Fernandes and C.A.F. Varandas

- **21st IEEE/NPSS Symposium on Fusion Engineering, September 26-29 of 2005, Knoxville, USA.**

- "*ITER LHCD plans and design*"
  Bibet, Ph., Beaumont, B., Belo, J.H., Bizarro, J.P.S., Delpech, L., Ekedahl, A., Granucci, G., Kazarian, F., Kuzikov, S., Litaudon, X., Mailloux, J., Mirizzi, F., Pericoli, V., Prou, M., Rantamäki, K., Tuccillo, A.A

- **47thAnnual Meeting of the Division of Plasma Physics, 24-28 of October of 2005, Denver, USA**

- *"Detection of Alfvén cascades in advanced JET plasmas"*
  Alper, B., S. Sharapov, S. Hacquin, D. Borba, C. Boswell, S. Pinches and JET-EFDA Contributors

- *"Testing the Porcelli Sawtooth Trigger Module"*
  Bateman, G., A. H. Kritz, *M.F.F.Nave,* V. Parail

- *"Axisymmetric Phase Space Structures Driven by Fast Ions in JET"*
  Berk, H. L., C. J. Boswell, Mit-PSFC, S. E. Sharapov, T. Johnson, M. F. F. Nave, S. D. Pinches

- *"Edge Stability Analysis of JET Quiescent H-mode Experiments"*
  Nave, M.F.F., G. Huysmans, J-S. Lonnroth, V. Parail, M. Marascheck, W. Suttrop and EFDA-JET Contributors

- **6th Int. Workshop Electrical Probes in Magnetized Plasmas (IWEP 2005), Seoul, Korea, 2005**
- *"Overview of electrical probe measurements on ISTTOK"*
  Varandas, C.A.F., C. Silva, I. Nedzelsky, H. Figueiredo, H. Fernandes, R. Schrittwieser, C. Ioniță, P. Balan

- **Int. Conf. Nuclear Energy for New Europe 2005 (Bled, Slovenia, Sept. 5-8, 2005)**
- *"Probe Diagnostics for Edge Plasmas in Fusion Experiments"*
  Ioniță, C., R. Schrittwieser, P.C. Balan, J. Stöckel, J. Adámek, M. Hron, C.A.F. Varandas, H.F.C. Figueiredo, C. Silva, M. Tichý, E. Martines, G. Van Oost, J.P. Gunn, T. Klinger

- *"Edge Plasma Fluctuations Measurements in Fusion Experiments" Oral presentation*
  Schrittwieser, R., C. Ioniță, P.C. Balan, C.A.F. Varandas, H.F.C. Figueiredo, C. Silva, J. Stöckel, J. Adámek, M. Hron, M. Tichý, C. Hidalgo, M.A. Pedrosa, E. Calderón, E. Martines, G. Van Oost, J.P. Gunn, T. Klinger

- **9th IAEA TCM on Energetic Particles, Takayama, Japan, November 9-11, 2005**
- *"Axisymmetric Phase Space Structures Driven by Fast Ions in JET"*
  Berk, H. L., C. J. Boswell, D. Borba, T. Johnson, M. F. F. Nave, S. D. Pinches, S. E. Sharapov, and JET EFDA contributors

- *"Fishbones Activity in JET Low Density Plasmas"*
  Nabais, F., D. N. Borba, M. J. Mantsinen, S. E. Sharapov and JET-EFDA contributors

- *"Alfvén cascades in JET discharges with NBI-heating"*
  Sharapov, S., B. Alper, Y. Baranov, H. Berk, D. Borba, C. Boswell, B. Breizman, C. Challis, M. de Baar, E. de la Luna, E. Evangelidis, S. Hacquin, N. Hawkes, V. Kiptily, S. Pinches, P. Sandquist, I. Voitsekhovitch, N. Young and JET-EFDA Contributors

- **7th IEA Workshop International workshop on Beryllium Technology for Fusion, Santa Barbara, USA, 29 Nov. - 2 Dec. 2005**
- *"Structural and oxidation studies of titanium beryllides"*
  Alves, E., L.C. Alves, N. Franco, M.R. da Silva, A. Paúl

- *"Beeeryllium breeder blankets-status of the European R&D"*
  Moeslang, A., E. Alves, L.V. Bocaccini, J.B.J. Hegeman, P. Kurinsky, et al.

- **12th International Conference on Fusion Reactor Material, Santa Barbara, USA, 5-10 December 2005**
- *"Oxidation and stability studies of Beryllium Titanate"*
  Alves, E., L. C. Alves, N. Franco, M.R. da Silva, A. Paúl

- *"Microstructural characterisation of reduced activation EUROFER ODS alloy after long-term annealing"*
  Paúl, A., L. C. Alves, E. Alves, J. A. Odrizola

- **XI Latin-American Workshop on Plasma Physics, Mexico, 5-9 December 2005**
- *" ELMy Studies in ITER Relevant Regimes in ASDEX Upgrade Broadband FM-CW Reflectometry Techniques" (Oral presentation)*
  Manso, M.E., A. Silva, P. Varela, D. Borba, P. Lang, L. Cupido, I. Nunes, G. Conway and the ASDEX
  Upgrade Team.

- *"Real time plasma control tools for advanced tokamak operation" (Invited talk)*
  Varandas, C.A.F., J. Sousa, A.P. Rodrigues, B.B. Carvalho, H. Fernandes, A.J. Batista, N. Cruz, A. Combo and the CFN Control and Data Acquisition Group

- **55th Annual Meeting of the Austrian Phys. Soc. (Vienna, Austria, 2005)**
- *"Measurements of edge plasma fluctuations in toroidal plasmas with probes"*
  Ioniță, C., P.C. Balan, R. Schrittwieser, J. Stöckel, J. Adámek, M. Hron, M. Tichý, E. Martines, G. Van Oost, C.A.F. Varandas, H.F.C. Figueiredo, C. Silva, J.J. Rasmussen, V. Naulin

- **6th International Balkan Workshop on Applied Physics (Constanța, Romania, 2005)**
- *"Edge plasma fluctuations in magnetized plasmas", invited lecture*
  Balan, P., C. Ioniță, R. Schrittwieser, J. Stöckel, J. Adámek, M. Hron, M. Tichý, E. Martines, G. Van Oost, H.F.C. Figueiredo, J.A. Cabral, C. Varandas, C. Silva, M.A. Pedrosa, C. Hidalgo

19.1.4. Papers in nacional conferences

- **14ª Conferência Nacional de Física 2005, Dezembro 1-3, Porto**
- *"Computação de turbulência na periferia de plasmas de tokamaks".*
  Ribeiro, T. T., B. Scott, D. Coster e F. Serra Druyts F and E. Alves

- *"O papel do tokamak ISTTOK no programa europeu de fusão"*
  Silva, C., H. Fernandes, B.B. Carvalho, I. Carvalho, P. Carvalho, R. Coelho, J. Ferreira, H. Figueiredo, J. Figueiredo, J. Fortunato, R. Gomes, I. Nedzelskij, A. Neto, T. Pereira, V. Plyusnin, A. Soares, D.F. Valcárcel, C.A.F. Varandas

- **As Energias do Presente e do Futuro, Lisboa, 21-22 Novembro, 2005**

- *"Fusão nuclear: uma opção energética para o futuro"*
  Manso, M.E., (Oral presentation)

- *"O Sistema de Controlo em Tempo-Real do Tokamak ISTTOK"*
  Valcárcel, D.F., I.S. Carvalho, A. Neto, P. Ricardo, J. Fortunato, A.S. Duarte, A.J.N. Batista, B.B. Carvalho, C. Silva, H. Fernandes, J. Sousa, C.A.F. Varandas

- *"Energia nuclear: uma opção para o futuro"*
  Varandas, C.A.F. (Invited talk)

19.1.5. Articles in newspapers

- *"Um marco importante para a energia de fusão nuclear"*
  Carlos Varandas
  Público, 29 June 2005

- *"ITER: oportunidade de trabalho para as Empresas e Unidades de Investigação Portuguesas"*
  Carlos Varandas
  Diário Económico, 22 November 2005

19.1.6. Laboratorial Prototypes

- *"Retarding Field Energy Analyzer"*

Nedzelskij, I., C. Silva and H. Fernandes

- *"Multi-pin array of emissive probes"*

Silva, C. and H. Figueiredo

- *"Real-time test facility"*

Batista, A. and J. Sousa

- *"PCI transient recorder module with galvanic isolation"*

Correia, M. and J. Sousa

1.9.1.7. Prizes and Awards

- Bruno Gonçalves received the Ph.D Research Award for an outstanding Doctoral Thesis, given by the Plasma Physics Division of the European Physical Society, in June 2005

- Prof. C. Varandas was awarded the degree *of "Grande Oficial da Ordem do Infante D. Henrique"* for his contributions to Physics in Portugal by the President of the Portuguese Republic in November 2005

19.2. TECHNOLOGIES OF PLASMAS AND LASERS

19.2.1. Ph.D thesis

- *"Coulomb explosion of large clusters"*
  Fabio Peano
  Politecnico di Torino, March 2005

19.2.2. Book chapters

- Guerra,V., P. A. Sá, and J. Loureiro,
  Kinetic modeling of the nitrogen afterglow, in V. Haubrecht e J. Bartl (editores)
  16th Symposium on Physics of Switching Arc, Brno University of Technology, Brno-Letohrad, Czech Republic, 2005.

19.2.3. Articles in scientific journals

- *"The effect of the gas flow-rate on the radial structure of a torch-like helium plasma"*
  Álvarez, R., M.C. Quintero and A. Rodero
  IEEE Trans. Plas. Sci. 33(2), 422–423, 2005

- *"Radial description of excitation processes of molecular and atomic species in a high-pressure helium microwave plasma torch"*
  Álvarez, R., M.C. Quintero and A. Rodero
  J. Phys. D: App Phys. 38(20), 3768-3777, 2005

- *"Thermal inequilibrium of atmospheric helium microwave plasma produced by an axial injection torch"*
  Álvarez, R., A. Rodero, M. C. Quintero, A. Sola, A. Gamero and D. Ortega
  J. Appl. Phys. 98, 093304, 2005

- *"Oxygen plasma surface interaction in treatments of polyolefines"*
  Belmonte, T., C.D. Pintassilgo, T. Czerwiec, G. Henrion, V. Hody, J.M. Thiebaut, and J. Loureiro
  Surface and Coatings Technology 200, 26-30, 2005

- *"Wave kinetic treatment of forward four-wave stimulated scattering instabilities"*
  Bingham, R., L. O. Silva, R. M. G. M. Trines, J. T. Mendonça, P. K. Shukla, W. B. Mori, R. A. Cairns
  Journal of Plasma Physics 71, 899, 2005

- *"Broadband amplification in non linear crystals using controlled angular dispersion of signal beam"*
  Cardoso, L., G. Figueira
  Optics Communications 251, 405, 2005.

- *"Bandwidth increase by controlled angular dispersion of signal beam in optical parametric amplification"*
  Cardoso, L., G. Figueira, N. Lopes, J. Wemans, J. T. Mendonça,
  Proc. SPIE Vol. 5777, 775, 2005.

- *"Exact orbital motion theory of the shielding potential around an emitting, spherical body"*
  Delzanno, G. L., A. Bruno, G. Sorasio, G. Lapenta,
  Phys. Plasmas 12, 062102, 2005

- *"Effects of Landau quantization on the equation of state (EOS) in intense laser plasma interactions with strong magnetic fields"*
  Eliezer, S., P. Norreys, J. T. Mendonca, K. Lancaster,
  Phys. Plasmas 12, 052115, 2005

- *"A new diagnostic for very high magnetic fields in expanding plasmas"*
  Eliezer, S., J. T. Mendonca, R. Bingham, P. Norreys
  Physics Letters A 336, 390, 2005

- *"Mirrorless tilted pulse front single-shot autocorrelator"*
  Figueira, G., L. Cardoso, N. Lopes, J. Wemans,
  Journal of the Optical Society of America B 22, 2709, 2005

- *"Performance and characterization of a 2.8 TW Ti:sapphire-Nd:glass chirped pulse amplification laser system"*
  Figueira, G., et al.
  Proc. SPIE Vol. 5777, 636, 2005.

- *"Densities of N and O – atoms in N2-O2 flowing glow discharges by actinometry"*
  Henriques, J., S. Villeger, J. Levaton, J. Nagai, S. Santana, J. Aamorin AND A. Ricard,
  Surface and Coating Tech. 200, 814 (2005).

- *"Ion acoustic instability triggered by finite amplitude polarized waves in the solar wind"*
  Gomberoff, L., J. Hoyos and A.L. Brinca,
  J. Geophys. Res.109, A06101, 2005;

- *"Self-confinement of a fast pulsed electron beam generated in a double discharge"*
  Goktas, H., M. Udrea, G. Oke, A. Alacakir, A. Demir, and J. Loureiro,
  Journal of Physics D: Applied Physics 38, 2793-2797, 2005

- *"New mechanism of vacuum radiation from non-accelerated moving boundaries"*
  Guerreiro, A., J. T. Mendonça, A. M. Martins,
  J. Optics B: Quantum and Semiclassical Optics 7, S69, 2005

- *"Characterization of a surface-wave sustained plasma discharge in a coaxial structure"*
  Letout, S., L.L. Alves, C. Boisse-Laporte and P. Leprince,
  J. Optoelectronics and Advanced Materials Vol. 7, No. 5, 2005

- *"Creation and expansion of a magnetized plasma bubble for plasma propulsion"*
  Loureiro, J., J. T. Mendonça, A. L. Brinca, R. Fonseca, L. O. Silva, I. Vieira
  Journal of Atmospheric and Solar-Terrestrial Physics 67, 1315, 2005

- *"Double Sheaths in RF Discharges"*
  Marques, L., G. Gousset and L.L. Alves
  IEEE Trans.Plasma Sci. - Special Issue on Images In Plasma Science 33, 358-359, 2005

- *"Three-dimensional wakes driven by intense relativistic beams in gas targets"*
  Martins, S. F., R. A. Fonseca, L. O. Silva, F. S. Tsung, W. B. Mori, S. Deng, T. Katsouleas
  IEEE Transactions on Plasma Science 33, 558, 2005

- *"Long-time evolution of magnetic fields in relativistic GRB shocks"*
  Medvedev, M., M. Fiore, R. A. Fonseca, L. O. Silva and W. B. Mori
  The Astrophysical Journal Letters, 618, L75, 2005

- *"Micrometeoroid flight in the upper atmosphere: Electron emission and charging"*
  Mendis, D. A., Wai-Ho Wong, M. Rosenberg, and G. Sorasio,
  J. Atmos. Sol.-Terr. Phys. 67, 1178, 2005

- *"Physical problems of artificial magnetospheric propulsion"*
  Mendonça, J. T., A. L. Brinca, R. Fonseca, J. Loureiro, L. O. Silva, I. Vieira
  Journal of Plasma Physics 71, 495, 2005

- *"A coupled two-step plasma instability in PW laser plasma interactions"*
  Mendonça, J T, P Norreys, R Bingham and J R Davies
  Plasma Phys. Control. Fusion 47 B799, 2005

- *"Beam Instabilities in Laser-Plasma Interaction: Relevance to Preferential Ion Heating"*
  Mendonça, J. T., P. A. Norreys, R. Bingham, and J. R. Davies
  Phys. Rev. Lett. 94, 245002, 2005

- *"Wakefield of Bose-Einstein condensates in a background thermal plasma"*
  Mendonça, J. T., P. K. Shukla, R. Bingham,
  Physics Letters A 340, 355, 2005

- *"Parametric excitation of neutrino pairs by electron plasma waves"*
  Mendonça, J. T., A. Serbeto, R. Bingham, P. K. Shukla,
  J. Plasma Physics 71, 119, 2005

- *"A kinetic approach to Bose-Einstein condensates: self-phase modulation and Bogoliubov oscillations"*
  Mendonça, J.T., R. Bingham and P.K. Shukla,
  Journal of Experimental and Theoretical Physics (JETP) 101, 942-948, 2005

- *"Time refraction and the quantum properties of vacuum"*
  Mendonça, J.T. and A. Guerreiro,
  Physical Review A 72, 044512, 2005

- *"Absolute Time-Resolved X-Ray Laser Gain Measurement"*
  Mocek, T., S. Sebban, G. Maynard, Ph. Zeitoun, G. Faivre, S. Hallou, M. Fajardo, S. Kazamias, B. Cros, J. P. Rousseau, and J. Dubau
  Phys. Rev. Lett. 95, 173902, 2005

- *"Observation of ion temperatures exceeding background electron temperatures in petawatt laser-solid experiments"*
  Norreys, P. A., K. L. Lancaster, H. Habara, J. R. Davies, J. T. Mendonça, R. J. Clarke, B. Dromey, A. Gopal, S. Karsch, R. Kodama, K. Krushelnick, S. D. Moustaizis, C. Stoeckl, M. Tatarakis, M. Tampo, N. Vakakis, M. S. Wei and M. Zepf
  Plasma Phys. Control. Fusion 47, L49, 2005

- *"Particle Statistics in quantum information processing"*
  Omar, Y.
  Int. J. Quantum Information 3, 201, 2005

- *"Characterization and crystal structure of the bimetallic cyano-bridged [(eta 5-C5H5) (PPh3)(2) Ru (mu-CN) Ru (PPh3)2(eta(5)-C5H5)][PF6], Synthesis, Inorganica Chimica"*

Ornelas, C., C. Candum, J. Mesquita, J. Rodrigues, M. H. Garcia, N. C. Lopes, M. P. Robalo, K. Nattinen, K. Rissanen, Acta 358 (8) 2482-2488, May, 2005.

- *"Dynamics and control of shock shells in the Coulomb explosion of very large deuterium clusters"*
  Peano, F., R. A. Fonseca, L. O. Silva,
  Physical Review Letters 94, 033401, 2005; also in Virtual Journal of Ultrafast Science 4, issue 2, 2005

- *"Modelling of a N2-O2 flowing afterglow for plasma sterilization"*
  Pintassilgo, C.D., J. Loureiro, and V. Guerra,
  Journal of Physics D: Applied Physics 38, 417-430, 2005

- *"Pair production by a strong wakefield excited by intense neutrino bursts in plasmas"*
  Rios, L. A., A. Serbeto, J. T. Mendonça, P. K. Shukla, R. Bingham,
  Physics Letters B 606, 79, 2005

- *"Wigner-Moyal description of free variable mass Klein-Gordon fields"*
  Santos, J. P., and L. O. Silva,
  Journal of Mathematical Physics 46, 102901, 2005

- *"Periodic structures on an ionic-plasma-vacuum interface"*
  Shukla, P. K., and L. Stenflo,
  Physics of Plasmas 12, 044503, 2005

- *"Molecular Dissociation in N2-H2 Microwave Discharge"*
  Tatarova, E., F. M. Dias, B. Gordiets and C. M. Ferreira
  Plasma Sources and Science Technology 14 19-31, 2005.

- *"A Large scale Ar Plasma Source Excited by a TM33 mode"*
  Tatarova, E., F. M. Dias, J Henriques and C. M. Ferreira,
  IEEE Transactions on Plasma Science 33 866-875, 2005

- *"A quasi-particle approach to modulational instabilities in wave-plasma interactions"*
  Trines, R., R. Bingham, L. O. Silva, J. T. Mendonça, P. K. Shukla, and W. B. Mori,
  Physica Scripta T116, 75, 2005

- *"Quasi-particle approach to the modulational instability of drift waves coupling to zonal flows"*
  Trines, R., R. Bingham, L. O. Silva, J. T. Mendonça, P. K. Shukla, and W. B. Mori,
  Physical Review Letters 94, 165002, 2005

- *"An update of argon inelastic cross-sections for plasma discharges"*
  Yanguas, A., J. Cotrino and L.L. Alves
  J. Phys. D: Appl. Phys. 38, 1588-1598, 2005

- *"Characterisation and optimisation of a multiterawatt CPA laser system using SPIDER"*
  Wemans, J., G. Figueira, N. Lopes, L. Cardoso,
  Proc. SPIE Vol. 5777, 642, 2005.

19.2.4. Papers in conference proceedings

- *"Modelo hidrodinâmico de difusão-convexão em grelha adaptativa, para plasmas de descarga micro-ondas em geometria coaxial"*
  Alves, L.L.
  Congreso de Métodos Numéricos en Ingeniería (CMNI-05), Granada, Spain 2005.

- *"New features on surface-wave discharges: boundary phenomena and power deposition"*
  Alves, L.L.
  XIth Conference on Plasma Physics and Applications, Iasi, Rumania 2005.

- *"Bandwidth increase by controlled angular dispersion of signal beam in optical parametric amplification"*
  Cardoso, L., G. Figueira, N. Lopes, J. Wemans, J. T. Mendonça,
  Proc. SPIE Vol. 5777, 775 (2005)

- *"On the possibility to restore time-averaged Langmuir probe characteristics"*
  Dias, F. M. Tsv. K. Popov
  FLTPD VI "Frontiers in Low Temperature Plasma Diagnostics VI", Les Houches, France, 2005, 56

- *"Precise Determination of the Electron Density in Intermediate Pressure Gas Discharges Using Langmuir Probe Measurements"*
  Dimitrova, M., Tsv. K. Popov, F. M. Dias,
  FLTPD VI "Frontiers in Low Temperature Plasma Diagnostics VI", Les Houches, France, 2005, 47

- *"Performance and characterization of a 2.8 TW Ti:sapphire-Nd:glass chirped pulse amplification laser system"*
  Figueira, G., N. Lopes, L. Cardoso, J. Wemans, J. Dias, M. Fajardo, C. Leitão, T. Mendonça,
  Proc. SPIE Vol. 5777, 636, 2005

- *"Simulation of plasma radiation in Earth and Mars atmospheric entries"*
  Silva, M. Lino da, V. Guerra, J. Loureiro, and M. Dudeck,
  4th International Symposium on Atmospheric Reentry Vehicles and Systems, Arcachon (France) 2005.

- *"Kinetics of Particles in Relativistic Collisionless Shocks, in Particle Acceleration in Astrophysical Plasmas: Geospace and Beyond"*
  Mikhail V. Medvedev, Luis O. Silva, Ricardo A. Fonseca, J. W. Tonge, and Warren B. Mori
  Edited by D. Gallagher, J. Horwitz, J. Perez, R. Preece, and J. Quenby, Geophysical Monograph Series, Volume 156, 2005

- *"Experimental study and modelling of the afterglow of an N2-O2 microwave discharge"*
  Pintassilgo, C.D., M. Mrázková, P. Vašina, V. Kudrle, V. Guerra and A. Tálský,
  27th International Conference on Phenomena in Ionized Gases (ICPIG), Eindhoven (The Netherlands) 2005.

- *"Kinetic study of the flowing afterglow of a N2-CH4 microwave discharge for metal nitrocarburising"*
  Pintassilgo, C.D., C. Jaoul, T. Belmonte, T. Czerwiec, and J. Loureiro,
  16th International Symposium on Plasma Chemistry (ISPC), Toronto (Canada) 2005.

- *"Simple techniques to restore time-averaged Langmuir probe characteristics"*
  Tsv. K. Popov, F. M. Dias,
  IW&SSPP I "First International Workshop & Summer School on Plasma Physics", Kiten, Bulgaria, 2005, P6

- *"Production and study of Titan´s aerosols analogues with a RF low pressure plasma discharge"*
  C. Szopa, G. Cernogora, J.J. Correia, L. Boufendi, A. Jolly, P. Coll, and C. Pintassilgo,
  Geophysical Research Abstracts, vol.7, 08006, Proceedings General Assembly European Geosciences Union (EGU), Viena (Austria) 2005.

- *"Characterisation and optimisation of a multiterawatt CPA laser system using SPIDER"*
  J. Wemans, G. Figueira, N. Lopes, L. Cardoso,
  Proc. SPIE Vol. 5777, 642 (2005)

19.2.5. Invited talks in international conferences

- *"Modelo hidrodinâmico de difusão-convexão em grelha adaptativa, para plasmas de descarga micro-ondas em geometria coaxial"*
  Alves, L.L.
  Congreso de Métodos Numéricos en Ingeniería (CMNI-05), Granada, Spain 2005.

- *"New features on surface-wave discharges: boundary phenomena and power deposition"*
  Alves, L.L.
  XIth Conference on Plasma Physics and Applications, Iasi, Rumania 2005.

- *"Plasma laboratory simulations of Titan's aerosols, Invited Topical Review Letters"*
  Cernogora, G., C. Szopa, L. Boufendi, P. Coll, J.-M. Bernard, and C. Pintassilgo,
  4th International Conference in Physics of Dust Plasmas (ICPDP) 2005, Orléans–France

- *"Basic physics issues in fast ignition"*
  Davies, J. R.
  8th International Workshop on Fast Ignition of Fusion Targets 2005, Tarragona, Spain.

- *"The Alfvén Limit Revisited*
  Davies, J. R.
  2nd International Conference on the Frontiers of Plasma Physics and Technology 2005, Goa, India.

- *"Plasma Physics Applications"*
  Fajardo, M.
  Research Courses on New X-ray Science: New Science in the VUV to Soft X-ray Domain, Hamburg, Germany, March 15-17, 2005

- *"Tablletop Ultra-Intense XUV Sources, Lasernet Task 2" Fajardo, M.*
  workshop: Plasma-based x-ray lasers; Prague 1-2 Sep 2005

- *"Large-scale molecular plasma sources" (Invited lecture)*
  Ferreira, C. M., E. Tatarova, F. M. Dias, and J. Henriques,
  XXVII International Conference on Phenomena in ionized Gases, July 17-22, Eindhoven, The Netherlands, 2005

- *"Kinetic processes in molecular microwave plasmas" (Invited lecture)*
  Ferreira, C. M., E. Tatarova, V. Guerra, J. Henriques and F. M. Dias
  XIV International Summer School on "Vacuum, Electron and Ion Technologies", 12-16 September, Sunny Beach, Bulgaria, 2005

- *"The Laboratory for Intense Lasers at IST"*
  Figueira, G.
  LaserLab Users Meeting, St. Catherine's College, Oxford, UK, April 2005

- *"Computational Methods for Laser Plasma Interactions"*
  Fonseca, R. A.
  NATO Advanced Studies Institute – Scottish Universities Summer School in Physics, SUSSP60, August 2005. [invited computational workshop organizer]

- *"Computational Challenges in Laser Plasma Interactions"*
  Fonseca, R. A.
  NATO Advanced Studies Institute – Scottish Universities Summer School in Physics, SUSSP60, August 2005.

- *"An integrated tool for modeling astrophysical and laboratory plasmas"*
  Fonseca, R. A., osiris.framework:
  Congreso de Métodos Numéricos en Ingeniería 2005, Granada, Spain, July 2005.

- *"Visualization and data analysis of computer simulations"*
  Fonseca, R. A.
  7th International School Symposium for Space Simulations – ISSS 7, Kyoto, Japan, March 2005.

- *"Kinetic modeling of the nitrogen afterglow"*
  Guerra,V., P. A. Sá, and J. Loureiro
  16th Symposium on Physics of Switching Arc, Nové Město – Moravě (Czech Republic) 2005.

- *"Mutual interactions between finite laser beams in plasmas"*
  Lopes, N. C.
  2005 SSAAP Symposium, Las Vegas, NV- USA, August 2005

- *"Acceleration processes in the Peta-Watt regime"*
  Mendonça, J. T.

RAL Christmas Meeting, Abingdon, U.K., 19th to 20th December 2005.

- *"New results in photon kinetics"*
  Mendonça, J. T.
  Brazilian Conference on Plasma Physics, Rio de Janeiro, Brazil, 27th to 30th November 2005.

- *"Recent advances in wave kinetics"*
  Mendonça, J. T.
  Autumn College on Plasma Physics, International Centre for Theoretical Physics,Trieste, Italy, 5th to 30th September 2005.

- *"Acceleration of photons and quasi-particles"*
  Mendonça, J. T.
  Scottish Universities Summer School in Physics, St. Andrews, Scotland UK, 14th to 27th August 2005.

- *"The artificial magnetosphere concept"*
  Mendonça, J. T.
  IAGA 2005 - 10th Scientific Assembly of the International Association of Geomagnetism and Aeronomy, Toulouse, France, 18th to 29th July 2005.

- *"Extreme states of matter"*
  Mendonça, J. T.
  6th International Summer School-Conference "Let's Face Chaos through Nonlinear Dynamics, Maribor, Slovenia, 26th June to 10th July 2005.

- *"Photon acceleration in plasma and gravitational fields"*
  Mendonça, J. T.
  The Rank Prize Funds, Mini-Symposium on High Intensity Laser Plasma Interactions, Grasmere, U.K., 4th to 7th April 2005.

- *"Photons, Gravitons and Einstein"*
  Mendonça, J. T.
  RAL Lecture included in the commemoration of "The World Year of Physics, 31th March 2005.

- *"Magnetic field effects in ultra-intense laser plasmas"*
  Mendonça, J. T.
  International Workshop on Physics of High Energy Density in Matter, Hirschegg, Austria, 30th January to 4th of February 2005.

- *"A two-step process for ion heating in IFE"*
  Mendonça, J. T.
  8th International Workshop on Fast Ignition of Fusion Targets 2005, Tarragona, Spain.

- *"N2-O2 afterglow for plasma sterilization" Topical Invited Lecture*
  Pintassilgo, C.D.
  18th European Conference on the Atomic and Molecular Physics of Ionised Gases (ESCAMPIG) 2006, Lecce–Italy

- *"Physical problems (microphysics) in relativistic plasma flows, Relativistic Jets: The Common Physics of AGN, Microquasars, and Gamma-Ray Bursters"*
  Silva, Luís O.
  Ann Arbor, Michigan, December 2005

- *"White light parametric instabilities in plasmas"*
  Silva, Luís O.
  Autumn College on Plasma Physics, Abdus Salam ICTP International Centre for Theoretical Physics, Trieste, Italy, September 2005.

- *"PIC simulations of relativistic shocks, Astrophysical sources of high energy particles and radiation"*
  Silva, Luís O.
  Torun, Poland, June 2005
- *"Formation of strong shocks by laser pulses"*
  Silva, Luís O.
  April 2005 Meeting of the American Physical Society, Tampa, Florida, April 2005

- *"Photon kinetics, Multiscale Processes in Fusion Plasmas"*
  Silva, Luís O.
  IPAM/UCLA Workshop, Los Angeles, California, January 2005

- *"Very High Mach Number Shock Waves Resulting from Collisions of Plasma Slabs"*
  Sorasio, G.
  Autumn College on Plasma Physics, Abdus Salam ICTP International Centre for Theoretical Physics, Trieste, Italy, September 2005.

- *"Shielding potential around a body immersed in a plasma: effect of electron emission"*
  Sorasio, G.
  IAGA 2005 - 10th Scientific Assembly of the International Association of Geomagnetism and Aeronomy, Toulouse, France, 18th to 29th July 2005.

- *"Wave driven plasma sources" (Invited lecture)*
  Tatarova, E., F. M. Dias, J. Henriques and C. M. Ferreira,
  XIV International Summer School on "Vacuum, Electron and Ion Technologies" (12-16 September 2005, Sunny Beach, Bulgaria)

- *"Large-Scale Microwave Plasma Sources Interdisciplinary" (Invited lecture)*
  Tatarova, E.
  Workshop on Electronic Materials and Interaction of Plasmas with Matter (University of Minho, Guimarães, 16 December, Portugal)

19.2.6. Laboratorial Prototypes

- *"Device to measure simultaneously a laser pulse-front inhomogeneity and its intensity autocorrelation in a single-shot fashion"*
  Figueira, G., L. Cardoso, N. Lopes, J. Wemans

- *"Device to produce a plasma waveguide for intense lasers"*
  Lopes, N.C, C. Clayton, F. Fang

- *"Setup for time-resolved measures of plasma waveguide density profiles"*
  Macedo, R., N.C. Lopes, C. Clayton

- *"High-voltage ultra-short pulser"*
  Sampaio, J., N.C. Lopes, C. Clayton

19.2.7. Prizes and Awards

- Prof. Matos Ferreira was awarded the degree *of "Grande Oficial da Ordem do Infante D. Henrique"* for his contributions to Physics in Portugal by the President of the Portuguese Republic in November 2005

- Bruno Brandão received the prize *"Best 2nd year LEFT/IST student",* in October 2005.

- Jorge Vieira received the Best Poster Prize at the 32nd EPS Conference Plasma Physics and Controlled Fusion 2005, Tarragona, in July 2005, with the work *"Optimizing Wave Breaking and Self Injection in the Laser Wake-field Accelerator"*

- Jorge Vieira received the Best Poster Prize at the 60th Scotish Universities Summer School in Physics Best Poster Prize, St. Andrews, Scotland, in August 2005, with the work *"Self Injection in the Laser Wake-field Accelerator"*